THE UNIVERSITY OF HULL

Positron Emission Tomography Imaging Probes Targeting Chemokine Receptors

Being a Thesis submitted for the Degree of Doctor of Philosophy in The University of Hull

By

Seraj Omar Alzahrani B.Sc (Hons) M.Sc.

May 2016

I. Abstract

Positron emission tomography (PET) is a highly sensitive nuclear medicine imaging technique. PET is used to accurately diagnose cancer and can detect early stage tumours. Molecular probes containing a positron emitting metal radioisotope (such as ^{64}Cu or ^{68}Ga) need to give a stable complex *in vivo* as well as targeting biomarkers or metabolic processes within the tumour. The roles of chemokine receptors in multiple disease stages have been demonstrated. The CXCR4 and CCR5 chemokine receptors have been implicated in cancer, as well as other disease states including HIV infection and chronic inflammatory diseases, including asthma and rheumatoid arthritis. Incorporation of a positron emitting radioisotope into a CXCR4 or CCR5 specific antagonist compound could allow visualisation of physiological locations with high expression levels of these receptors to characterise the disease.

The small molecule CXCR4 antagonist AMD3100 (Plerixafor) has been approved for clinical use as a haematopoietic stem cell mobilising agent and also exhibits anti-HIV, anti-inflammatory and anti-tumour activity. Configurationally restricted analogues of AMD3100 complexed to metal ions have improved binding characteristics compared to AMD3100 and its metal complexes. A synthetic pathway to obtain series of configurationally restricted macrocyclic compounds (analogues of AMD3100) fixed in the *trans IV* configuration, has been developed and the copper(II), zinc(II) and nickel(II) complexes characterised. Their biological properties (anti-HIV, cytotoxicity and Ca^{2+} signalling inhibition) were evaluated to allow selection of compounds to be radiolabelled with $^{64}Cu^{2+}$ for evaluation as a PET imaging agent targeting CXCR4. The most active *trans IV* complexes, bis(zinc(II))-1,4-xylyl bis(methyl side-bridged cyclam and bis(zinc(II))-1,4-xylyl bis(benzyl side-bridged cyclam) have EC_{50} values of 516 and 247 nM respectively in the anti-HIV assay with cyotoxicity (CC_{50}) values of 42800 and 39600 nM respectively. However, the novel mixed metal *trans II* complex (copper(II)zinc(II))-1,4-xylyl bis(side-bridged cyclam) has a higher binding affinity with an EC_{50} value of 3 nM (four times more potent than AMD3100) and cytotoxicity CC_{50} value greater than 10 µM. Bis(zinc(II))-1,4-xylyl bis(side-bridged cyclam) was successfully radiolabelled with $^{64}Cu^{2+}$ *via* transmetallation to form (^{64}Cu (zinc(II))-1,4-xylyl bis(side-bridged cyclam) with a crude radiochemical yield of 92%.

A derivative of known CCR5 antagonist TAK-779 containing a carboxylic acid functional group 2-(p-tolyl)-6,7-dihydro-5H-benzo[7]annulene-8-carboxylic acid **18** was prepared. A DO3A compound with a spacer terminating in a primary amine (tri-tert-butyl 2,2',2''-(10-(2-((2-aminoethyl)amino)-2-oxoethyl)-1,4,7,10-tetraazacyclododecane-1,4,7-triyl)triacetate) was successfully conjugated to compound **18** forming a potential CCR5 targeting compound that could be radiolabelled with gallium-68 for PET imaging applications. Preliminary *in vitro* affinity assays indicated that the modification of the structure had disrupted the CCR5 binding and some structural modification redesign may be required. Radiolabelling of the conjugate compound 2-(p-tolyl)-6,7-dihydro-5H-benzo[7]annulene-8-amidoethyl-DOTA with gallium-68 was carried out. A crude radiochemical yield of ca. 100% was achieved to give ^{68}Ga-**(**2-(p-tolyl)-6,7-dihydro-5H-benzo[7]annulene-8-amidoethyl-DOTA) which is stable in buffer and against transferring challenge for over four hours.

II. Risk Assessment

All experiments were carried out in accordance with the University of Hull's Health and Safety guidelines. A full COSHH (Control of Substances Hazardous to Health) and risk assessment was carried out for each new experiment, signed by the undertaking student, supervisor, (Prof. S.J. Archibald) and the departmental safety officer (Dr T. McCreedy or Dr D. Lacey) before any practical work started. The COSHH forms carry the reference numbers SZ01 and SZ032.

III. Acknowledgements

I would like to express my deep thanks to my supervisor Prof. S. Archibald, for his continues guidance, constant support, encouragement, for all the knowledge he has imparted to me and opportunities as well as patience throughout my work. I am also grateful to Prof. R. Boyle for his help throughout my PhD.

Moreover, I would like to thank Dr. B. Burke and Dr. Rahul Saurabh for their assistance and special thanks to all past and currents members of C222 lab. Thanks to technical staff in the Department of Chemistry must certainly not be forgotten.

Finally, my sincere thanks also go to my family: my great father for his incessant backing, and support, my brothers and my sisters for everything they have done for me throughout my life and without whom none of this would have been achieved.

IV. Abbreviations

AIDS	Acquired immune deficiency syndrome
Asp	Aspartate
Bq	Becquerel's
CB	Cross bridge
CC_{50}	Cytotoxic concentration required to reduce a population by 50%
CHN	Carbon, Hydrogen, Nitrogen analysis
COSHH	Control of Sustances Hazardous to Health
CT	Computed tomography
d	Doublet
DCM	Dichloromethane
DMSO	Dimethylsulphoxide
DO2A	4,10-bis(Carboxymethyl)-1,4,7,10-tetraazabicyclo[5.5.2]tetradecane
DOTA	1,4,7,10-Tetraazacyclododecane-1,4,7,10-tetraacetic Acid
EC_{50}	Effective concentration required to reduce an effect by 50%
ECL1,2 or 3	Extra Cellular Loop 1, 2 or 3
EDC	1-Ethyl-3-(3-dimethylaminopropyl) Carbodiimide
EGF	epidermal growth factor
ESI	Electrospray ionisation
ET	Emission tomography
EtOH	Ethanol
FDG	2-Fluoro-2-deoxy-D-glucose
G-CSF	Granulocytes colony stimulation factor
Glu	Glutamate
GPCR	G-protein coupled receptor
HIV	Human immunodeficiency virus
HPLC	High performance liquid chromatography
HRMS	High resolution mass spectrometry
IC_{50}	Concentration required to inhibit binding by 50%

K_D	Langmuir isotherm
K_d	Rate of dissociation
KDa	kilo Daltons
KeV	Kilo electron volt
logP	Partition coefficient
m	Multiplet
M	Molar
MeCN	Acetonitrile
MeOH	Methanol
MIP1a or b	Macrophage inflammatory protein a or b
MRI	Magnetic Resonance Imaging
MS	Mass spectrometry
MT-4	Meta Trader 4
MTT	3-(4,5-dimethylthiazol-2-yl)-2,5-diphenyltetrazolium bromide
nBuLi	n-Butyl Lithium
NMR	Nuclear Magnetic Resonance
NP	Nanoparticles
PBS	Phosphate buffer solution
PEG	Polyethyleneglycol
PEG	Polyethyleneglycol
PET	Positron Emission Tomography
ppm	Parts per million
RCY	Radiochemical yield
R_f	Retention factor
RT	Room temperature
s	Singlet
SB	Side bridge
SPECT	Single photon emission computed tomography
t	Triplet

$t_{1/2}$	Half-life
TEA	Triethylamine
TLC	Thin layer chromatography
TM	Transmembrane
UV	Ultra-Violet
UV-vis	Ultra-Violet-visible
v/v	Volume/volume
w/w	Weight/weight
β-	Electron (beta minus)
β+	Positron (beta plus)
δ	Chemical Shift
λ_{max}	Maximum wavelength
3D	Three dimensional

V. List of Figures

VI. List of Schemes

VII. List of Tables

VIII. Table of Contents

Chapter 1

Introduction

1. Introduction

1.1. Chemokine and Chemokine Receptors

A combination of the words chemoattractant and cytokine form the word chemokine.[1] Cytokines are small protein water-soluble polypeptides (8-30 kDa) signalling molecules sending messages to both adjacent and distant cells.[2] Chemokines belong to the sub family of cytokines and are mainly associated with chemotaxis activities (the mediation of cell movement).[3] They have a main role to act as a chemoattractant and guide the movement of cells to regulate cell trafficking.[3] The chemokines play a key role in the immunophysiology and also contribute to immune and inflammatory responses.[4] The chemokine proteins are mainly composed of basic amino acids with conserved cysteine motifs to allow disulphide bond formation between the first and third, and second and fourth cysteine positons. On the basis of cysteine residue position, the chemokines are classified into four subtypes (CC, CXC, C and CX3C) the X represented by the number of residues that separate the cysteine residues as shown in Figure 1.[5] The CC and CXC are the main classes of chemokines of which over 40 have been identified.[6] The first two-cysteine residues of the CC subgroup of chemokine found next to one another whereas in CXC chemokines, the first two-cysteine residues are separated by a non-conserved amino acid.[6, 7]

Chemokines can be activated through a widely variant family of seven-transmembrane receptors belonging to the G-protein coupled receptor (GPCR) super family controlling recruitment of leukocytes to the sites of inflammation. Disease can occur in a breakdown of the regulation of such process.[8] A number of chemokines can bind to multiple receptors whilst some receptors can bind to more than one chemokine and this enables many biological effects.[3, 9] The involvement and overexpression of chemokines and their receptors are well recognised in various diseases, such as, cancer, inflammatory bowel disease, AIDS, asthma, multiple sclerosis, arthritis and allergic disorders.[7], [10] In many of these small molecule receptor antagonists can mediate the progression of the disease.[11, 12]

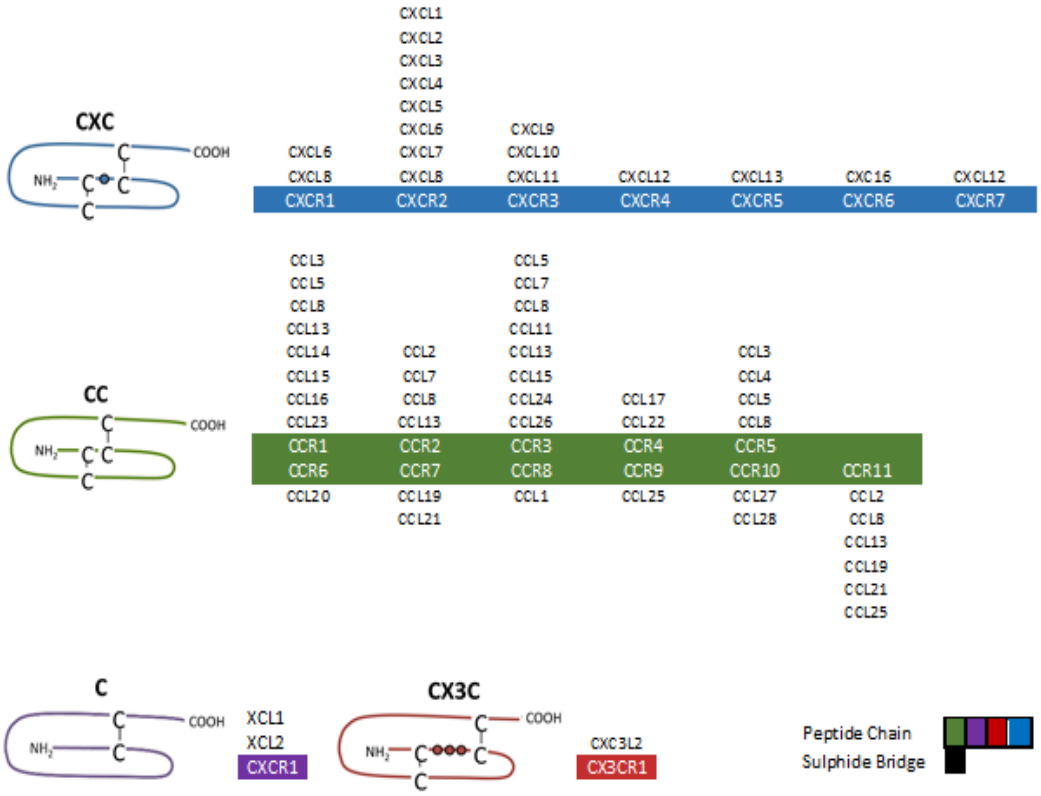

Figure 1 Schematic diagram of chemokine subfamilies and cysteine residues configuration

1.1.1. The Chemokine Receptor CXCR4

CXCR4 is one of the most prominent members of the chemokine receptor family and a central component of the signalling pathways in the body.[13] CXCR4 is involved in three fundamental stages of various cancer types (e.g., in lung, breast, prostate, ovarian, colon, melanoma, brain cancers): primary tumour growth, migration of cancer cells, and establishment of metastases. CXCR4 has been shown to be overexpressed in more than 70% of cancers, generating the need for personalised medicine through a combination of diagnosis and treatment.[13, 14] CXCR4 is 340-370 amino acids in length as shown in Figure 2, and has a negative charge of −9 at physiological pH.[14]

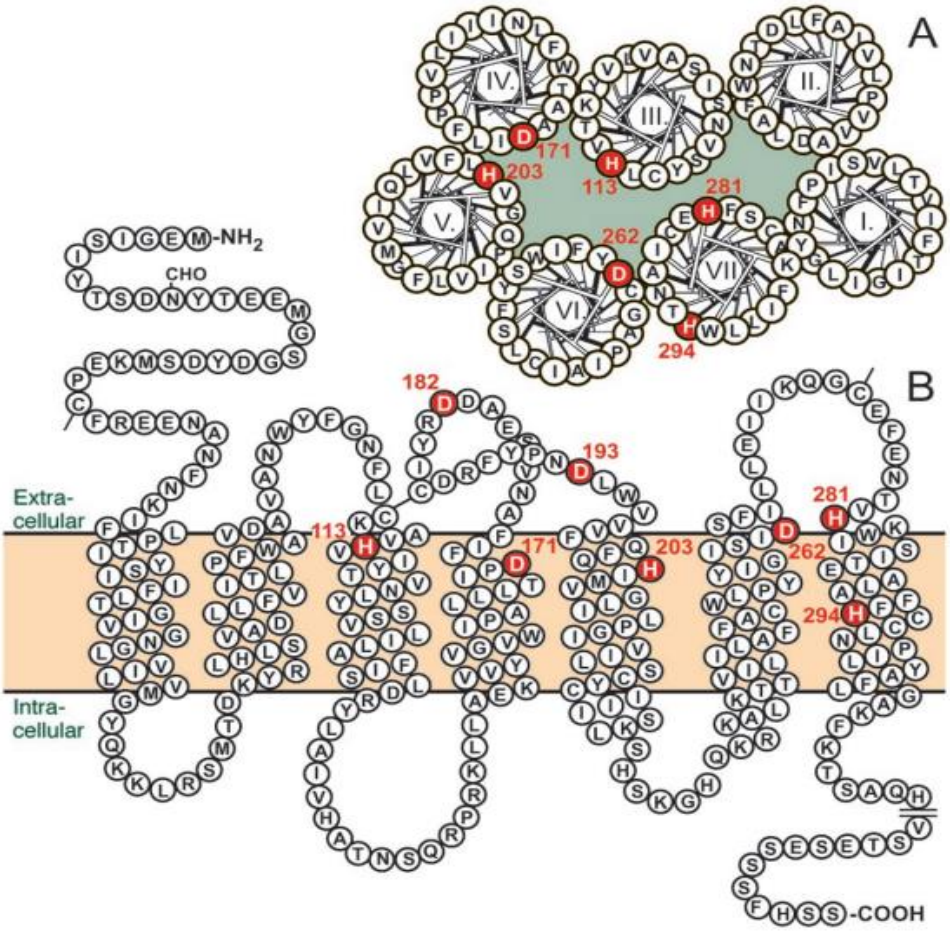

Figure 2 Helical wheel (A) and serpentine diagram (B) of the CXCR4 receptor (reproduced from Gerlach *et al*., 2001)[15]

In 2001, Muller *et al.* published a paper showing that the chemokines CXCR4 and CCR7 and their respective ligands play a critical role in determining the metastatic destination of breast cancer by acting directly on tumour cell migration and invasion.[16] They noted that CXCR4 is highly expressed in several breast cancer cell lines but also that CXCL12 is at peak levels of expression in organs representing the first destination of breast cancer metastasis. Breast cancers metastasise to lymph nodes, lung, liver and bone marrow and in the study they were able to correlate this with the level of CXCL12 expression observed in these organs.

The expression and concentration of chemokine receptor, CXCR4, and its ligand CXCL12 is associated with embryonic cell migration allowing the embryo to develop and grow normally. It is a lethal knockout at this stage but can be blocked

without impact in a mature organism. These migrational cues can be exploited in tumour progression and metastasis. Therefore, the blocking of the CXCR4 receptors may provide an opportunity to locate, diagnose and prevent the diseases such as cancer and AIDS.[17] CXCR4 antagonists have already been recognised as potential therapeutic agents hence they have been investigated for the treatment of HIV infection, cancer, and rheumatoid arthritis.[7, 18] CXCR4 antagonists have been reported for the clinically licensed application in the mobilisation of haematopoietic stem cells for stem cell transplantations, the attenuation of pain, the treatment of asthma, and the treatment of neurological diseases.[7]

1.1.1.1. CXCR4 Antagonists

The involvement of CXCR4 in many diseases has motivated the development of a number of receptor antagonists. CXCR4 antagonists have been characterised as substances that either block the receptors ability to be involved in HIV cell entry or block the binding of the natural ligand CXCL12 to abrogate the cellular signalling process which can be involved in the metastatic spread of cancer cells. The antagonists will bind to the CXCR4 receptors but produce no biological response whilst blocking the site; this differs from agonists that activate the receptor when bound.[19, 20] There have been numerous compounds such as antibodies, peptidic compounds, non-macrocyclic small molecules and macrocyclic molecules that have been developed to antagonise CXCR4 and have been analysed as anti-HIV agents. Much of the published data refers to the anti- HIV activity.[7]

BMS-936564/MDX-1338 is a human IgG4 monoclonal antibody that specifically recognises human CXCR4. *In vitro* studies show that MDX-1338 binds to CXCR4-expressing cells with low nanomolar affinity, blocks CXCL12 binding to CXCR4-expressing cells, and inhibits CXCL12- induced migration and calcium flux with low nanomolar EC_{50} values. When given as monotherapy, MDX-1338 exhibits antitumor activity in established tumours including AML, NHL, and multiple myeloma xenograft models. It has also been demonstrated that MDX-1338 can induce apoptosis in multiple cell lines and suggested that antibody-induced apoptosis is the key response that results in tumour growth inhibition.[21]

T140 is a 14 residue peptide derivative of T22 which was found to be active against HIV-1 through binding to the CXCR4 chemokine receptor, see Figure 3, and it is more effective at blocking infection than T22.[22] A number of T140 analogues were investigated in an attempt to reduce the cytotoxicity. The most successful approach was to replace arginine and lysine residues with residues that are non-basic and polar such as L-citrulline and glutamine.[23, 24] Some of the new compounds displayed similar anti HIV activity to T140 (IC_{50} values in the range of 8 to 50 nM).[23] The *in vivo* stability of the T140 analogues was increased by addition of a 4-fluoro-benzoyl group by N-terminal acylation. The development of these T140 analogues and their therapeutic potential have been discussed in several recent reviews.[18, 24]

ALX40-4C, see Figure 3, is a polypeptide consisting of arginine residues that mimics the TAT domain of HIV and is shown to have a high anti-HIV activity against X4 strains in the nanomolar range (IC_{50} of 3 nM) in a MT4 assay.[25, 26] However, in human clinical trials no significant impact on viral load was observed and so clinical investigations were not continued.[27] ALX40- 4C and AMD3100 are the only drugs of this type that have been administered to humans in clinical trials against HIV.

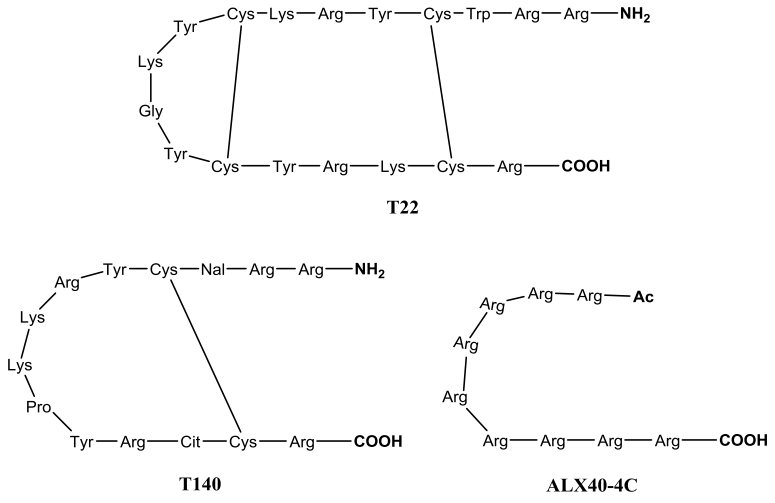

Figure 3 Some peptide CXCR4 antagonists

To understand the diagnosis and treatment of diseases associated with the overexpression of CXCR4 receptor, numerous small CXCR4 antagonist molecules

have been synthesised. One of the well-known small CXCR4 antagonist molecules, KRH-1636, see Figure 4, has been tested for its potential in the treatment of HIV. KRH-1636 inhibits X4 strains and shows potent antiviral activity in peripheral white blood cells of an immunodeficient mouse model (hu-PBL-SCID).[28] KRH-3955 and KRH-3140, orally bioavailable derivatives of KRH-1636, have been synthesised to demonstrate the efficacy in protection of mice from HIV infection on oral administration.[29,30] Another small molecule CXCR4 antagonist, AMD070, see Figure 4, has been synthesised and shown to be an effective anti-HIV agent which is also orally bioavailable..[31] A dual CCR5/CXCR4 antagonist, AMD3451 (*N*-pyridinylmethyl cyclam) see Figure 4, has been investigated which can inhibit infection by several viral strains, although it requires relatively high concentrations (1.2 - 26.5 μM) and it is regarded as a low potency antagonist.[32]

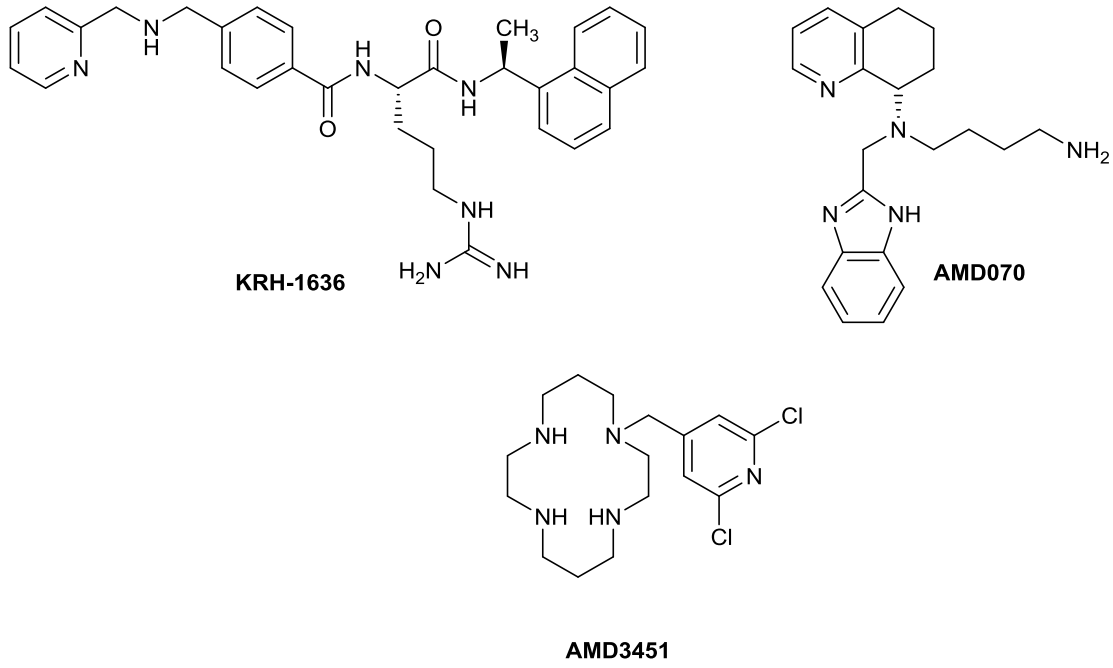

Figure 4 Chemical structures of some small molecules CXCR4 antagonists

1.1.1.1.1. Mono-Macrocycles

In the last few years numerous mono-azamacrocyclic compounds have been synthesised, many of which have applications outside the medical field.[33-35] There has also been extensive work conducted on mono-macrocyclic compounds with biological applications. Moreover, monomacrocyclic ligands have good potential for improved pharmacological properties such as oral bioavailability due to their reduced molecular charge and lower molecular weight in comparison to their bismacrocyclic counterparts.[36]

Gerlach *et al.* determined that binding of cyclam to CXCR4 receptor was dependent only on Asp^{171} and mutation of Asp^{262} did not impact binding.[15] This trend was observed for mono-macrocycle, AMD3465; see Figure 5, which suggests that for mono-macrocycles only one aspartate residue is required for binding.

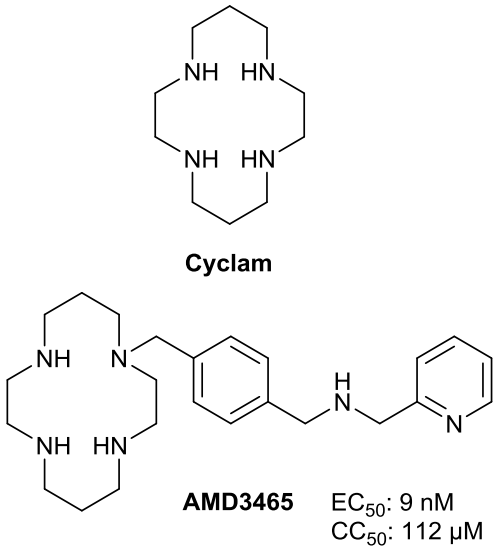

Figure 5 Chemical Structure of mono-macrocycle AMD3465, in vitro data from Bridger *et al.*[37]

In 2010, Bridger *et al.* investigated the minimum structural features required for a potent CXCR4 inhibitor developing a series of mono-macrocycle analogues of AMD3100 based on the scaffolds shown in Figure 6.[37] They found that substituting one cyclam with benzylamine, **L**^{1} significantly reduced the anti-HIV activity, EC_{50} value of 0.491 μM, which was 100 fold higher than AMD3100, EC_{50}: 4 nM; nonetheless the compound was still active at a micromolar concentration. An EC_{50} value shows the effective concentration of a substance that induces 50% of the maximal response, it is commonly used to measure a drug's potency. *Ortho* and *para* amino-phenyl substituents to form **L**^{2} and **L**^{3} respectively see Figure 6, did not alter activity, although, the ortho amino-phenyl substituent showed a higher degree of toxicity with a CC_{50} value of 24 μM. CC_{50} is the concentration of a substance required to reduce a cell population by 50%, it is a measure of a compounds cytotoxicity. The aromatic group was then substituted for 2-pyridine which resulted in a significant increase in activity, showing an EC_{50} of 9 nM; this led to the development of AMD3465, see Figure 6.

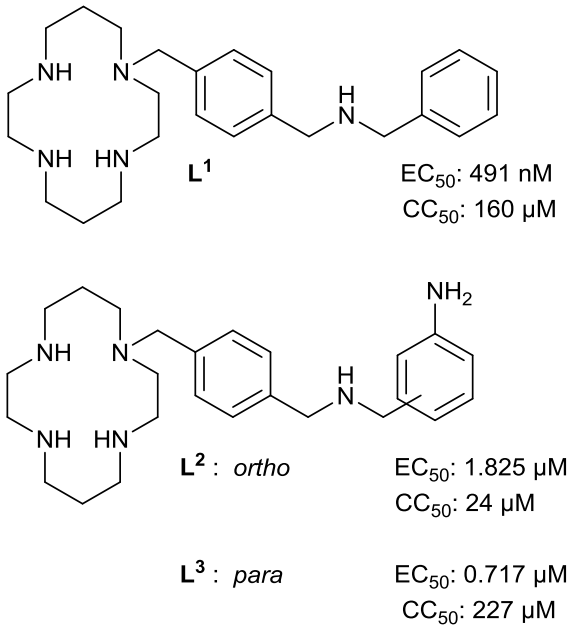

Figure 6 Scaffold of structures synthesised by Bridger *et al.*[37]

1.1.1.1.2. Bis-Macrocycles

The original discovery of the activity of molecules of this type started with an anti-HIV activity for several batches of commercial cyclam (1,4,8,11-tetraazacyclotetradecane) see Figure 7. They were found to be poor inhibitors of HIV replication in MT-4 cells but one of the batches of cyclam showed anomalously high activity and was therefore evaluated in further detail. This was the result of an impurity present in the sample which was eventually identified as AMD1657 a bis-cyclam connected by a direct C-C link, see Figure 7. This compound has an EC_{50} value of 0.1-0.2 μg/mL and a selectivity index of > 5,000.[38] The selectivity index is a ratio of the CC_{50} to EC_{50}. As a comparison, AZT, a current clinical drug used for HIV treatment has a selectivity index of > 1,000.[39, 40] Through the systematic preparation of analogues of AMD1657 connected with different aliphatic and aromatic linkers, AMD3100 was eventually synthesised.AMD3100 is a bicyclam composed of two cyclam rings tethered via an aromatic linker, see Figure 7.[41, 42] In the 1990s it was considered as pharmaceutical candidate.[43-45] A decade later, AMD3100 was successfully trailed for haematopoietic stem cell mobilisation and was granted FDA approval under the tradename Plerixafor and it is now used in patients routinely.[46-49]

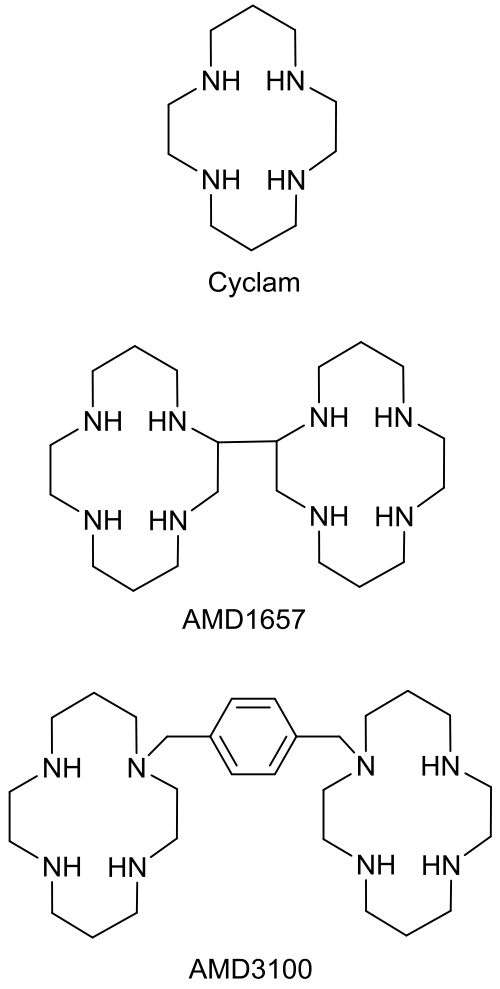

Figure 7 Important chemical structures in the development of AMD3100

In Phase 1 trials an unexpected side effect of AMD3100 was identified; an increase in the number of white blood cells in circulation. An application for this side effect was autologous stem cell transplantation which collects stem cells in sufferers of Hodgkin's disease, non-Hodgkin's lymphoma and multiple myeloma, who produce insufficient amounts of blood cells, and return them when needed. The standard mobilisation agent, granulocyte-colony stimulation factor (G-CSF) is not always sufficiently effective, however in conjunction with a single dose of AMD3100 much higher cell numbers were mobilised.[41] A single subcutaneous injection of AMD3100 was found by Calandra *et al.* to enable two thirds of sufferers of Hodgkin's disease, non-Hodgkin's lymphoma and multiple myeloma to generate enough cells for autologous transplantation.[50] Additional research by Gazitt *et al.*,

Flomenberg *et al.* and Devine *et al.* showed that tumour cells were not mobilised in multiple myeloma and non-Hodgkin's lymphoma patients on administration of AMD3100.[51-53] AMD3100, now called Plerixafor, was approved for haematopoietic stem cell mobilisation in non-Hodgkin's lymphoma and multiple myeloma patients.[41, 53, 54]

AMD3100 has now also been investigated as an anti-metastatic agent as the over-expression of CXCR4 in breast cancer, in particular, is well documented. In complementary studies with other cancers, De Falco *et al.* showed that in nude mice inoculated with the rare thyroid cancer anaplastic thyroid carcinoma AMD3100 has shown an effective reduction in tumour growth.[55] Furthermore, Rubin *et al.* discovered that for the development of many malignant brain tumours CXCR4 plays a critical role, suggesting that AMD3100 should be clinically assessed as a treatment.[56] In addition to this, Li *et al.* showed by blocking CXCL12 from activating CXCR4 with AMD3100, in colorectal cancer, a decrease in invasiveness was noted.[57] In summary, targeting the CXCR4 receptor with AMD3100 can prevent invasion and metastasis of multiple cancers. Analogues of AMD3100 could increase the potency further or lead to its use in other applications such as medical imaging.

Bis-macrocycles are a highly potent class of CXCR4 antagonists that have shown significantly greater affinity for CXCR4 receptor than mono-macrocycles due to additional interactions with the CXCR4 receptor.[37] In an effort to increase the understanding of how AMD3100 binds to CXCR4, Este *et al.* investigated numerous analogues of bis-cyclam connected by linkers of different types and lengths, see Figure 8.[58] Fused macrocycles were considered inactive and low activity was observed for macrocycles linked with an aliphatic linker group. Aromatic linkers proved to have increased activity, however the length of connector between the aromatic ring and the macrocycle affected the activity as AMD3390 showed very poor activity, see Figure 8. Therefore, the more aliphatic component to the linker the lower activity obtained. The effect of substituents on the linker groups resulted in lower activity or even inactive compounds with the exception of the 2-(methoxy)-*p*-xylyl linker which exhibited an EC_{50} value of 38 nM. The low activity was likely due to steric hindrance effects by the substituents which reduced the amount of

rotational freedom that the macrocyclic rings had. None of these bis-macrocyclic compounds investigated at the time were more active than AMD3100.

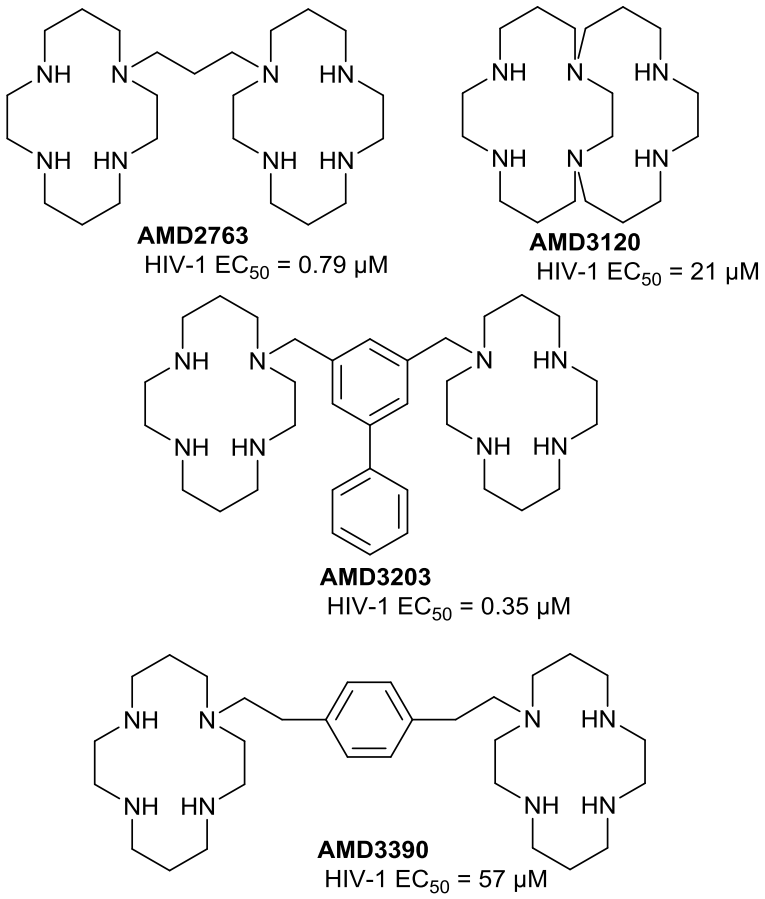

Figure 8 Chemical structures and EC^{50} values for a selection of the bis-macrocycles synthesised by Este *et al.*

De Clercq *et al.* and Bridger *et al.* have studied the structure-activity relationship of the bicyclams in detail.[44, 45, 59, 60] The potency of 12 to 16 membered bis-macrocycles as anti-HIV-1 and HIV- 2 agents connected via an aromatic linker with either *meta* or *para* substitution, was investigated by Bridger *et al.*, see Figure 9, it was found that for both the *meta* and *para* substituted bis-macrocycles the activity increases from 12 membered rings **L**[4] and **L**[5] to 14 membered rings **L**[6] and **L**[7], although activity decreases for rings larger than this **L**[8] and **L**[9]. The investigation of the toxicity was seen to decrease from 12 to 14 membered rings and then increase when the rings extended beyond 14 members.[44]

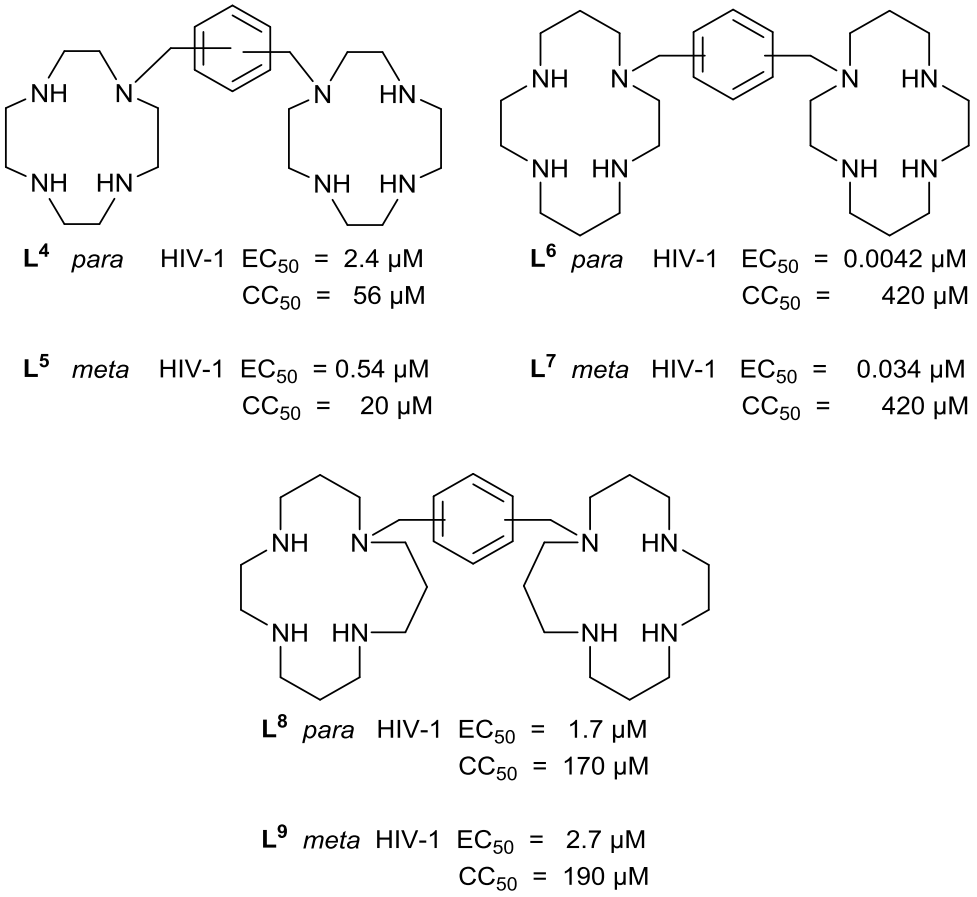

Figure 9 A small selection of chemical structures the bis-macrocycles synthesised by Bridger *et al*.[44, 45]

Moreover, Bridger *et al.* also examined the importance of symmetry in bis-macrocycles synthesising bis-macrocycles that contained different macrocycles. The activity of unsymmetrical bis-macrocycles was comparable to that of AMD3100 showing that symmetry was not crucial for activity, although, the macrocyclic ring was important for activity. The highest potency for the 12 and 13 membered rings was seen with the *meta* substitution whilst for the 14 membered rings a *para* substitution was preferable. Further studies revealed that activity of bis-macrocycles was not affected by the presence of electron withdrawing groups or electron donating groups on the *para* linker, nonetheless, the presence of halogens significantly increased macrocycle cytotoxicity, and this could be an important consideration in the development of radiotracers using radioactive fluorine. Moreover, bulky groups substituted on the linker resulted in adverse effects on activity; the reasoning for this was that the bulky group restricted the position of the cyclam rings. As mentioned previously, the optimum linker in this study was an aromatic group with methylene groups attaching the two macrocycles to it. It was concluded that, two azamacrocyclic rings tethered by a para-substituted aromatic linker result in extremely potent anti-viral activity.[44] Archibald and co-workers found that macrocycle configurational restriction and transition metal complexation enhances the binding affinity of bridged bis-cyclams for CXCR4 as a result of a further binding site on the molecule provided by configurational restriction. EC_{50} values of 74 nM and 2.5 nM were generated for the nickel(II) and zinc(II) complexes of $\mathbf{L^{10}}$ respectively.[61, 62] Valks *et al.* restricted the configuration with ethyl side bridges of a zinc(II) bis-macrocycle, $[Zn_2\mathbf{L^{10}}]^{4+}$ finding that it produced optimised binding to the CXCR4 receptor significantly improving the anti-HIV properties relative to AMD3100 and its metal complexes.[62] The copper(II) complex of a cross bridged cyclam chelator $[Cu_2\mathbf{L^{11}}]^{4+}$ was found to be one of the most active antagonists known and demonstrated to have a long receptor residence time that is thought to improve biological response in vivo. Smith *et al.* synthesised a nickel(II) coordinated *meta*-linked CB bis-macrocycle, $\mathbf{L^{11}}$**,** to target the CXCR4 receptor.[61] $[Ni_2\mathbf{L^{11}}]^{4+}$ along with $[Ni_2\mathbf{L^{10}}]^{4+}$, a previously published bis-macrocycle by McRobbie *et al.*, were tested as anti-HIV-1 agents.[63] IC_{50} values were calculated following calcium signalling assays and compared with AMD3100.[61] $[Ni_2\mathbf{L^{10}}]^{4+}$ was found to be the most effective CXCR4 antagonist with an IC_{50} value of 14 nM, this is comparable to

AMD3100. Cytotoxicity assays revealed that all the nickel complexes have a CC_{50} of more than 125 μM. Anti-HIV assays were carried out using an X4 strain which utilises the CXCR4 receptor for viral cell entry. The *para*-complex, $[Ni_2\mathbf{L^{10}}]^{4+}$, was more active than $[Ni_2\mathbf{L^{11}}]^{4+}$ but less than AMD3100, EC_{50} values of 74 nM, 398 nM and 11 nM respectively were observed showing that the nickel(II) complexes have high anti-HIV-1 activity and low cytotoxicity.

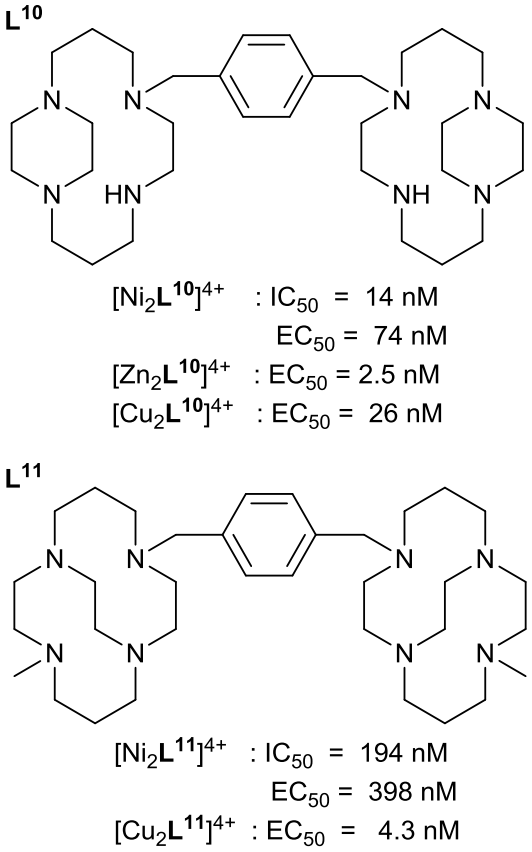

Figure 10 Chemical structures of Bis-macrocycles synthesised by Archibald and co workers[61, 63, 64]

1.1.2. The Chemokine Receptor CCR5

The CCR5 is composed of 352-amino-acid and its basic structure is consistent with other members of G protein-coupled receptor (GPCR), see Figure *11*.[65] The natural ligands of CCR5 reviewed by Mueller and Strange include the chemokines known as macrophage inflammatory protein (MIP)-1a, MIP-1b known as CCL3 and CCL4 respectively, and (RANTES) CCL5.[66] The observation that these ligands can inhibit HIV-1 entry led to the identification of CCR5 as a co-receptor for HIV-1.[67] [68] CCR5 is important because macrophage tropic (R5-) HIV-1 strains predominate during the initial step of the infection and are an important target for the pathogenesis of AIDS.[36, 69, 70] *In vitro*, cells cannot be infected by the macrophagetropic (R5-) HIV-1 strains without expression of CCR5. CCR5Δ32 homozygous individuals are resistant to R5-tropic HIV-1 infection, and appear to have delayed disease progression, suggest that CCR5 is a validated target for the treatment of HIV-1 infection.[70, 71] In addition, CCR5 and its ligand, CCL5, are found in solid tumors and blood cells. The role of CCL5 and CCR5 in cancer cell proliferation and metastasis has been reviewed by Aldinucci and Colombatti.[72]

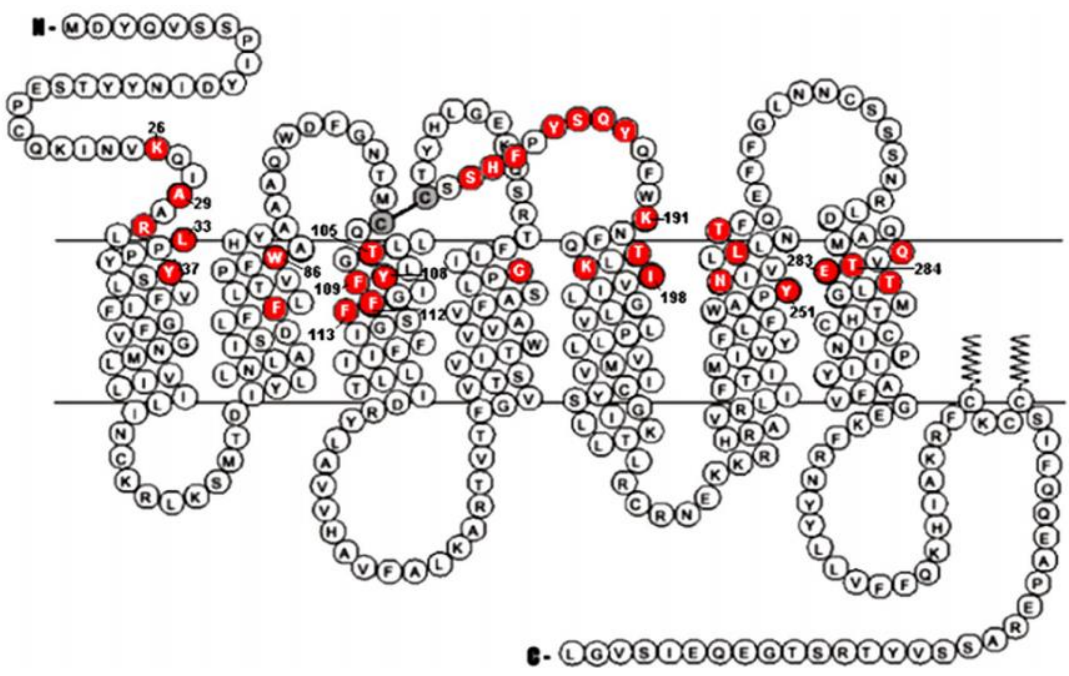

Figure 11 Snake plot representation of CCR5 (reproduced from Labrecque *et al.*, 2011)[73]

1.1.2.1. CCR5 antagonists

The CCR5 inhibitors can be divided into large-molecule inhibitors and small-molecule inhibitors. Several classes of small-molecule CCR5 inhibitors reported in recent times are under preclinical studies and clinical trials for HIV-1 including small molecules derived from natural products. Small-molecule CCR5 inhibitors can be divided into seven classes based on different structural features (benzocycloheptene derivatives, spiropiperidine derivatives, piperidino-iperidine / piperidino-piperazine derivatives, 1,4-disubstituted piperidine derivatives, tropane Derivatives, pyrrolidine derivatives and denzyloxybenzene derivatives).[70] The chemokine receptor CCR5 antagonist TAK-779 inhibited inflammatory tumour cells from response to chemokine CCL5, this finding suggests that development of appropriate chemokine receptor CCR5 antagonists could provide a novel cancer therapy.[71, 74]

1.1.2.1.1. Benzocycloheptane derivatives of CCR5 inhibitors

The first small molecular CCR5 inhibitor synthesised and reported by Takeda was TAK-779 see Figure 12, which was developed through high-throughput screening (HTS). TAK-779 is a potent and selective nonpeptide CCR5 inhibitor with an IC_{50} value of 1.4 nM in the RANTES binding assay. It inhibits the replication of macrophage (M)-tropic HIV-1 (Bal strain) in both MAGI-CCR5 cells and peripheral blood mononuclear cells (PBMCs) with EC_{50} values of 1.2 and 3.7 nM, respectively.[70] Based on the interaction mode between TAK-779 and CCR5, Liu and co-workers designed and synthesised a series of compounds incorporating some of the favourable pharmacophoric elements identified. Anti-HIV activity assays indicated that compound **L**^{12} and **L**^{13}, see Figure 12, show potent activty with IC_{50} values of 57 and 68 nM, respectively (in TZM- bl cells infected by HIV-1 Bal(R5)).[75]

Although TAK-779 showed no cytotoxicity to the host cells, the development of it was halted due to its poor oral bioavailability and the emergence of irritation at the injection site. Replacement of the quaternary ammonium moiety of TAK-779 with a polar sulfoxide moiety, a ring expansion of (6,7)- fused nuclei to (6,8)-fused

nuclei, and substitution of a 4-(2- butoxyethoxy) group for a methyl group led to an increase in bioavailability and potency. TAK-652 shown in Figure 12, shows potent anti-HIV-1 activity (IC_{90} = 0.81 nM in MOLT4/CCR5 cells), it inhibits the replication of six macrophage-tropic (CCR5-using or R5) HIV-1 clinical isolates in PBMCs (mean IC_{90} = 0.25 nM), and is well absorbed after oral administration in rats, dogs, and monkeys. TAK- 652, which was named TBR-652 when Takeda granted it to Tobira for further development in 2007, was taken into Phase II clinical trials but has not yet been licensed for clinical use.[70]

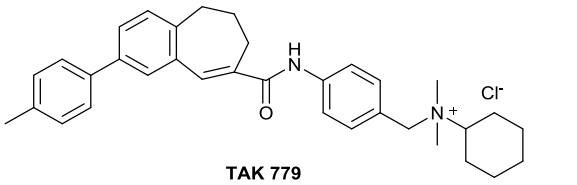

TAK 779

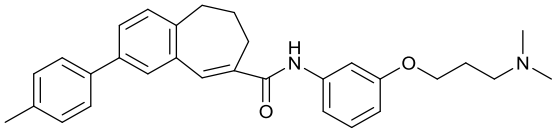

L[12]

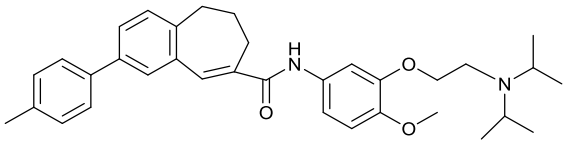

L[13]

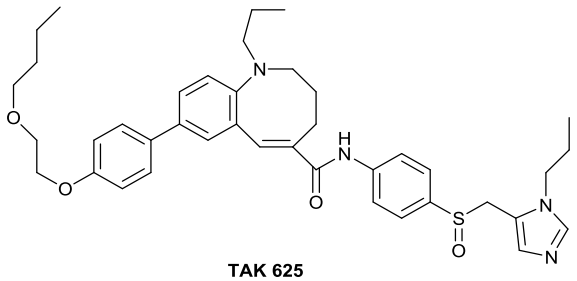

TAK 625

Figure 12 Some chemical structures of benzocycloheptane derivatives act as CCR5 inhibitors[70]

1.2. Molecular Imaging

The term molecular imaging defines the procedure of imaging a cell surface receptor or particular tissue type with a molecule,[76] in many cases allowing relevant information for the diagnosis and treatment of patients to be obtained.[77] As a result it is possible to diagnose patients that are suffering from or that may be susceptible to specific diseases and so, new chemotherapeutics have been designed to target specific disease biomarkers and by using an imaging and therapeutic pair, a treatment can be targeted to reduce impact on healthy tissue and improve therapeutic response.[78] There are different types of imaging techniques including: positron emission tomography (PET), magnetic resonance imaging (MRI), computed tomography (CT) and single-photon emission computed tomography (SPECT), all of which can be used in hospitals to scan patients non-invasively. For preclinical research, smaller, although in some cases more sensitive and higher resolution, analogues of the scanners are also used.[79] In general, diagnostic imaging is a non-invasive technique that is used to evaluate the disease states and screen the effects of treatment. The two nuclear medicine modalities of diagnostic imaging are of high interest, single photon emission computed tomography (SPECT) and positron emission tomography (PET), and are used in combination with CT scanning. These modalities offer complementary images and sensitivity in deep tissue.[80]

1.2.1. Imaging Cancer using PET

1.2.1.1. Positron Emission Tomography (PET)

Positron emission tomography (PET) is a non-invasive functional imaging technique with good resolution, high sensitivity and accurate quantification.[81] PET has the advantage of being able to detect molecular events and physiological processes in living subjects. MRI and X-ray techniques (CT) are often combined with PET and provide mostly organ structure and detailed anatomical images to complement the PET scan. PET can measure chemical changes before macroscopic anatomical signs and patient symptoms are observed.[82, 83] The most commonly used

positron emitting radiopharmaceutical isotopes are ^{11}C ($t_{1/2}$ = 20 min), ^{13}N ($t_{1/2}$ = 10 min), ^{15}O ($t_{1/2}$ = 2 min) and ^{18}F ($t_{1/2}$ = 110 min).[84]

1.2.1.1.1. Basic principles of PET

PET is a way of indirectly detecting an emission of radioactivity. A fragment of decay (a positron, ß$^+$) is emitted which travels a short distance until the positron encounters an electron. The resulting annihilation gives two γ ray photons with energy of 511 KeV which are at nearly 180^o to each other. Simulation detection *via* a circular ring of detectors around the patient gives the location of the radiolabel, see Figure 13, with each detector connected in a coincidence circuit with a detector located on the opposite side of the ring. A large amount of computing power using complex mathematical models is needed to process the raw data into quantified data to build a 3D volume for the whole body or studied organ.[85]

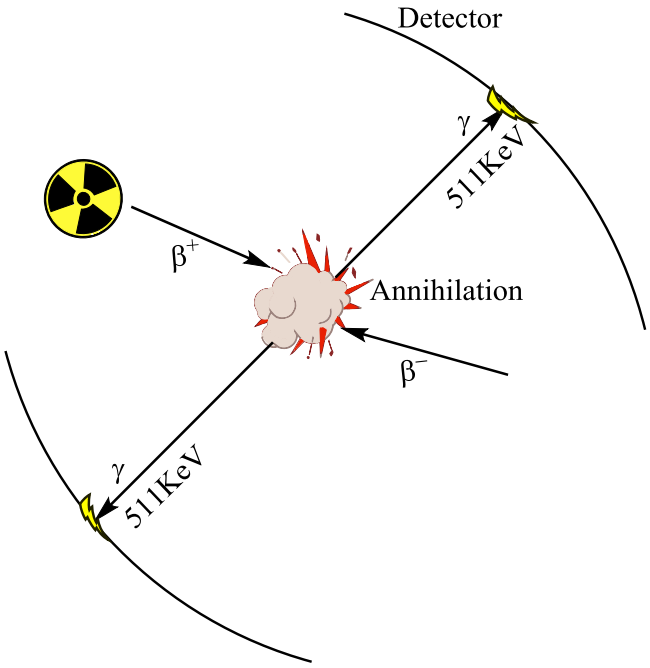

Figure 13 Schematic representation of the principle of PET[82]

1.2.1.2. Selection of radioisotope

The first thing to consider when imaging a target area is that you need a radiopharmaceutical that will interact with the body, accumulate in the desired location and produce a valuable image. A radiopharmaceutical has two components: the tracer, to target the specific area of the body, and the radioactive label, the part that emits the radiation which is used to generate an image.[86] In nuclear medicine, there are two types of radioactive labels: positron emitters and single-photon emitters. Positron emitters are used in PET, the most common are ^{18}F, ^{82}Rb, ^{11}C, ^{15}O, ^{13}N and ^{64}Cu. Single-photon emitters are those used in SPECT, the most widespread ones are ^{99m}Tc, ^{201}Tl, ^{123}I, ^{111}In and ^{67}Ga. Table 1 shows the half-lives of the commonly used isotopes. Many radioisotopes are made using a cyclotron by bombarding the appropriate isotopically pure substance with a beam of protons. An alternative method is through isotope generators the method in which ^{68}Ga and ^{99m}Tc are produced. The positron emitting isotope is extracted from a more slowly decaying parent isotope, in the case of ^{68}Ga, ^{68}Ge is used in the generator.[87]

Positron Emitters	
Isotope	**Half-Life ($t_{1/2}$)**
^{11}C	20.4 min
^{13}N	9.96 min
^{15}O	124 s
^{18}F	110 min
^{82}Rb	1.25 min
^{68}Ga	68 min
^{64}Cu	12.7 h

Single photon Emitters	
Isotope	**Half-Life ($t_{1/2}$)**
^{67}Ga	78.3 h
^{99m}Tc	6.02 h
^{111}In	2.83 d
^{201}Tl	68 min
^{123}I	13.2 h

Table 1 Half-life values of some frequently used radioisotopes

An advantage of using radioactive tracers is that they can efficiently target particular biological processes. This is useful as there are multiple processes involved in cancer progression and PET is a versatile technique when it comes to oncology. One of the applications is characterising the tumour in terms of the potential response to therapy in addition to the location of the tumour.[86, 87] PET is often used as the imaging modality of choice as it offers unparalleled sensitivity of detection coupled with the potential for quantitation.[80]

1.2.1.2.1. ^{64}Cu as Radioisotope

Copper radionuclides offer a selection of diagnostic (^{60}Cu, ^{61}Cu, ^{62}Cu, and ^{64}Cu) and therapeutic (^{64}Cu and ^{67}Cu) isotopes. The diagnostic nuclides are positron-emitters with a wide range of half-lives (10 min to 12.7 h).[88] The short half-life (9.7 min) of ^{62}Cu allows repeated doses without causing a significant radiation load on the patient.[89] The intermediate half-life (12.7 hours) of ^{64}Cu offers an opportunity for production and delivery across different sites and also allows its use with a wide range of biomolecules including antibodies.[80, 90] The low percentage of β^+ decay (18% β^+) of ^{64}Cu will have a negative effect on the resolution of the image and when the isotope decays to a gamma product by other decay pathways can cause both unnecessary radiation to patients and make image reconstruction more challenging. This can be considered as an advantage in some cases especially when it therapy is considered with a higher dose of the same isotope as it decays with 40% β^- and can therefore be used as a simultaneous diagnosis/treatment isotope. Generally the oxidation state of copper in aqueous environments is 2+ and shows Jahn-Teller distortion for the octahedral complexes, as expected for the $3d^9$ electron configuration. Copper(II) is a moderate/hard Lewis acid and prefers donors such as nitrogen.[87, 91] A common coordination number of copper is six.[92] The electron configuration of copper(I) is $3d^{10}$ and is therefore much more labile to ligand exchange, therefore increasing the kinetic inertness of the copper(II) chelate complex and avoiding reduction to copper(I) are of primary importance for *in vivo* stability.[80, 93, 94]

1.2.1.2.2. ^{68}Ga as Radioisotope

^{68}Ga a highly interesting metallic PET radioisotope for two main reasons, the relatively short half-life (68 min) and its production by radioactive decay of a parent isotope. ^{68}Ge as a parent isotope, decays to ^{68}Ga to give a daily supply of the isotope from an on-site generator.[87, 95] Recently efforts have been focused on developing a commercial system for continuous production of ^{68}Ga for laboratory use over one to two years.[96, 97] Generators for ^{68}Ga are now commercially available but expansion in the area of generator production is on-going with improvements required in the areas of HCl elution and possible metal ion impurity issues.[87] However, these restrictions do not influence the overall advantage that ^{68}Ga can be produced on site from a long term generator without the need for a cyclotron or daily isotope delivery, a characteristic that could have significant future clinical applications.[94] Current examples show that small molecules, peptides and antibody fragments are ideal biomolecules (BMs) for the development of ^{68}Ga-based PET pharmaceuticals.[80, 89, 98 89]

As mentioned above an ideal short half-life of ^{68}Ga makes it suitable for radiochemistry, being long enough to perform synthetic procedures but not so long to cause radiosynthetic handling challenges which are a concern for longer lived isotopes. High patient dose of radioactivity, one of the clinical issues, is not a major factor with a 68 minute half-life. Targeting molecules such as small molecules, peptides and antibody fragments which localise relatively quickly are exploited in the routine application of ^{68}Ga.[99, 100] The oxidation state of ^{68}Ga in aqueous solution at physiological pH is 3+ and it is generally eluted from a ^{68}Ge/^{68}Ga generator using 0.1M hydrochloric acid.[87, 101, 102] To avoid the formation of insoluble $Ga(OH)_3$ and soluble $Ga(OH)_4^-$, the majority of synthetic procedures are performed in the presence of weakly coordinating ligands such as citrate, acetate or oxalate.[103]

1.3. Aims in the design and testing of new compounds for chemokine receptor imaging

There have been many structurally different compounds tested as CXCR4 antagonists and interest in this research area has dramatically increased over recent years as the drive to develop new anti-cancer agents increases. Currently, there is not a clinically approved imaging agent or therapy specifically targeting CXCR4 expressing cancers, although there has been significant activity in this area. The CXCR4 receptor plays such an important role in the development of invasive cancers that the interest in a potent and safe CXCR4 antagonist is high. The aim of the first part of the project was to develop some new configurationally restricted macrocyclic based metal complexes and to evaluate their binding capability and potency *in vitro* using anti-CXCR4 mAb competition assays. In chapter 2 the synthesis of novel mono- bis macrocycles and their copper(II), nickel(II) and zinc(II) complexes is discussed. These new molecules were designed taking into account previous work within the research group into configurationally restricted derivatives. This new group of compounds, which included mono and bis-cyclam derivatives, were probed in order to fully characterise the impact on potency by fine tuning the metal ion coordination with the receptor. This had the potential further understanding of how configurational fixing would impact the affinity to design an optimal CXCR4 antagonist. Chapter 3 includes in vitro biological evaluation and radiolabelling of some of the macrocyclic ligands discussed in the previous chapter as CXCR4 antagonists. The second part of the project was to develop modified CCR5 antagonists with the potential for imaging applications and evaluate their interaction with the CCR5 receptor A study was then carried out to investigate radiolabel methodology using gallium-68. Finally, the work is summarised and concluded in chapter 5 and potential future work is outlined.

Chapter 2

Novel configurationally restricted transition metal cyclam complexes as CXCR4 antagonists

2. Novel configurationally restricted transition metal cyclam complexes as CXCR4 antagonists

2.1. Aim

AMD3100 is a drug that interacts with the chemokine receptor CXCR4 *via* hydrogen bonding interactions or as the metal complex *via* coordinate bonds with aspartate residues.[104] On metal complex formation, the tetraaza macrocyclic rings in AMD3100 show multiple configurations in solution.[105] Configurationally restricted macrocycles have the advantage of being present in only one configuration in solution. Configurational fixing may be a route to optimise interactions with the chemokine receptor CXCR4, with metal complexed *trans II* and *cis V* complexes showing increased receptor affinity and residence time.[62, 64] The aim of the research work reported in this chapter was to develop a method of making macrocyclic compounds which are structurally analogous to the high affinity *trans II* and *cis V* compounds but in this case, restricted to the *trans IV* configuration. A novel pathway to obtain a series of bis and monocyclam macrocyclic derivatives metal complexes (nickel(II), zinc(II) and copper(II)) that are highly rigid and fixed to only one configuration *trans IV* is presented. The development of synthetic pathways to obtain the target compounds is discussed and compared with methods previously reported in the literature.

2.2. Introduction

2.2.1. Binding to the Chemokine Receptor CXCR4

The 'free' cyclam ring has an overall 2+ charge under physiological conditions.[106] It has also been reported that protonated cyclam can form hydrogen-bond stabilised interactions with carboxylate groups.[107, 108] Gerlach *et al.* proposed that the aspartate residue 171 on the extracellular part of TM-IV (Asp^{171}) is important for cyclam and AMD3100 competition binding with CXCL12 for the CXCR4 receptor. AMD3100 binding to CXCR4 was also shown to be dependent on the aspartate residue 262 on the extracellular part of TM-VI (Asp^{262}). Cyclam could bind to Asp^{262} but with low affinity relative to Asp^{171}. When Asp^{171} is eliminated the

affinity decreases to 400 μM, which could represent the affinity of cyclam to Asp^{262}.[104] Given the fact that AMD3100 binding is dependent on both Asp^{171} and Asp^{262} and the compound can interact with carboxylate groups it is thought that one cyclam ring binds to Asp^{171} and the other to Asp^{262}.[106, 107]

2.2.2. Binding Model of Metal Complexes of AMD3100

Bis-macrocycle metal complex activity is highly reliant on the metal ion-protein complex stability. It was found by Este *et al.* that the binding affinity could be increased by ten-fold when AMD3100 was coordinated to transition metals.[58] Este *et al.* also found that there was a close correlation between anti-HIV activity and the CXCR4 interaction for the metal complexes, with the order of activity being Zn > Ni > Cu > Co > Pd. Metal ions allow not only stronger interactions at the CXCR4 receptor due to the formation of coordinate bonds (over weaker hydrogen-bonding interactions) but also a more stable interaction because of the geometry they cause the macrocycle to fold into.

To explain the enhancement coordinated to transition metals in binding, Gerlach *et al.* synthesised mono copper(II), zinc(II) and nickel(II) coordinated AMD3100 and found that they showed similar affinity to the bis-coordinated AMD3100 indicating that only one metal ion was responsible for the majority of the increase in binding affinity.[104] $[Ni_2AMD3100]^{4+}$ exhibited the highest affinity for the receptor, equivalent to the zinc(II) complex, both were higher affinity than the copper(II) complex.

It has been suggested that the increased binding affinity of transition metal complexes could arise from a direct coordination interaction from only one of the macrocyclic rings, with Asp^{262}.[104] Metal ion dependent enhancement can be eliminated by Asp^{262} mutation. These data confirm that Asp^{262} is essential for binding but the interaction with Asp^{171} is less well defined. It is possible that the receptor binding pocket may only allow the optimisation of one coordination interaction. Alternatively, hydrogen bonding interactions with the secondary amine nitrogen atoms of the metal complex may also be important. For example, a *trans III*

metal bound configuration can potentially form up to three hydrogen bonds with carboxylate oxygen atoms.[109]

2.2.3. Restricting the configurations of cyclam based complexes

The role that cyclam complexes play in medicine has been reviewed by Liang and Sadler.[110] Modification of the cyclam complexes may provide an opportunity to optimise binding to the CXCR4 receptor and prompts the need for further study. The different electronic arrangements of the metal ions will influence the binding geometries and affinities with the increase in affinity attributed to the formation of strong coordinate bonds between the metal ion and aspartate residues on CXCR4.[111]

Cyclam is known to form highly stable metal complexes with the majority of the first row transition metals, for example, its nickel(II) complex has a demetallation half-life of around 30 years in acidic media.[112, 113] The flexibility of the macrocycle means that it can adopt the most thermodynamically stable configuration for a chosen metal ion. Metal ions with an ionic radius of less than 0.75 Å afford the best fit into the macrocyclic cavity (e.g. first row transition metals).[112-114] Once the metal is bound, each nitrogen atom becomes chiral, giving rise to six possible configurations that the macrocycle can adopt see Figure 14.[7, 115] Therefore configurational fixing may be a route to optimise interactions with CXCR4. Indeed several cyclam derivatives which have shown high affinity for the CXCR4 receptor adopt a *cis V* configuration in the solid state, e.g. $[Zn_2AMD3100]^{4+}$, but they are in equilibrium in solution.

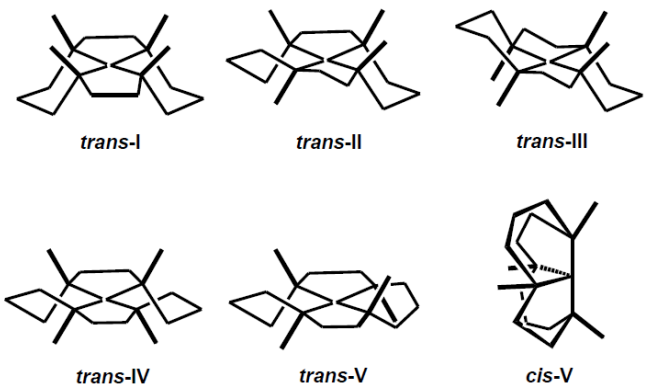

Figure 14 Metal complexes of cyclam can adopt up to six configurations (five *trans* and a folded *cis*) (Reproduced from Sadler *et al*., 2004).[110] The inclusion of an ethylene bridge can be used to restrict the compounds formed to a single configuration

The six-membered chelate rings adopt either chair or twist boat conformations and the five-membered rings are either gauche or eclipsed. *Trans V* can fold along its N-N diagonal to give the *cis V* configuration, where the six membered rings adopt the lower energy chair conformation. The configuration adopted by a complex will depend greatly on the coordination number and donor preference of the metal ion and also on the presence of any additional donor groups on the macrocyclic moiety.[115, 116]

Free-cyclam interacts with CXCR4 through three hydrogen bonds to the oxygen atoms on the carboxylate group of aspartate residues. These three bonds are not equivalent and vary from weak to strong, whereas transition metal complexes of cyclam form one hydrogen bond and one metal ion coordination bond in a docked model of the protein-metal complex interaction.[110] There is a high concentration of zinc(II) in the blood plasma, approximately 20 μM which strongly binds to cyclam, with a logK of around 15, despite the low levels of free zinc(II) ions (ca. 1 nM).[117, 118] Metal complexes with *cis V* configuration can bind to carboxylate groups on aspartate residues of CXCR4 in a mono- or bidentate manner via an equatorial bond (5 or 6 coordinate) whereas those in the *trans II* configuration bind to aspartate residues through an axial coordination site.[115, 119]

2.2.3.1. Configuration restriction:

The interaction with the chemokine receptor CXCR4 could be optimised by developing configurationally restricted macrocycles. Archibald and co-workers investigated the impacts of configurational fixing in improving biological properties.[62, 63, 120, 121] Conclusions from those investigations showed that when macrocycles were restricted to the *trans II* or *cis V* configurations, see Figure 15, biological properties were enhanced with IC_{50} values in the nanomolar range.[63, 64]

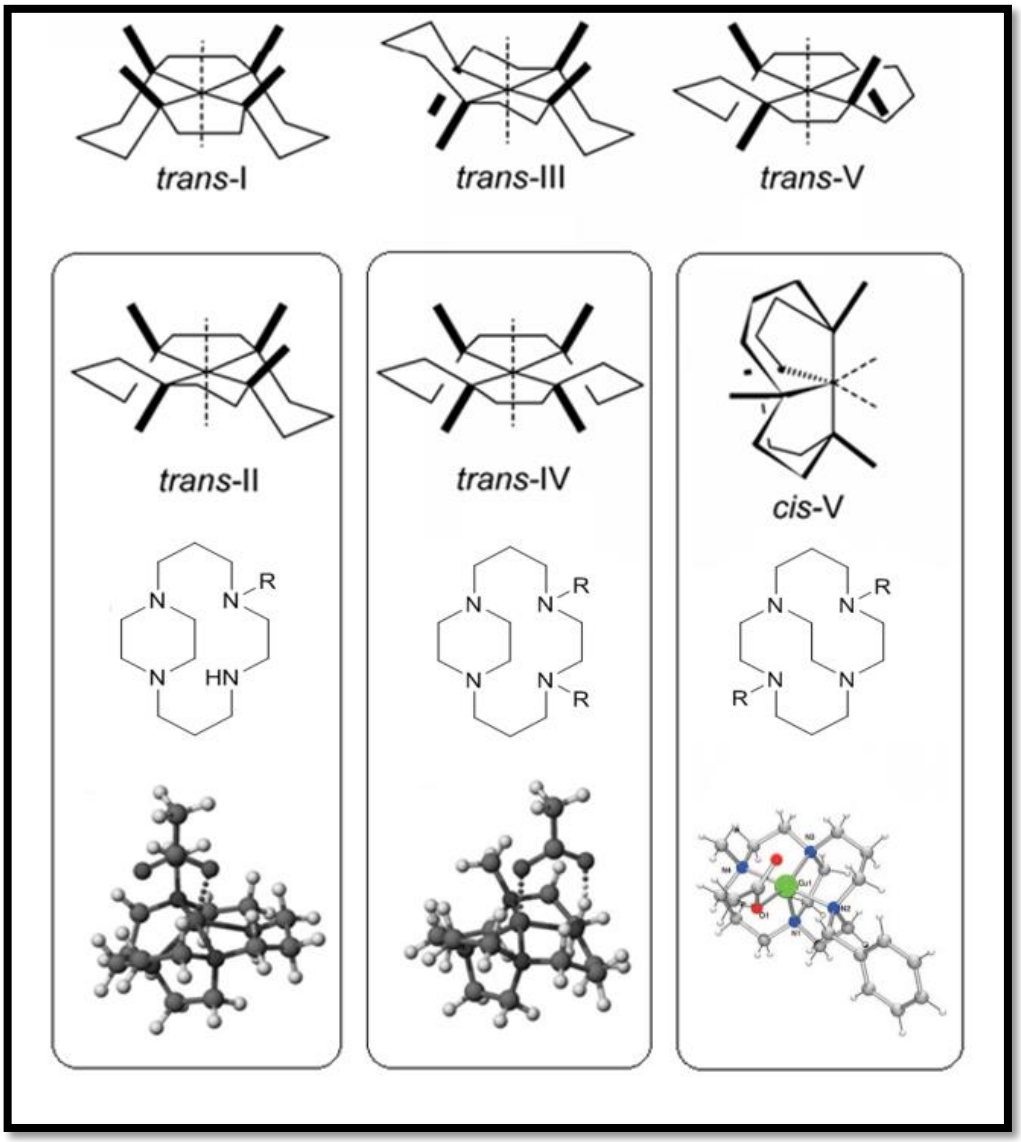

Figure 15 Configurations fixed macrocycles and their crystal structures developed by Archibald's group, *trans II* [63] and *cis V*. [64] *trans IV* was developed in this work

A *meta*-xylyl linked cross bridged bis-macrocyclic compound was synthesised by Smith *et al.* **L^{14}** see Figure 16, to target the CXCR4 receptor.[121] [Ni$_2$**L^{14}**]$^{4+}$ along with a previously published bis-macrocycle complexed with nickel(II) [Ni$_2$**L^{10}**]$^{4+}$. Anti-HIV assays were carried out using a strain which replicates through the CXCR4 receptor as opposed to CCR5.[62, 122] The ethylene bridge added between adjacent nitrogen positions to form a piperazine ring or side bridge **L^{10}** see Figure 16, sterically restricts the macrocycle to the *trans II* configuration on complex formation.[63] Calcium signalling assays were also conducted on [Ni$_2$**L^{14}**]$^{4+}$ and [Ni$_2$**L^{10}**]$^{4+}$ in conjunction with AMD3100 for comparison and from this data IC$_{50}$ values were determined. [Ni$_2$**L^{10}**]$^{4+}$ was found to be the most effective CXCR4 antagonist with an IC$_{50}$ value of 14 nM, around 2 fold less than AMD3100. The zinc complex, [Zn$_2$**L^{10}**]$^{4+}$, has a lower IC$_{50}$ value than [Zn$_2$AMD3100]$^{4+}$ and AMD3100. Cytotoxicity assays revealed that all the Ni complexes had a CC$_{50}$ of more than 125 μM hence are non-toxic at concentration where they are active.

Further work from our group by Khan *et al.* involved the synthesis and biological evaluation of **L^{11}** see Figure 16. **L^{11}** is forced into a folded arrangement *cis V* by the ethylene bridge between non-adjacent nitrogens, and the ring nitrogens occupy three of the equatorial sites and an axial site. The study showed that rigidify the macrocycle structure so that the copper(II) complex would favour metal coordination bonds with oxygen atoms from the carboxylate groups on the aspartate residue. The cross-bridged Cu(II) complex showed 2.5 fold greater activity than AMD3100 when tested on HIV-1 infected MT-4 cells, the EC$_{50}$ generated for [Cu$_2$**L^{11}**]$^{4+}$ was 4.3 nM. It was concluded that the increase in activity was originated from the coordinate bonds with the Cu(II) complex, as opposite to weaker hydrogen bonds observed in AMD3100. However, this increase also relates to the configuration and coordination sphere since simply complexing AMD3100 to copper(II) gives a decrease in the biological activity.[123]

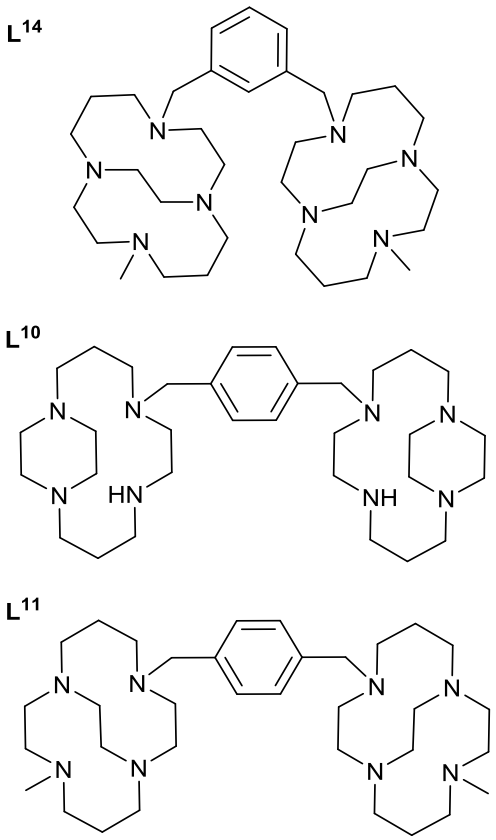

Figure 16 Chemical structures of SB bis-macrocycle *trans II* **L**[10], and CB meta bis-macrocycles **L**[14] and CB bis-macrocycle *Cis V* **L**[11]

2.2.4. Synthetic methodologies to form *trans IV* macrocyclic complexes

The importance of the configuration of the macrocyclic rings in relation to receptor binding is clear. Configurationally restricted monomacrocyles and bis-macrocycles are more potent in binding to CXCR4 when compared to AMD3100 as they only present one shape to the binding site. In addition, the ability of the macrocycle to retain its metal ion will be important for *in vivo* studies as demetallation could have serious side effects due to the toxicity of the metal ion or loss of a radioisotope.[111] Therefore, complexes possessing increased kinetic stability are highly desirable for *in vivo* applications. Based on X-ray crystallographic results reported by Kaden *et al.* and the previous work from the Archibald group in characterising configurationally restricted cyclam complexes it is clear that the degree of substitutions of at the N-atoms of the macrocycle influences the structure of the metal complexes.[124] These data indicate that if all of the N-atoms of the macrocycle have been substituted the configuration of the macrocycle will be restricted to the formation of the *trans IV* configuration on complex formation with first row transition metal ions. The N-tetramethyl derivative of the cyclam macrocycle (TMC) has been demonstrated to form the *trans I* configuration. A mixture of square planar and pentacoordinate geometries have been observed for Ni^{2+} complexes with this macrocycle.[125] However, as the substituents at the N-atoms become more sterically demanding, the pentacoordinate geometry cannot be formed anymore and only distorted square planar complexes are observed. To control the structure of macrocyclic ligand an additional bridge between two N-atoms can be added, this is called a reinforced macrocycle.[126] Configurationally restricted monomacrocylic and bis-macrocyclic ligands have been used in this work and are discussed. An introduction to the chemistry which has been developed in order to prepare configurationally rigid transition metal complexes is presented herein.

2.3. Synthetic Discussion

Novel copper(II), zinc(II) and nickel(II) mono and bis side bridged macrocycle that are restricted to the *trans IV* configuration that have been synthesised are shown below, see Figure 17, followed by the synthetic pathways used to obtain them.

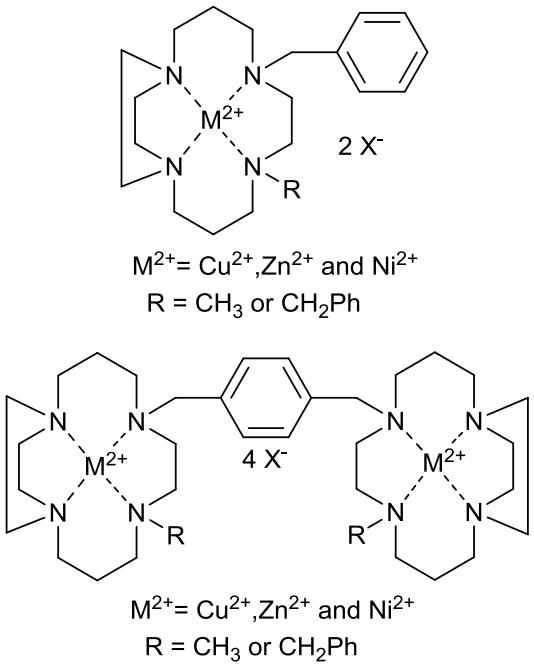

Figure 17 Metal containing mono and bis mono macrocycle synthesised in this work

2.3.1. Bis-aminal precursors

Glyoxal cyclam, **2**, was synthesised following an adapted method based on the protocol published by Le Baccon *et al.* This was repeated on multiple occasions and all reactions gave excellent yields (in excess of 80%) which are comparable to the reported yield for this compound.[127] The reaction was cooled to −10ºC and glyoxal was added slowly to avoid polymerisation. The crude product was purified by extracting into diethyl ether to separate it from any polymeric material and then thoroughly dried to remove water produced during the reaction see Scheme 1. The rigid bis-aminal bridging moiety fixes the geometry of the macrocycle with the aminal protons located *cis* to each other. **2** was characterised by NMR, in which the

characteristic aminal peaks were present in the ^{1}H and ^{13}C NMR spectra, and the molecular ion was detected by mass spectrometry.

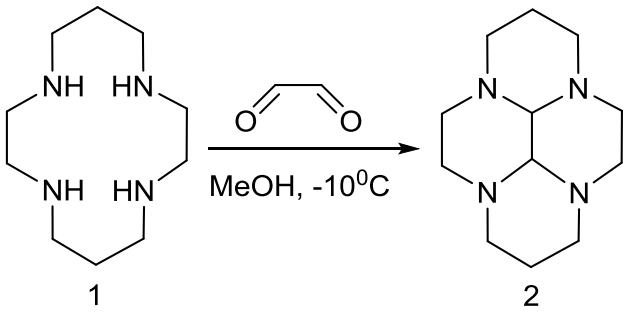

Scheme 1 Synthetic pathway to bridged cyclam

On first inspection of the structure of **2**, it would seem that all four nitrogen atoms are in the same environment and should react in similar fashion. However, this is not the case because of the rigidified nature of the macrocycle, the lone pairs on the nitrogen atoms fall into two chemically different groups. The first is where the lone pair is pointing directly into the macrocyclic cleft see Figure 18.

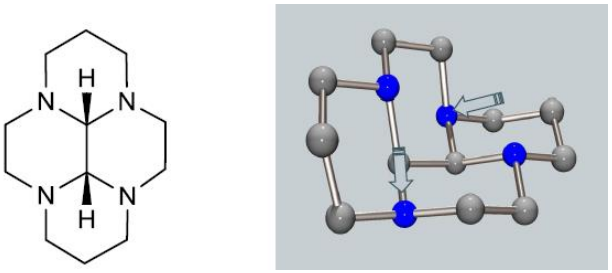

Figure 18 Molecular structure of bridged cyclam showing a cis configuration (left). Ball and stick representation, of the X-ray crystal structure of **2** indicating the presence of two exo and two endo lone pairs (right). Grey = carbon atoms, blue = nitrogen atoms.[128]

The incorporation of an ethylene bridge into the macrocycle to form a bisaminal species is important because it mediates the reactivity of the amine groups. This is more clearly seen in the structures of glyoxal cyclam reported by Gluzinski *et al.*[128] It can be seen that the rigid bis-aminal bridge creates a chair conformation

causing two of the nitrogens to point onto the fold of the macrocycle, termed *endo* nitrogens, and two to point outwards, termed *exo* nitrogens. The *endo* nitrogens are sterically hindered and therefore do not act as nucleophiles, however the *exo* nitrogens are available, resulting in reaction of groups solely on the non-adjacent nitrogen atoms.

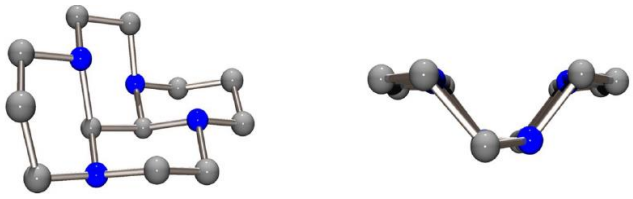

Figure 19 Representations of the X-ray crystal structure of **2**. Grey balls represent carbon atoms and blue balls nitrogen atoms, hydrogen atoms have been omitted for clarity.[128]

2.3.2. Alkylation

The first method for adding pendant arms was established by Kolinski *et al.* in 1995, Archibald and co-workers have led the research into incorporation of novel pendant arms.[62, 129-133] Previous work within our group includes the synthesis of a number of mono-ring structures with an aniline pendant group.[129] However, having the primary amine directly attached to the aromatic ring created problems in subsequent reactions that were attributed to the nitrogen lone pair being delocalised into the aromatic ring reducing its reactivity.

In this work, alkylation with (bromomethyl)benzene in a 4:1 ratio and para-xylene dibromide in a 1:2 ratio were then carried out in either dry acetonitrile or dry THF to form **3** and **4** respectively, see Scheme 2, the extra carbon between the phenyl ring and primary amine will prevent delocalisation. The choice between these two solvents has no significant impact on the reaction yield as long as they have been freshly dried. Addition of a pendant arm to give **3** and **4** was performed following a modified method based on the protocol reported by Le Baccon *et al.*[130] Whilst Le Baccon *et al.* continued the reaction for 10 days attaining a yield of 87% the yield was not impeded by work-up after 3 days to give an 88% yield for **4** in

THF. The bis-ammonium salt **3** and **4**, precipitate out of solution and can be collected by filtration and washed with diethyl ether.[55]

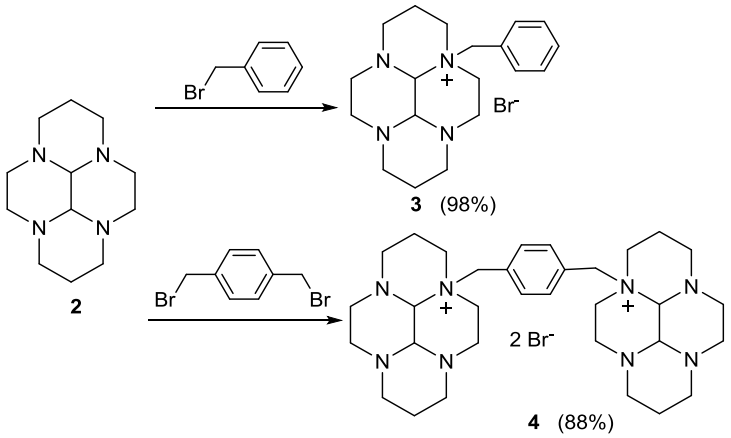

Scheme 2 Synthetic pathways of alkylation

All compounds were produced in good yields and fully characterised. Compounds **3** and **4** gave clean NMR spectra showing the expected peaks. CHN and MS analysis confirmed the purity of these compounds.

2.3.3. Reductive ring cleavage

Compounds **3** and **4** can be reduced following modified procedures based on Kolinski's route that was used with mono-macrocyclic compounds.[134] The success of this reaction depends on the quality and the amount of hydride reducing agent employed. Optimum results were obtained when twenty molar equivalents of sodium borohydride were used per macrocycle, see Scheme 3.

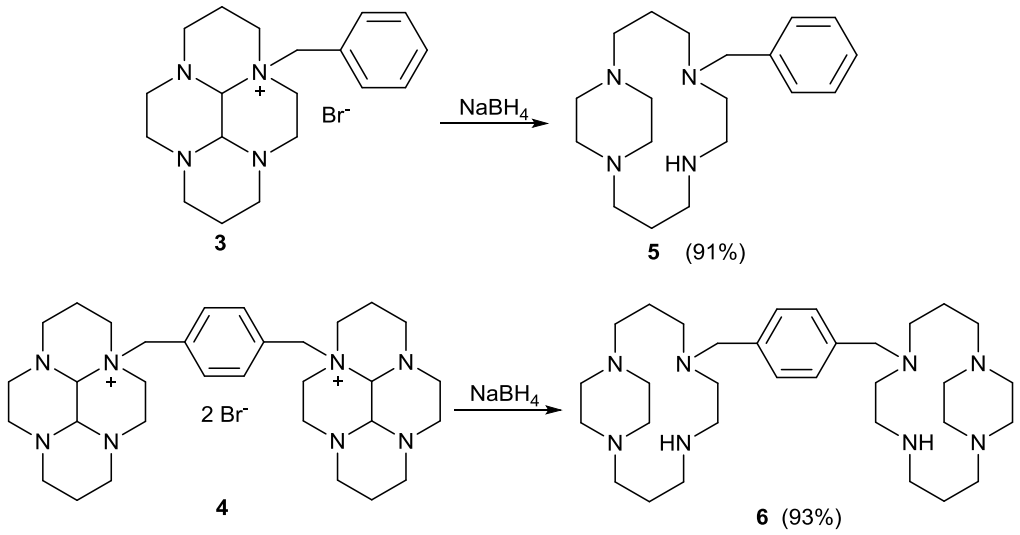

Scheme 3 Synthetic pathway to reduction of macrocycle quaternary salts

A mechanism for the reduction has been proposed previously and is shown in Figure 20.[134] Cleavage of the quaternary nitrogen to carbon bond results in the formation of a highly unstable tricyclic aminal, **L**[15] see Figure 20, which is either reductively cleaved or hydrolysed on aqueous work up. An extraction in the work-up utilises a strongly basic (pH 14) aqueous layer to deprotonate the macrocycle and facilitate extraction into organic solvent. Overall, very good yields were obtained (91% and 93%) and NMR spectra showed the expected peaks. Mass spectrometry confirmed the purity of desired products with peak at 317 for the molecular ion of **5** and 554 for molecular ion of **6**.

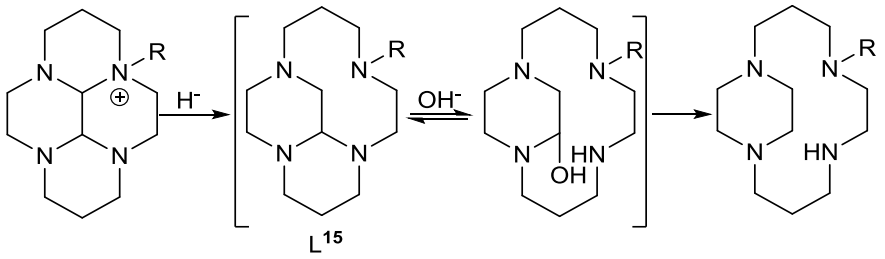

Figure 20 Mechanism of hydride reduction

2.3.4. Configurationally restricted complexes

Copper(II), nickel(II) and zinc(II) were the transition metal ions of choice since previous studies have shown improved binding affinities for CXCR4 when macrocyclic antagonists have been complexed with these metals. A series of nickel(II) salts, copper(II) acetate monohydrate, and zinc(II) acetate hexahydrate were used to make a novel series of metal complexes, see Figure 17. Standard preparation procedures were followed for all of the complexation reactions.[135, 136] All complexes were purified using size exclusion chromatography (Sephadex LH20). Complexes were characterised by mass spectrometry, elemental analysis and, where applicable, UV-vis spectroscopy.

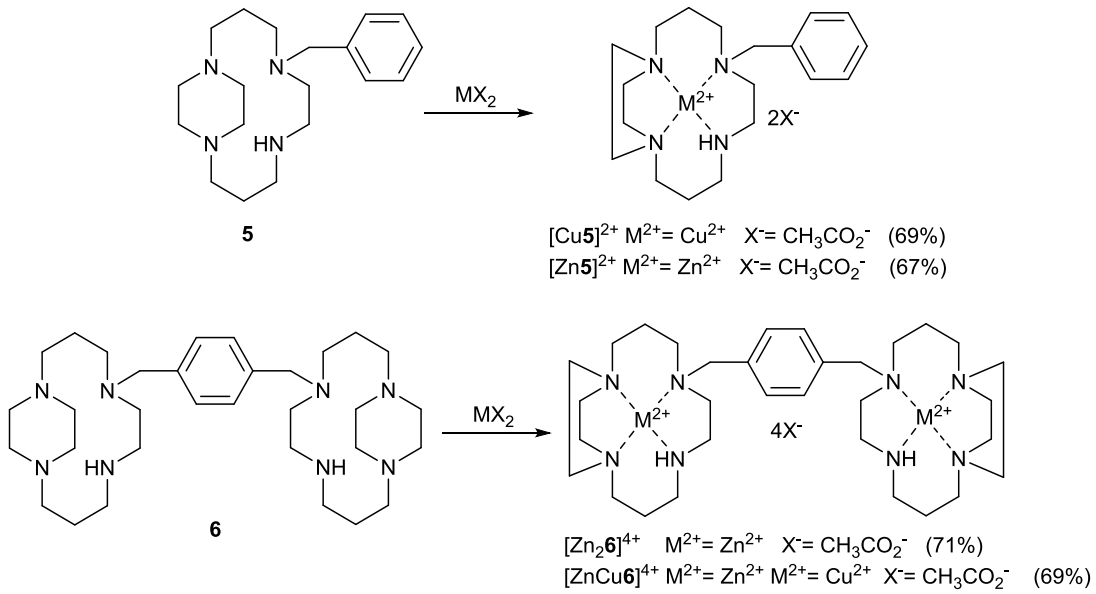

Scheme 4 Synthetic pathway to obtain Cu and Zn metal complexes of mono and novel mixed metal [ZnCu**6**]$^{4+}$ *trans II* bis macrocycle

Copper(II) is a stable oxidation state although the reduction to copper(I) can be accessible in biological systems. Preferred coordination numbers with the tetraazamacrocycles are likely to be five or six coordinate with either one or two additional ligands from the solvent or counter anions. The existence of copper radioisotopes also make it a metal of interest since incorporation of such isotopes could be used to form structurally identical diagnostic probes.

The $[Zn\mathbf{5}]^{2+}$ and $[Zn_2\mathbf{6}]^{4+}$, see Scheme 4, are of interest as their properties will demonstrate the impact of variation in the metal centre. It could argued that the choice of the anion (in the metal salt) is not important as it is likely to exchange when the compound is administered *in vivo*. However, it is worth noting whether there is an impact of the variation of anion appropriate reaction conditions were determined and elemental analysis data for each of the four metal complexes described shows successful insertion of the metal ion into the cavity to form pure compounds, solvent molecules (water and methanol (MeOH)) were noted but this is not unexpected as solvent molecules are usually observed in the unit cell of X-ray structures of such compounds. Mass spectrometry analysis confirmed that the metal ion was coordinated to the chelator. Nickel(II) displays some interesting coordination properties. It can either form diamagnetic square planar complexes or expand its coordination sphere to octahedral through incorporation of additional donors, with the dark brown colour observed indicating a higher coordination number.

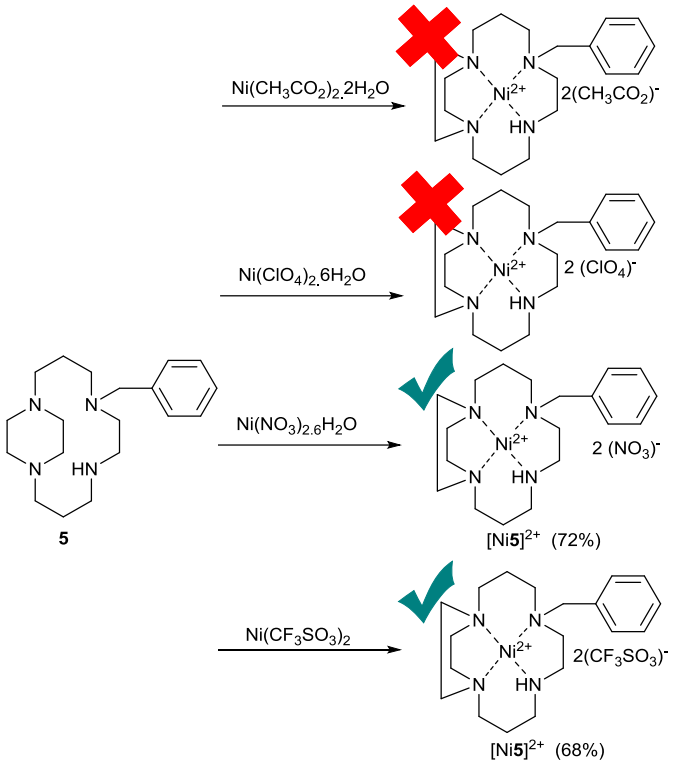

Scheme 5 Complexation attempts of 5 using different Ni(II) salts

A variety of different counter anions were used to form $[Ni\mathbf{5}]^{2+}$ derivatives including acetate, perchlorate, trifluoromethanesulfonate and nitrate as shown in Scheme 5. There were two main reasons for this approach: firstly, obtaining the square planer nickel(II) macrocyclic complexes as precursors, and secondly, giving a variety of compounds to be tested in reactions where solubility and anion may influence the properties. The acetate and perchlorate salts did not give the desired compound in sufficient purity. When nickel(II) trifluoromethanesulfonate, and nitrate were used it formed the desired products of $[Ni\mathbf{5}]^{2+}$. The bright orange colour of the nickel(II) nitrate complex $[Ni\mathbf{5}]^{2+}$ (λ_{max} = *ca.* 480 nm), and all of those formed with chelators **5** indicates a square planar coordination environment.

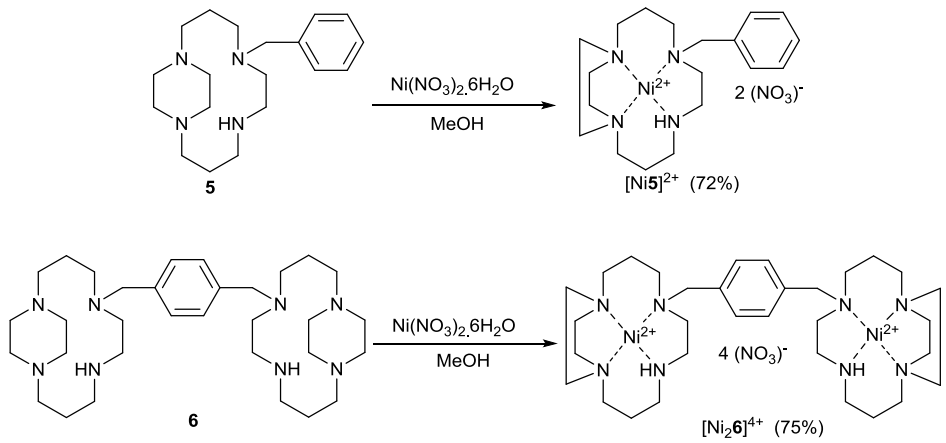

Scheme 6 Synthetic pathway to $[Ni\mathbf{5}]^{2+}$ and $[Ni_2\mathbf{6}]^{4+}$

2.4. Alkylation using nickel(II) macrocyclic complex precursors

2.4.1. Novel configurationally restricted metal mono- macrocyclic chelators

Whilst searching for synthetic procedures for the alkylation of secondary amines, a potential route that could be modified for the preparation of $[Ni\mathbf{7}]^{2+}$ see Scheme 1, was found in the literature. Kaden and co-workers, following a modification of a reaction initially reported by Barefield *et al*., prepared the side-bridged macrocycle, $\mathbf{L^{17}}$, in a three step process via the nickel(II) complex see Figure 21. [124, 137] The initial nickel(II) complexation of $\mathbf{L^{16}}$ proceeds in reasonable yield (65%), resulting in a complex which can be deprotonated by nBuLi in dry DMSO solvent. The orange solution undergoes a colour change to blue after the addition of nBuLi. Addition of methyl iodide results in the reappearance of the orange solution which was then transferred into a saturated ethanolic solution of ammonium hexafluorophosphate to precipitate the product as an orange solid. After recrystallisation, the reported yield of $\mathbf{L^{17}}$ is 62%.

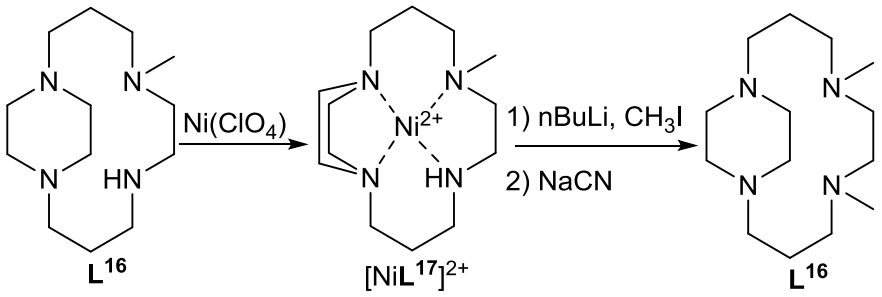

Figure 21 Kaden's synthesis of **L**^{21}

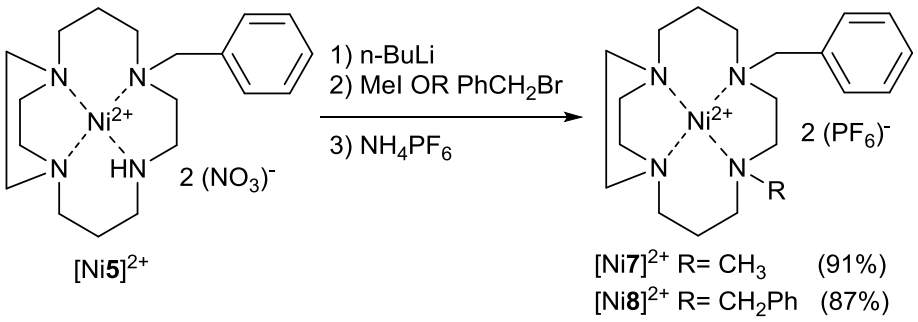

Scheme 7 Synthetic pathway to tetra substituted [Ni**7**]$^{2+}$ and [Ni**8**]$^{2+}$

2.4.2. Novel configurationally restricted metal bis-macrocyclic

In this work, a modified version of Kaden's method was followed, see Scheme 8. The nickel(II) complex of $[Ni_2\mathbf{8}]^{4+}$ was prepared by refluxing the ligand with a slight excess of nickel(II) nitrate hexahydrate (ratio 1:1.1) in methanol overnight. After determining the optimum conditions for the complexation with nickelII) using the mono-macrocyclic compounds the same procedures were followed to obtain the new nickel(II) bis(macrocyclic) complexes with an increase of the ratio of metal salt to chelator (2.2:1)as we have two cavities to be complexed. The crude orange solid was purified via size exclusion chromatography to remove the excess metal salt. The yields for the complexation reaction were excellent (72-75%). The nickel(II) metal centre would be expected to coordinate to each of the four nitrogen atoms of the macrocyclic ring in a square planar geometry. This would have the effect of disrupting the hydrogen bonding network in the macrocycle which has been reported by Kotek *et al*. This should result in the secondary amine position becoming the most reactive site and it could, therefore, be deprotonated by a strong base, such as n-butyl lithium n-BuLi. The addition of n-BuLi to the orange DMSO solution gave the expected blue solution indicating the formation of the amido complex. Subsequent addition of excess methyl iodide or bromomethyl benzene to the blue solution results in the formation of an orange solution. The hexafluorophosphate salt of the methyl and benzyl alkylated derivatives $[Ni\mathbf{7}]^{2+}$, $[Ni\mathbf{8}]^{2+}$,$[Ni_2\mathbf{9}]^{4+}$ and, $[Ni_2\mathbf{10}]^{4+}$ have been obtained in excellent yield (~88%) by dripping the DMSO solution into a saturated solution of ammonium hexafluorophosphate in ethanol and filtering off the resulting orange precipitate.

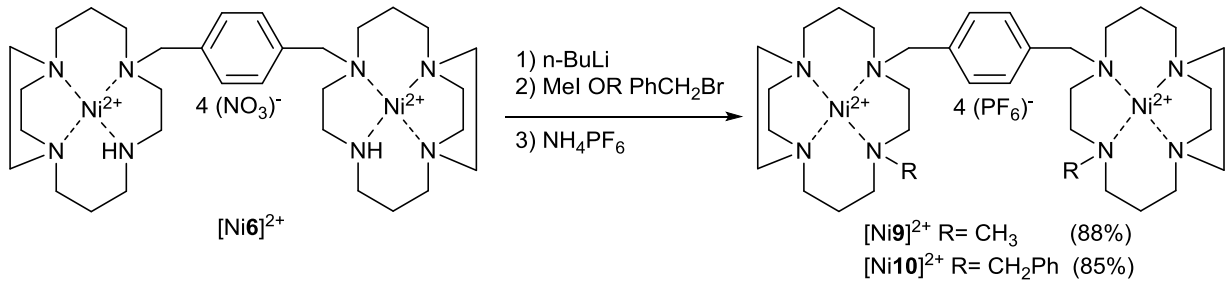

Scheme 8 Proposed synthetic route to form $[Ni_2\mathbf{9}]^{4+}$ $[Ni_2\mathbf{10}]^{4+}$

2.4.3. Demetallation using sodium cyanide

The decomposition of nickel(II) macrocyclic complexes with sodium cyanide is well known.[138] These reactions have traditionally been carried out in aqueous conditions. The choice of reaction solvent is dictated by the solubility of the starting material, $[Ni\mathbf{7}]^{2+}$, $[Ni\mathbf{8}]^{2+}$, $[Ni_2\mathbf{9}]^{4+}$ and $[Ni_2\mathbf{10}]^{4+}$ which have been found to only be highly soluble in acetonitrile. It was originally thought that the reaction could be carried out in this solvent. However, sodium cyanide is not sufficiently soluble in acetonitrile, hence the appropriate conditions were found to be heating at reflux for two hours in acetonitrile containing ca. 5% water. This resulted in the isolation of the novel bis(alkylated) side-bridged macrocyle ligands **7, 8 , 9** and **10,** see Scheme 9, in yields of *ca.* 90% yield.

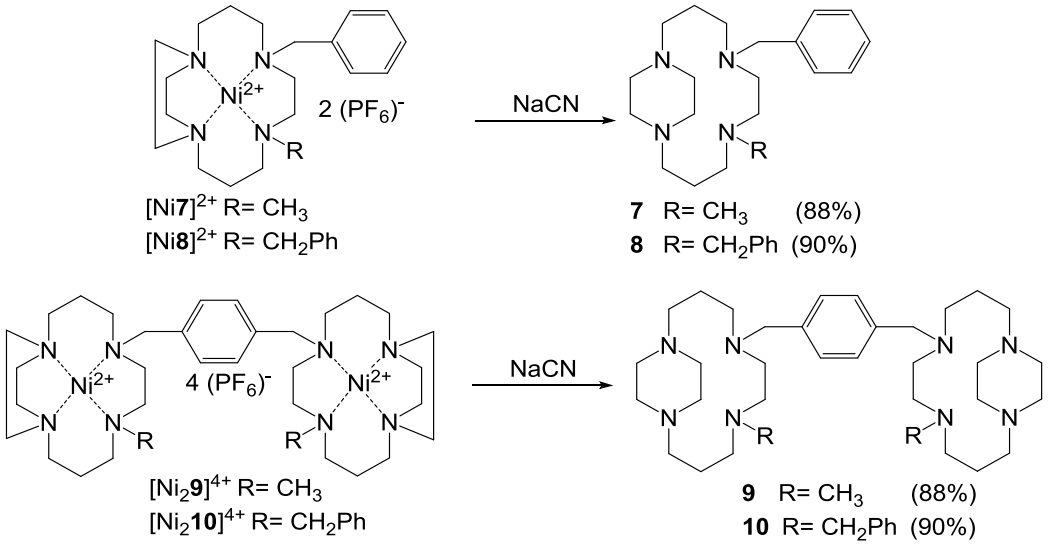

Scheme 9 Synthetic pathway of demetallation using sodium cyanide to form the novel free chelator

The ^{1}H NMR spectra of **7, 8, 9** and **10** gave peaks in the expected regions. For compound **7** the appearance of a singlet peak at 1.81 indicated the replacement of the amino hydrogen in compound **5** with a methyl group. For compound **8** the aromatic region shows the equivalent of 10 protons in the integration trace indicating that the benzyl group has replaced the amino hydrogen in compound **5**. The spectrum

of compound **9** showed a singlet peak at 2.01 which integrates to be equal to 6 protons, corresponding to the two methyl groups. Finally, for compound **10** an integration of 14 protons in the aromatic region in NMR spectra confirmed the presence of the two benzyl groups. Mass spectrometry analysis for the chelators confirmed the purity with a single molecular ion peak at 331, 406, 583 and 735 for compounds **7, 8, 9** and **10** respectively. CHN analysis confirmed the purity of the novel compounds.

Metal complexes could then be formed using copper(II) acetate, zinc(II) acetate and nickel(II) nitrate to form the novel configurationally restricted metal trans IV side bridged mono- and bis-cyclam derivatives shown in Scheme 10.

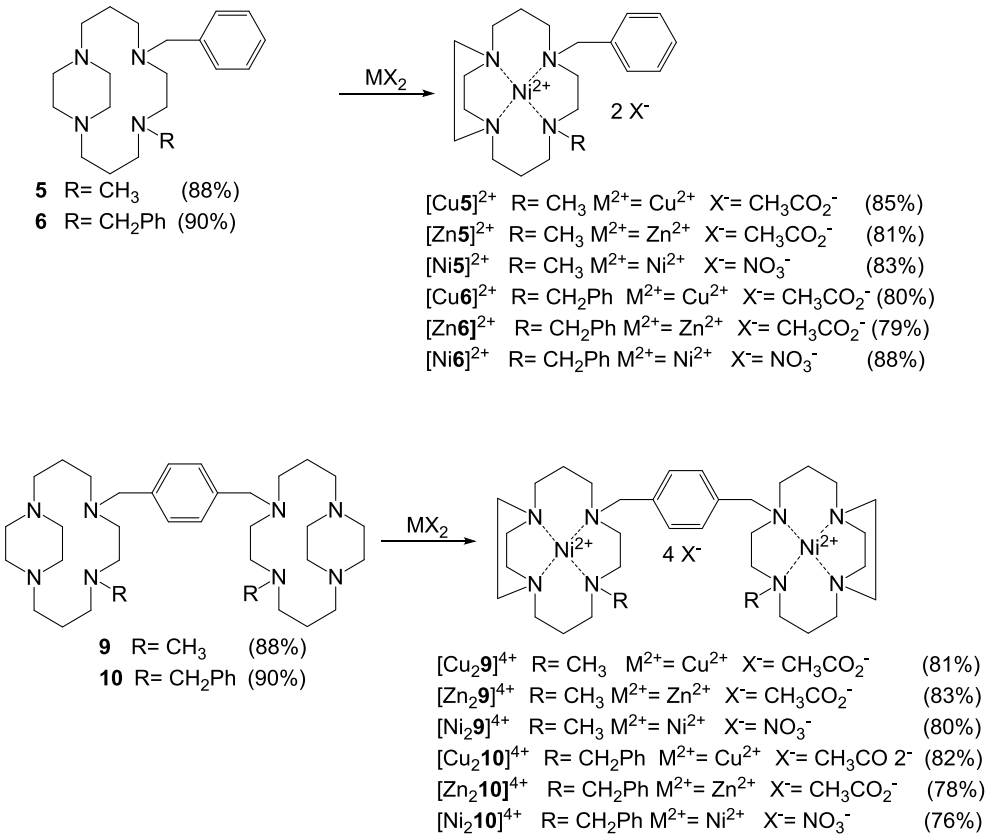

Scheme 10 Synthetic pathway to obtain novel *trans IV* metal complexes

2.5. Conclusion

Previous investigation of the structure-binding affinity relationship of a range of macrocyclic based complexes has shown and confirmed a number of key structural features that are important in trying to design a high affinity CXCR4 antagonist. In support of previous studies within Archibald's group inclusion of a metal ion is crucial in increasing the affinity of the complex. This chapter outlines the successful synthesis of a novel collection of configurationally restricted N-functionalised mono and bis-macrocycles that can potentially be used in imaging applications. Cyclam can adopt one of the six possible configuration when it is complexed to a first row transition metal ion. Configurational restriction is important because it ensures the macrocycle binds to the CXCR4 receptor target in a single configuration so the most biologically active configuration can be used rather than relying on an equilibrium of multiple configurations as seen with cyclam metal complexes.[110] Zinc(II), copper(II) and nickel(II) complexes of novel configurationally restricted mono and bismacrocycles have been synthesised and the biological profile of these complexes will be discussed in chapter 3. The synthetic route to a mono and bis-macrocyclic compound containing a side bridge that are thought to be restricted to only one configuration *trans IV* has been developed. This route has proven to be reproducible yielding the compounds in good overall yield.

Chapter 3

Imaging of the Chemokine Receptor CXCR4

3. Imaging of the Chemokine Receptor CXCR4

3.1. Aim

The aim of research presented in this chapter was to develop novel ^{64}Cu labelled CXCR4 antagonists for use as positron emission tomography (PET) imaging agents. In chapter 2, mono and bis-macrocyclic ligands containing an ethylene bridge between adjacent nitrogen atoms (side bridged) were synthesised. These transition metal complexes were configurationally restricted to either *trans II* or *trans IV*, see Figure 22. The initial aim of the work reported in this chapter is to determine how configuration (*trans II* vs. *trans IV*) effects binding to the CXCR4 receptor. After biological stratification of antagonists, the best candidate can then be radiolabelled with copper-64 to form a novel configurationally restricted CXCR4 targeting PET imaging agent.

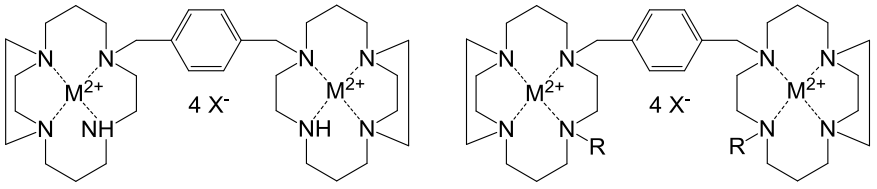

Trans II
M^{2+}= $Cu^{2+}$and Zn^{2+}

TransIV
M^{2+}= Cu^{2+}, Zn^{2+} and Ni^{2+}
R= CH_3 or $CH_2C_6H_5$

Figure 22 Chemical structure of CXCR4 binding *trans II* and *trans IV* macrocyclic antagonists

3.2. Introduction

3.2.1. PET imaging of CXCR4

Numerous physiological and pathological processes related to cell homing and migration, are found to be mediated by chemokines.[20, 139] The chemokine CXCL12 (stromal cell-derived-1 SDF-1) binds to the G-protein coupled receptor CXCR4 which through multiple pathways, leads to chemotaxis, enhanced

intracellular calcium, cell adhesion, survival and proliferation.[140, 141] CXCR4 has gained increasing attention over the last decade since it was initially discovered to have involvement in HIV entry and leukocyte trafficking.[142, 143] More recently, CXCR4 was found to be up-regulated in a wide variety of cancers.[20, 140] CXCR4 expression was found in 12% of early breast cancer samples analysed[144] and in 92% of ductal carcinoma in situ (DCIS) samples.[145] For non-small cell lung cancer (NSCLC)[146], gastric cancer[147] and prostate cancer more than 95% of the samples analysed showed CXCR4 expression.[148] In addition, the correlation between CXCR4 overexpression in tumour and poor survival, tumour aggressiveness, increased risk of metastasis and high probability of recurrence has been demonstrated.[149, 150]

Due to the important involvement of CXCR4 in oncology, a number of CXCR4 antagonists have been developed (see Chapter 1). Recently, these CXCR4 targeting moieties have been used to deliver multipurpose platforms for the synthesis of imaging agents using to diagnose primary tumours or a highly aggressive subpopulation of tumour cells. Important challenges must be met when a new CXCR4 imaging agent is developed and evaluated. First, the compound has to bind with high affinity to the CXCR4 receptor. The receptor affinity of a compound is described by the inhibitory concentration, which blocks 50% of binding (IC_{50}).[151, 152] This is determined *in vitro* using cell lines with intrinsic CXCR4 expression or cell lines that overexpress the CXCR4 receptor after transfection with the CXCR4 gene. Secondly, the antagonist is required to be highly specific, allowing differentiation between CXCR4 positive and negative cells, which can also be determined *in vitro*.[153] A primary concern is the possibility of binding to the closely related chemokine receptor CXCR7.[154] Thirdly, for clinical translation, the ideal imaging agent should have high tumour uptake, which can be evaluated *in vivo* in mouse tumour models.[153] For toxicity reasons, non-specific retention in vital organs should be minimal. This may be especially important for related studies wherein high doses of radiotoxic radionuclides are injected to give an analogous therapeutic response.[155] Finally, as CXCR4 is also naturally expressed in immune related cells residing in tissues (e.g. lymph nodes), background signal in these tissues must be taken into consideration when evaluating both biodistribution and *in vivo* imaging results.[156] As the uptake of an imaging agent is also influenced by the tumour morphology and its

vascular physiology, a transplantation-based model will generally provide a closer resemblance to a cancer patient than a cell line-based model but this is considerably more complex.

The groups of investigated CXCR4 imaging agents are derivatives of T140, FC131 and AMD3100. The natural protein signalling partners of CXCR4, CXCL12 can be used as an imaging agent. Nimmagadda *et al.* demonstrate that the CXCR4 antibody clone (12G5) binds the extracellular loop similar to CXCL12, studied on glioblastoma tumour model using radiolabelled with ^{125}I.[157] The PET image data showed an accumulation of ^{125}I-12G5 in the tumours. Tamamura *et al.* identified a potent CXCR4 antagonist, T140 (fourteen residue peptide with a disulphide bridge) showing that Arg^{2}, L-3-(2-naphthyl)alanine (Nal)^{3}, Tyr^{5}, and Arg^{14} in T140 are important to bind the CXCR4 receptor.[158] It is also reported thatT140 is unstable in serum.[24]

Fujii *et al.* synthesised a cyclic pentapeptide library comprising the smaller T140 analogues.[159] The peptide, cyclo(-Nal1-Gly2-D-Tyr3-Arg4-Arg5-), known as, FC131, showed the highest affinity with CXCR4. FC131 acts as inverse agonist of CXCR4 and does not bind to CXCR7, similar to T140.[160] FC131 has been radiolabelled with ^{123}I, ^{124}I and ^{125}I on D-Tyr^{3} for PET imaging.[161] Iodinated FC131 still binds with high affinity to CXCR4, K_D = 0.4 nM, (where K_D is the dissociation constant) and is relatively lipophilic for an imaging agent (partition coefficient logP = −0.35 as determined with octanol/PBS).[161] Despite the fact that tumour visualisation was possible with radioiodinated FC131, the compound was too lipophilic for *in vivo* applications. To decrease lipophilicity, Demmer *et al.* used the more hydrophilic label DOTA as an imaging chelator on FC131.[162] Arg^{4} was chosen as an attachment point and was replaced by N-a-methylated D-Orn to allow functionalisation. When N-a-methylated D-Orn^{4} was functionalised with DOTA (CPCR4-2, Pentixafor) see Figure 24, the binding affinity was further decreased to 150 nM. Indium (44 nM) and gallium (5 nM) complexation significantly restored the CXCR4 affinity[162] confirming the carboxylates possesses a negative impact on the binding affinity. The value of log P for ^{68}Ga-CPCR4-2 is −2.90, more than two orders of magnitude lower than ^{125}I-FC131.

Subsequently, Gourni *et al.* performed supplementary biodistribution and competition studies *in vivo*, dynamic PET studies, and studies on the metabolic stability and plasma protein binding to ^{68}Ga-CPCR4-2 in nude mice xenografted with metastasising OH1 human small cell lung cancer.[163] They found that, ^{68}Ga-CPCR4-2 shows great CXCR4 binding affinity (IC_{50} = 5±0.72 nM).[163] ^{68}Ga-CPCR4-2 also, showed low uptake in non-tumour tissue and particularly low kidney accumulation despite predominant renal excretion, leading to high-contrast delineation of tumours in small-animal PET studies.[163]

Recently, the first clinical application of ^{68}Ga- CPCR4-2-PET providing images with good specificity and contrast was reported by Wester *et al.* This imaging technology for quantitative assessment of CXCR4 expression could be used to further elucidate the role of the CXCR4/CXCL12 ligand interaction in the pathogenesis and treatment of cancer, cardiovascular diseases and autoimmune and inflammatory disorders, see Figure 23.[164] The first human evaluation of *in vivo* CXCR4 imaging in cancer of the lymphoid system, using the CXCR4-specific PET tracer, FDG was conducted by Philipp-Abbrederis *et al*.[165] ^{68}Ga-CPCR4-2, known as Pentixafor, evaluated for *in vivo* mapping of CXCR4 expression density. Out of 14 patients with advanced multiple myeloma (MM), the ^{68}Ga-CPCR4-2 PET/CT scans revealed the MM manifestations in 10 patients, whereas 9 patients were recognised as MM positive using standard ^{18}F-fluorodeoxyglucose (^{18}F-FDG) PET/CT scan.[165] There are still disadvantages to the use of peptides in terms of biological processing and hence it would be useful to also evaluate small molecule imaging agents for this application.

Figure 23 *In vivo* evaluation of ^{68}Ga-CPCR4-2. Left) For competition; right) ^{68}Ga-CPCR4-2 coinjected with AMD3100 (reproduced from Wester *et al.*, 2015)[164]

Small molecule tetraazamacrocyclic CXCR4 antagonists AMD3100 and AMD3465, see Figure 24, have been used to image the CXCR4 using PET. The first in vivo study reported the biodistribution and PET imaging of ^{64}Cu-AMD3100 in non-tumour bearing mice.[166] The accumulation was high in immune-related organs such as the spleen, lymph nodes and bone marrow, demonstrating the CXCR4 targeting ability of ^{64}Cu-AMD3100. However, the liver uptake was relatively high. Nimmagadda et al. and Weiss et al. described PET imaging and biodistribution of ^{64}Cu-AMD3100 in tumour bearing mice.[167, 168] The logP value of ^{64}Cu-AMD3100 is 0.52 ±0.0281.[167] Although expression of CXCR4 in the liver is low, accumulation of ^{64}Cu-AMD3100 seemed to be specific, indicating that it may bind to other binding sites. The high liver accumulation appears to be the main bottleneck for a clinical

application of ^{64}Cu-AMD3100.[163, 168] In human beings, the elimination of AMD3100 happens primarily via kidney, and approx. 70% of the drug removes within 24 hours, suggesting metabolic stability.[31, 32] This is happened probably due to the cyclam metabolites show low affinity to CXCR4. But it has been studied that bridged cyclam based inhibitors can produce the stable Cu-based CXCR4 imaging agents.[31, 32]

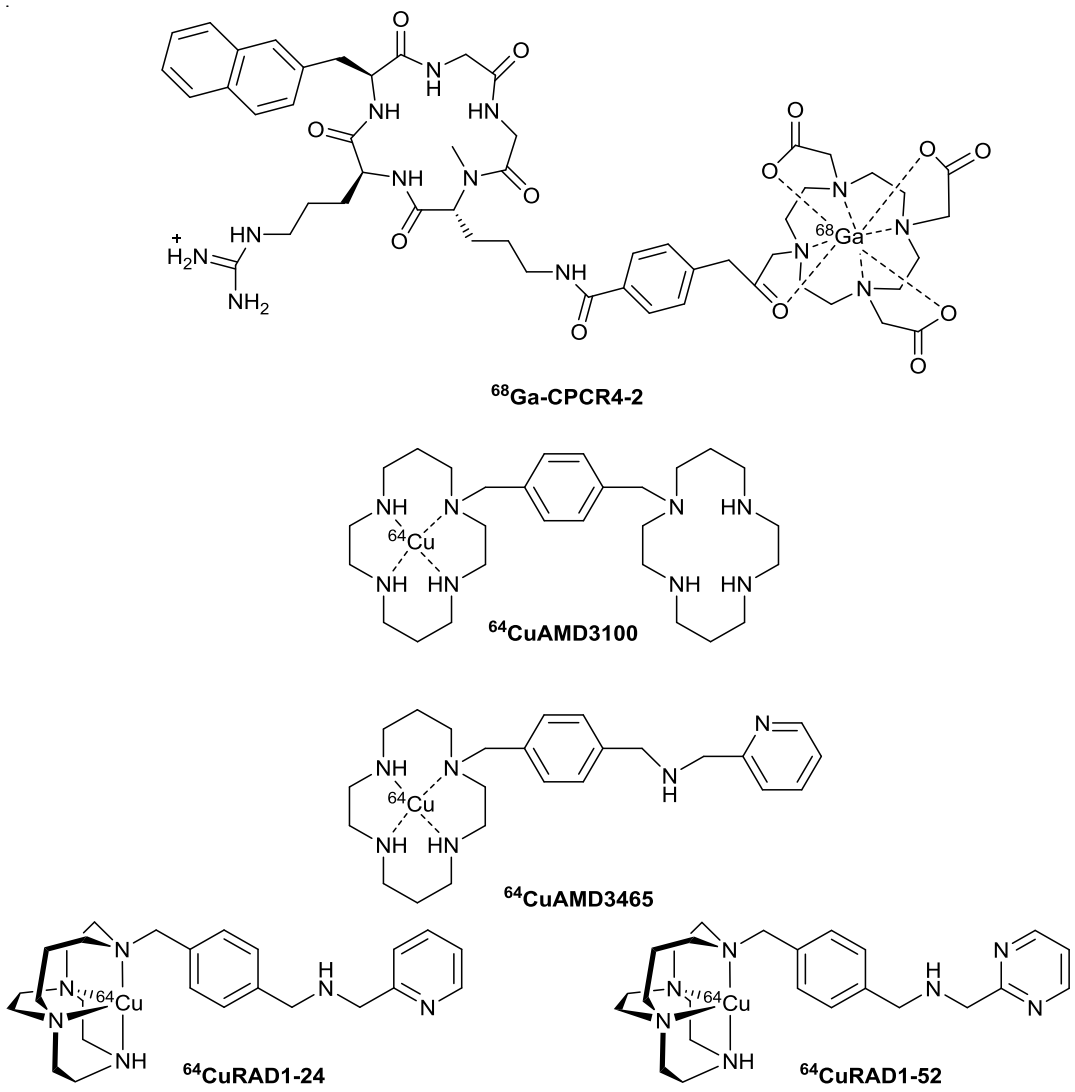

Figure 24 Chemical structures of radiolabelled CPCR4-2, AMD3100, AMD3465, RAD1-24 and RAD1-52

In AMD3465 see Figure 24, one cyclam group of AMD3100 is replaced by a pyridine group. AMD3465 has a slightly lower IC_{50} value than AMD3100 (18 nM and 33 nM, respectively, measured in the same assay) and is more hydrophilic than AMD3100.[36] De Silvia et al. evaluated the use of ^{64}Cu-AMD3465 as a PET agent to detect CXCR4 expression in tumour models with graded levels of CXCR4 expression.[169] Evaluation of a ^{64}Cu-AMD3465 was carried out in transfected U87 brain tumours and ex vivo bio-distribution was investigated using dynamic and whole-body PET. These PET/CT studies showed significant deposition of radioactivity in U87-stb-CXCR4 tumours model. Treatment with AMD3465 before administering the imaging agent stopped the uptake of radioactivity by the tumours.[169], [170] Addition of stabilising ethyl bridges is known to provide more robust chelator copper(II) complexes.[171] In addition, bridged cyclam based CXCR4 binding agents demonstrated increased receptor residence times relative to existing agents.[170] This reflects and references the published work already carried in the Archibald group. Woodard et al. synthesised several bridged cyclam analogues of AMD3465, to increase the retention time of the tracer bound to the receptor to allow for protracted imaging and improved target-to-non-target ratios.[170] Specific accumulation of two radiolabelled, cross-bridged analogues ^{64}Cu-RAD1-24 and ^{64}Cu-RAD1-52 see Figure 24, was observed in U87-stb-CXCR4 tumours in both PET/CT imaging and biodistribution studies.[170] However these tracers did not show optimum properties with liver uptake that could not be blocked hence is thought to be non-specific or insufficiently stable, which is unexpected. Further development work is required to provide azamacrocyclic compounds that can be used for imaging of the CXCR4 receptor.

3.3. Result and Discussion

3.3.1. *In vitro* biological assessment of side bridged tetrazamacrocycles

The aim is to conduct a variety of biological assays on the compounds shown in Figure 25, to test their binding to the CXCR4 receptor in cellular systems as well as analysing cytotoxicity. The receptor affinity of a compound is described by the concentration required to inhibit binding by 50% (IC_{50}).[150] The IC_{50} value can be determined *in vitro* using cell lines with intrinsic CXCR4 expression or cell lines that over-express the CXCR4 receptor after transfection with the (human) CXCR4 gene.

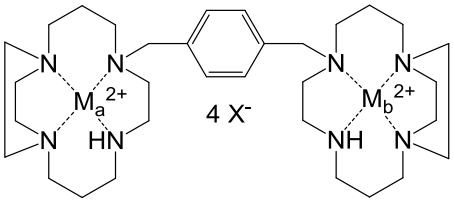

[ZnCu**6**]$^{4+}$ M_a^{2+}= Zn^{2+} M_b^{2+}= Cu^{2+}

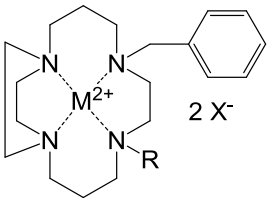

[Cu**7**]$^{2+}$ R= CH_3 M^{2+}= Cu^{2+} X^-= $CH_3CO_2^-$
[Zn**7**]$^{2+}$ R= CH_3 M^{2+}= Zn^{2+} X^-= $CH_3CO_2^-$
[Ni**7**]$^{2+}$ R= CH_3 M^{2+}= Ni^{2+} X^-= NO_3^-

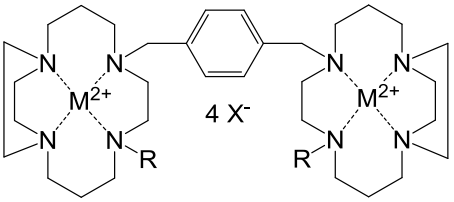

[Cu_2**9**]$^{4+}$ R= CH_3 M^{2+}= Cu^{2+} X^-= $CH_3CO_2^-$
[Zn_2**9**]$^{4+}$ R= CH_3 M^{2+}= Zn^{2+} X^-= $CH_3CO_2^-$
[Ni_2**9**]$^{4+}$ R= CH_3 M^{2+}= Ni^{2+} X^-= NO_3^-
[Cu_2**10**]$^{4+}$ R= CH_2Ph M^{2+}= Cu^{2+} X^-= $CH_3CO_2^-$
[Zn_2**10**]$^{4+}$ R= CH_2Ph M^{2+}= Zn^{2+} X^-= $CH_3CO_2^-$
[Ni_2**10**]$^{4+}$ R= CH_2Ph M^{2+}= Ni^{2+} X^-= NO_3^-

Figure 25 Chemical structure of CXCR4 *trans II* and *trans IV* macrocyclic antagonists

3.3.1.1. Displacement assay with antibody

Zinc(II), copper(II) and nickel(II) coordinated bis and mono-macrocyclic compounds were evaluated as CXCR4 antagonists and compared with the clinically licensed drug AMD3100 in the biological assays. Initially, displacement assays were conducted to screen the macrocycles as listed in Table 2. This assay was carried out using Jurkat cells which overexpress the CXCR4 receptor, normal cells express about 10,000 copies of the CXCR4 receptor whereas Jurkat cells express *ca.* 140,000 copies.[172] The macrocyclic antagonist is bound to the CXCR4 receptor and a CXCR4 specific mAb with a fluorescent label is introduced to determine whether it can bind by displacement of the antagonist; the label is detected and a percentage of inhibition is calculated. A high percentage corresponds to low displacement of macrocyclic compound by the mAb and means that the compound has competed efficiently for the CXCR4 receptor. A high fluorescence reading results in a low percentage because a high degree of mAb has displaced the macrocyclic compound from the CXCR4 receptor. To summarise the assay, the procedure can be broken down into four steps. To begin with, Jurkat cells (a human leukaemia cell line) are incubated with a large excess of the synthesised antagonist compound which saturates the receptor on the cells. After half an hour, excess compound is washed off. The cells are then incubated for an hour with a primary mAb which is specific to CXCR4, before a secondary (fluorescently tagged) mAb is added which binds to the primary mAb (or this process can be simplified if a fluorescently tagged primary mAb is used). The final step in the assay is to quantify the fluorescence intensity via flow cytometry in order to calculate the % binding inhibition of each antagonist compound. An example of a flow cytometry plot is shown in Figure 26.

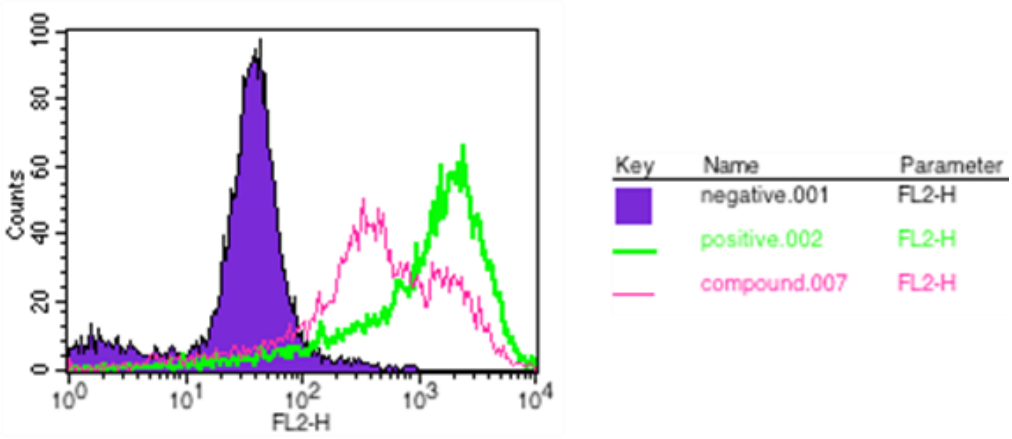

Figure 26 Typical flow cytometry plot showing negative control (purple), positive control (red) and an antagonists (green)

The negative control (purple) represents zero mAb binding and the positive control (red) represents mAb binding in the absence of antagonist. Therefore, the more effectively a compound competes for receptor binding, the closer the trace with the compounds present will be to the negative control. The higher the % binding inhibition, the more of the compound remains bound to CXCR4 in the presence of the CXCR4 specific mAb.

The metal containing monocyclam complexes $[Cu\mathbf{7}]^{2+}$, $[Zn\mathbf{7}]^{2+}$ and $[Ni\mathbf{7}]^{2+}$ show mAb inhibition in Jurkat cells of 33%, 20% and 39%, respectively. These metal monocylam complexes show low inhibition because only one coordinate bond can form with a single metal centre. They act as antagonists but they have effectively low rate of inhibition on the anti-CXCR4 mAb. This trend has been observed previously within our group and so was expected. The monocyclam metal complex derivatives displaced less mAb therefore they are considered as weak CXCR4 antagonists. However, these monomacrocyclic ligands may possess the potential to improve the pharmacological properties such as oral bioavailability due to their reduced molecular charge and lower molecular weight in comparison to their bismacrocyclic counterparts.

Bicyclam complexes containing $[Cu_2\mathbf{10}]^{4+}$, $[Zn_2\mathbf{10}]^{4+}$ and $[Ni_2\mathbf{10}]^{4+}$ with the benzyl group inhibited the binding to the receptor on the Jurkat cells by 62%, 59% and 52%, respectively. Whereas bicyclam metal complexes, $[Cu_2\mathbf{9}]^{4+}$, $[Zn_2\mathbf{9}]^{4+}$ and $[Ni_2\mathbf{9}]^{4+}$ with methyl groups inhibited the cell line by 38%, 46%, 34%, respectively. The data suggest that benzyl containing bicyclam metal complexes show more effective competition with the anti-CXCR4 mAb on the Jurkat cell line than the complexes with a methyl group. The metal complexes $[Cu_2\mathbf{AMD3100}]^{4+}$, $[Zn_2\mathbf{AMD3100}]^{4+}$, $[Cu_2\mathbf{L^{11}}]^{4+}$, $[Zn_2\mathbf{L^{11}}]^{4+}$ and $[Zn_2\mathbf{L^{10}}]^{4+}$ tested previously within our group showed almost100% inhibition. These metal complexes are more effective than AMD3100 (88%) as listed in Table 2. The bicyclam side bridge complex $[Cu_2\mathbf{L^{10}}]^{4+}$ showed similar inhibition to AMD3100. The free ligands; bicyclam side bridge $\mathbf{L^{10}}$ and crossbridge $\mathbf{L^{11}}$ gave values of 72% and 17%, respectively. The results indicate that the bicyclam side bridge complexes with the metal showed more effective inhibition than the bicyclam cross bridge without metal (similar to the AMD3100). The mAb displacement assay indicates that each metal complex synthesised inhibited CXCR4 less effectively than AMD3100, including $[Cu_2\mathbf{10}]^{4+}$, which is the most potent in blocking the binding of the anti-CXCR4 mAb.

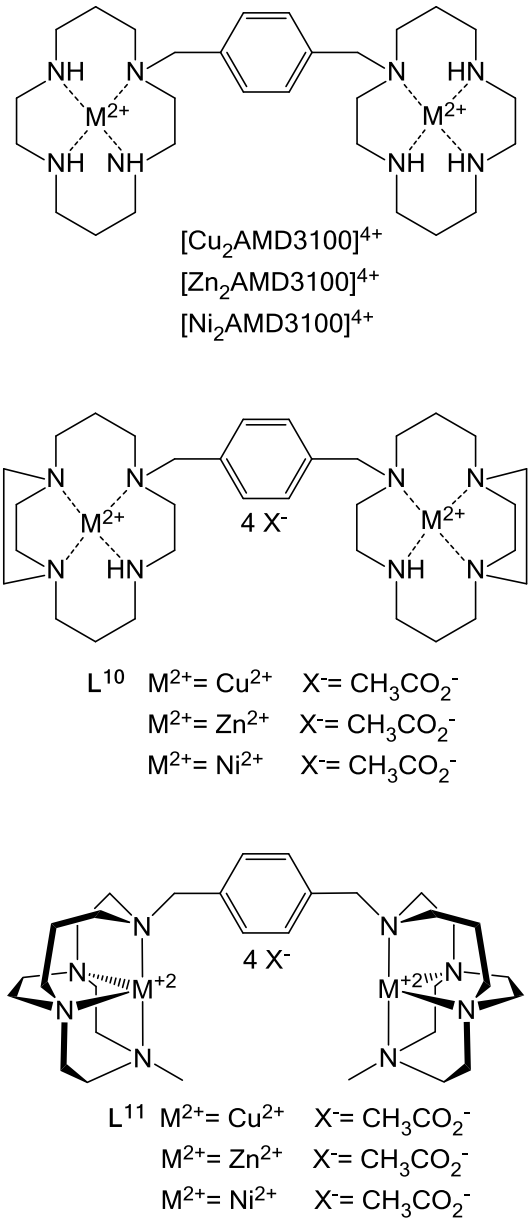

Figure 27 Chemical structures of complexes of Cu(II), Zn(II) and Ni(II) of AMD3100, side bridge **L**^{10} and cross bridge **L**^{11} bis macrocycles

Complex	Av % inhibition in Jurkat cells (based on MFI)
$[Cu7]^{2+}$	33
$[Cu_29]^{4+}$	38
$[Cu_210]^{4+}$	62
$[Zn7]^{2+}$	20
$[Zn_29]^{4+}$	46
$[Zn_210]^{4+}$	59
$[Ni7]^{2+}$	39
$[Ni_29]^{4+}$	34
$[Ni_210]^{4+}$	52
AMD3100	88
$[Cu_2AMD3100]$	96
$[Zn_2AMD3100]$	99
L^{10}	72
Cu_2L^{10}	90
Zn_2L^{10}	100
L^{11}	17
Cu_2L^{11}	97
Zn_2L^{11}	98

Table 2 CXCR4 antibody blocking activities of macrocycle based compounds (percentages are based on the mean fluorescence intensity of duplicates or triplicate results)

3.3.1.2. Anti-HIV and cytotoxicity assays

For the anti-HIV assay, different cell lines can be used. In our assay, U87.CD4.CXCR4, a human glioblastoma cell line cell line transfected with high levels of the CXCR4 receptor was used as well as MT-4 cells (a human T cell leukaemia cell line) and the TMZbl cell line. All assays were carried out by our collaborators at KU Leuven in Belgium. An AMD3100 resistant MT-4 cell line is also available and provides a test for macrocyclic compounds as some of the residues normally used for binding will have mutated. The assay determines anti-HIV activity

(whether cells have or have not been infected with HIV-1 or HIV-2) and cytotoxicity measurements assess the viability of the cells against different concentrations of antagonist.[173] The X4 virus strain was used because it infects cells using the CXCR4 receptor as opposed to the R5 virus strain which uses the CCR5 receptor to gain entry to the cells. The cytotoxicity assay involves culturing the cells for 5 days and quantifying the number of viable cells using the tetrazolium-based colourimetric method outlined by Pauwels *et al.*[174, 175] The cells were infected with HIV as described by Schols *et al.*[176] The anti-HIV assay records the replication of HIV in MT-4 cells over a period of five days. Therefore, the procedure can be separated into three steps; a) infection b) incubation and c) evaluation. The method relies on the HIV-induced cytopathogenic effect and measures the number of cells infected with HIV to give an effective concentration that reduces infection by 50% (EC_{50}).

The metal complexed monomacrocyclic compounds $[Cu\mathbf{7}]^{2+}$, $[Zn\mathbf{7}]^{2+}$ and $[Ni\mathbf{7}]^{2+}$ did not register an EC_{50} value (>63900, >108100 and >24600 nM) under the experimental conditions employed. These data are consistent with the displacement assay results in the previous section. The metal bismacrocyclic complexes $[Zn_2\mathbf{9}]^{4+}$ and $[Zn_2\mathbf{10}]^{4+}$ showed greater anti-HIV activity (516 and 247 nM) when compared to $[Cu_2\mathbf{9}]^{4+}$, $[Cu_2\mathbf{10}]^{4+}$, $[Ni_2\mathbf{9}]^{4+}$ and $[Ni_2\mathbf{10}]^{4+}$ bicyclam complexes (11000, 24500, >11020 and >10300 nM). These values can be related to the accessibility of forming the coordination interactions with the metal centre when the macrocycle is present in the *trans IV* configuration. This is lower than has previously been observed indicating that this configuration is not optimal. The higher activity of the zinc(II) complexes can be attributed to the greater flexibility in coordination geometry preferences for a d^{10} metal ion.

Our group previously synthesised and assessed $[Cu\mathbf{L^{11}}]^{4+}$ as an anti-HIV-1 agent and found it had greater activity than AMD3100 when tested on HIV-1 infected MT-4 cells.[64] The EC_{50} value for $[Cu\mathbf{L^{11}}]^{4+}$ is 4 nM. The increase in activity, which was attributed to more effective binding due to coordinate bonds forming with the copper(II) complex as opposed to weaker hydrogen bonds detected with AMD3100 is accompanied by a longer receptor residence time. The improvement in binding is thought to be due to the optimisation of the configuration because complex formation of AMD3100 with copper(II) leads to a decrease in activity. The

cis V macrocyclic structure favours the metal ion forming coordination bonds with oxygen atoms from the carboxylate groups on the aspartate residue when bound to the CXCR4 protein. All of these results were consistent with those obtained in this study.

Sample	Cytotoxicity (nM) CC_{50} [a]	Anti-HIV (nM) EC_{50} [b]	Calcium signalling (nM) IC_{50} [c]	Ref.
$[Cu7]^{2+}$	63900	>63900	AD	TW
$[Cu_29]^{4+}$	38000	11000	AD	TW
$[Cu_210]^{4+}$	32300	24500	AD	TW
$[Zn7]^{2+}$	108100	>108100	AD	TW
$[Zn_29]^{4+}$	42800	516	AD	TW
$[Zn_210]^{4+}$	39600	247	AD	TW
$[Ni7]^{2+}$	24600	>24600	AD	TW
$[Ni_29]^{4+}$	11020	>11020	AD	TW
$[Ni_210]^{4+}$	10300	>10300	AD	TW
AMD3100	>225000	11	31	[177]
$[Cu_2$AMD3100$]$	-	62	-	[64]
$[Zn_2$AMD3100$]$	>225000	8	8	[62]
$[Ni_2$AMD3100$]$		8	-	[58]
$Cu_2\,L^{10}$	>150000	3	330	[63]
$Cu_2\,L^{11}$	-	4	180	[120]
$Zn_2\,L^{10}$	60560	3	260	[63]
$Zn_2\,L^{11}$	-	6	250	unpublished
$Ni_2\,L^{10}$	-	74	14	[121]
$Ni_2\,L^{11}$	-	398	194	[121]

Table 3 Cytotoxicity, Anti-HIV activity and Calcium signalling for *trans IV* complexes in MT-4 cells, [a] (CC_{50}) is average concentration required to have a cytotoxic effect reducing MT-4 cell viability by 50%. [b] (EC_{50}) average effective concentration to reduce the HIV-induced cytopathic effect by 50% in MT-4 cells.). [c] IC_{50} (calcium signalling) concentration required to reduce the level of Ca^{2+} ions observed during a 'normal' signalling process by 50%. AD awaiting data and TW this work.

A cytotoxicity assay was performed, the cell survival can be measured dependent on the concentration of the compounds added. This can be measured spectrophotmetrically. The yellow 3-(4,5-dimethylthiazol-2-yl)-2,5-diphenyltetrazolium bromide (MTT) is reduced by mitochondrial enzymes to formazan which is a blue colour, see Scheme 11. The enzymes are only active when the cells are metabolically active and so the intensity of the colour indicates the number of viable cells remaining.

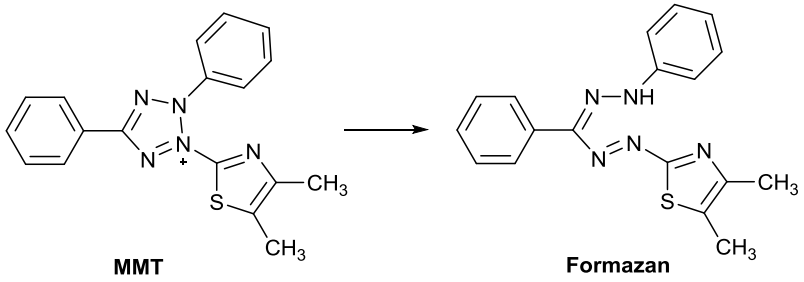

Scheme 11 Reduction of MTT to formazan

The CC_{50} of the compounds can be determined and defined as the concentration of the compound that is required to reduce the absorbance of the control sample by 50%. For compounds which are themselves coloured (for example the metal complexes in this work), their colour is taken into account when determining the cytotoxicity. Reference compounds are also included in the assays, which include AZT, heparin and dextran sulphate. As it can be seen in Table 3, all of the *trans IV* complexes were found to be non-toxic to the MT-4 cells in the assay, with CC_{50} values in general being >10300 nM compared to AMD3100 which showed >1000 nM in the same cell line as listed in Table 3. It was noted that the mono macrocyclic complexes showed higher toxicity than the bismacrocyclic counterparts in some cases.

As a further comparison, Smith *et al.* synthesised a nickel(II) complex of *meta*-linked CB bis-macrocycle, $[Ni\mathbf{L}^{\mathbf{11}}]^{4+}$.[121] $[Ni\mathbf{L}^{\mathbf{11}}]^{4+}$ was found to be an effective CXCR4 antagonist with an IC_{50} value of 14 nM. Cytotoxicity assays revealed that all of those published nickel(II) complexes have a CC_{50} of more than 125 μM. Anti-HIV assays were conducted using an X4 strain which exploits the CXCR4 receptor for

viral cell entry. The complex [Ni**L**^{11}]$^{4+}$ was less active than AMD3100, EC_{50} values of 74 nM and 11 nM respectively were observed showing that the nickel(II) complexes have high anti-HIV-1 activity and low cytotoxicity. The compounds studied in this work also had low cytotoxicity but the anti-viral assays showed lower potency.

3.3.1.3. Calcium signalling assay

The calcium signalling assay used in this work (which was performed at KU Leuven in Belgium by the group of Prof Dominique Schols) involves incubating a range of antagonist concentrations with U87.CD4.CXCR4 cells, a human glioblastoma cell line that has been transfected with CXCR4 receptors.[178] Firstly, the cells are washed after incubation with the antagonist at a range of concentrations. CXCL12 is then introduced to stimulate the calcium(II) release and the levels of intracellular calcium(II) are monitored. A control set of cells only exposed to CXCL12 with no antagonist present is run for comparison to the antagonist samples. A reduction in calcium(II) release, compared to the control, should be observed when the antagonist is present as the receptors are blocked and unable to activate calcium(II) release. The process is monitored by a calcium(II) sensitive dye which binds to calcium(II) and fluoresces. The assay is quantified using a fluorometric imaging plate reader, FLIPR. A 96-well plate is used to allow for relatively high-throughput. Use of a range of antagonist concentrations enables the IC_{50} value to be calculated. Unfortunately, the full set of data is not yet available from the collaborators at KU Leuven, hence more robust conclusions will be drawn once the full set of biological data is supplied.

3.3.2 Copper-64 radiolabelling

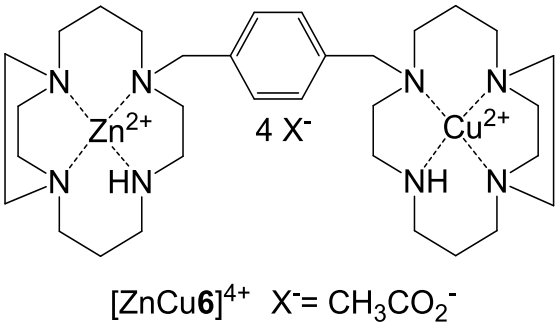

$[ZnCu\mathbf{6}]^{4+}$ $X^- = CH_3CO_2^-$

Figure 28 Chemical structure of novel SB bicyclam *trans II* Zn-Cu complex

This section includes the synthesis of radiolabelled bismacrocyclic complexes which have potential applications as PET imaging agents. As none of the novel *trans IV* compounds (reported in chapter 2) showed higher affinity for the receptor in the *in vitro* studies, than the *trans II* configurationally restricted side bridge bismacrocyclic compounds it was decided that the best option for radiolabelling was to pursue the trans II complexes. A novel mixed metal complex $[ZnCu\mathbf{6}]^{4+}$, see Figure 28, was synthesised as a non-radioactive standard for a potential imaging agent and showed a high receptor affinity with EC_{50} 3 nM in the anti-HIV assay. The cytoxicity assay showed that $[ZnCu\mathbf{6}]^{4+}$ is not significantly more toxic than AMD3100 see Table 4. $[Zn_2\mathbf{6}]^{4+}$ could be radiolabelled with $^{64}Cu(II)$ *via* transmetalation to give $[ZnCu\mathbf{6}]^{4+}$. The development of efficient radiolabelling protocols for the macrocycles was investigated in this work.

Sample	Cytotoxicity (nM) CC_{50} [a]	Anti-HIV (nM) EC_{50} [b]	Calcium signalling (nM) IC_{50} [c]
$[Cu6]^{2+}$	78750	4	AD
$[Cu_2L^{10}]^{4+}$	>150000	3	330
$[Zn_2L^{10}]^{4+}$	60560	3	260
$[ZnCu6]^{4+}$	102178	3	AD
AMD3100	225000	11	31

Table 4 Cytotoxicity, Anti-HIV activity and Calcium signalling for *trans II* complexes in MT-4 cells, [a] (CC_{50}) is average concentration required to have a cytotoxic effect reducing MT-4 cell viability by 50%. [b] (EC_{50}) average effective concentration to reduce the HIV-induced cytopathic effect by 50% in MT-4 cells.). [c] IC_{50} (calcium signalling) concentration required to reduce the level of Ca^{2+} ions observed during a 'normal' signalling process by 50% in. AD awaiting data

3.3.2.1. Synthesis of ^{64}Cu Radiolabelled 1,4-bis((1,5,8,12-tetraazabicyclo[10.2.2]hexadecan-5-yl)methyl)benzene di-zinc (II) acetate $[Zn_2 6]^{4+}$

Copper(II) should effectively undergo transmetalation.[62, 179, 180] with zinc(II) because the binding constant for $[Zn\text{-cyclam}]^{2+}$ is 11 orders of magnitude lower than that of $[Cu\text{-cyclam}]^{2+}$ thus the formation of $[Cu\text{-cyclam}]^{2+}$ is thermodynamically favoured. Furthermore, in addition to the hgher stability of copper(II) cyclam, the rate of complexation to cyclam is faster for copper(II) than zinc(II).[110, 181] Displacement of zinc(II) by copper(II) was observed by Paisey *et al.*, initially zinc(II) bound to cyclam when both metal ions were added to a solution of cyclam, however copper(II) displaced zinc(II) slowly at RT and 37 ^{o}C.[181]

In this work, the novel mixed metal copper-zinc(II) SB *trans II* bicyclam complex was synthesised by reacting $[Zn_2\mathbf{6}]^{4+}$ with a molar equivalent of copper(II) acetate monohydrate and heating at 60 ^{o}C for 2 hours, see Scheme 12. This reaction time was selected as it matched with the known time for incorporation of a metal ion

into a SB macrocycle and more importantly matches with a potential reaction time for radiolabelling with the copper-64 radioisotope.[132, 136] A molar equivalent was used because the aim was to replace only one zinc(II) ion.[182]

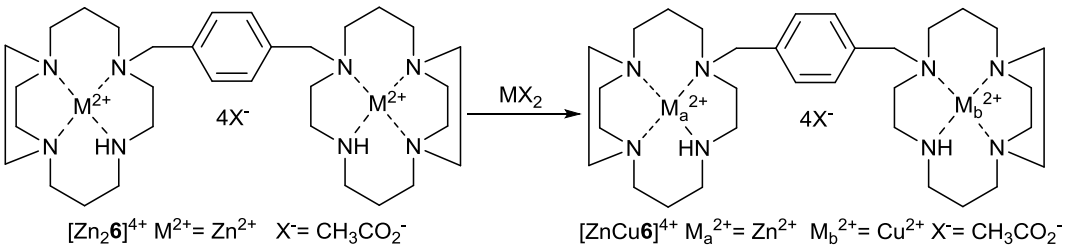

Scheme 12 Transmetaliation of $[Zn_2\mathbf{6}]^{4+}$to form novel mixed metal *trans II* complex $[ZnCu\mathbf{6}]^{4+}$

The side bridged structure was selected over the cross bridged structure as the flexibility of the CB structure is lower than the SB therefore the SB is may offer more rapid transmetallation. On addition of the copper(II) acetate monohydrate methanolic solution the bis-macrocycle solution immediately turned deep blue. $[CuZn\mathbf{6}]^{4+}$ was purified by size exclusion chromatography using Sephadex LH20 to yield the blue product in 74% yield. The complex $[CuZn\mathbf{6}]^{4+}$, was eluted in 95:5 water:MeOH on neutral alumina tlc plates saturated with NaCl as a test for a procedure to monitor the progress of the radiochemical reaction. These unusual conditions were selected as they enabled the macrocyclic complex to travel on the TLC plate.

Following the successful 'cold' (i.e. non-radioactive) transmetalation reaction of $[Zn_2\mathbf{6}]^{4+}$, radioactive transmetalation was explored. Woodard *et al.* afforded their radiolabelled CB-cyclam analogues by dissolving the macrocycle in water, adding 0.1 M sodium acetate pH 8.0 before addition of $[^{64}Cu]CuCl_2$ in HCl and heating at 95°C for 1 h.[170] This differed from the method outlined by Jacobson *et al.* who began by converting $[^{64}Cu]CuCl_2$ to $[^{64}Cu]Cu(CH_3CO_2)_2$ by adding 0.4 M ammonium acetate buffer, pH 5.5, with the buffer facilitating the anion exchange.[166] The $[^{64}Cu]Cu(CH_3CO_2)_2$ solution was then added to AMD3100 dissolved in 0.4 M ammonium acetate buffer pH 5.5 and stirred for 1 h at RT. Boswell *et al.* used a

similar method to synthesise ^{64}Cu-SB-TE1A1P, except [^{64}Cu]$CuCl_2$ was added directly to the macrocyclic compound in ammonium acetate buffer pH 7.5.[183]

The method used in this work was comparable to Jacobson *et al.* although heat was introduced due to the additional challenge of the transmetallation aspect. [^{64}CuZn**6**]$^{4+}$, see Figure 29, was synthesised by mixing a solution of macrocycle and 0.4 M ammonium acetate buffer pH 5.5. This was added to a [^{64}Cu]$CuCl_2$ solution that had been incubated at 60^{o}C with 0.4 M ammonium acetate buffer pH 5.5, heated at 90^{o}C to form the acetate salt for reaction.

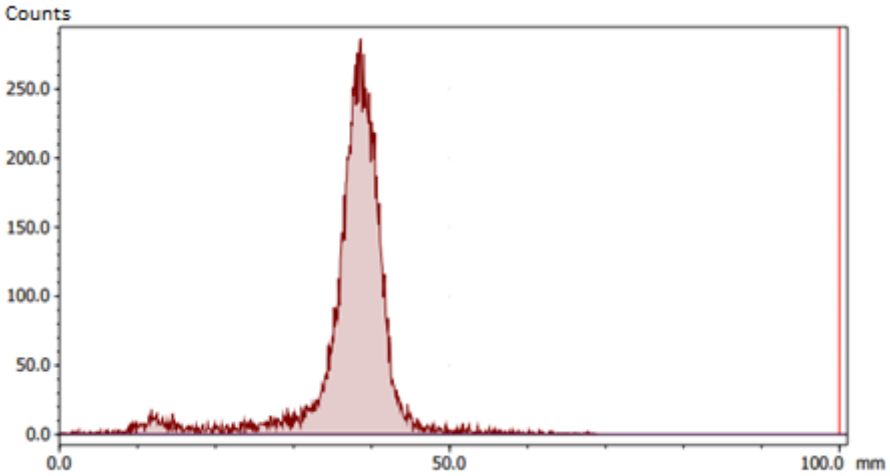

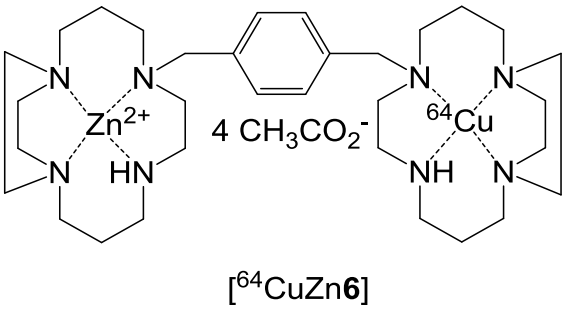

[^{64}CuZn**6**]

Figure 29 Chromatogram of radio TLC [^{64}CuZn**6**]$^{4+}$ after 75 minutes showed main peak corresponding to [^{64}CuZn**6**]$^{4+}$ and very little amount of free ^{64}Cu and chemical structure of radiolabelled bis-macrocycles [^{64}CuZn**6**]$^{4+}$

The conversion of $[Zn_2\mathbf{6}]^{4+}$ into $[^{64}CuZn\mathbf{6}]^{4+}$ was monitored via radioTLC as described earlier. The chromatograms obtained from the radio-TLCs, show the transmetallation of the zinc(II) complex to form the corresponding radiolabelled complex at each time point measured. The radiolabelled macrocycle was eluted with 95:5 water : MeOH, saturated with NaCl, which allowed reaction progress to be monitored.

Moreover, radio TLCs of diluted sample of 0.04 mM $[Zn_2\mathbf{6}]^{4+}$ showed that after just 15 minutes a considerable amount of $^{64}Cu^{2+}$ was incorporated into the macrocyclic cavities of $[^{64}CuZn\mathbf{6}]^{4+}$ about 51%. It was noted that, an increase in ^{64}Cu incorporation over the course of the reaction that was run for 75 min. After 75 min full incorporation of $^{64}Cu^{2+}$ was observed. The crude-RCY based on the TLC was 82% for $[^{64}CuZn\mathbf{6}]^{4+}$. The reaction was monitored at 15 minute intervals but insufficient reaction solution was added to the radio-TLC plate to give an accurate determination of the yield at each time point, see Figure 30, however they show a qualitative progression of the reaction over time, see graph plot in Figure 31.

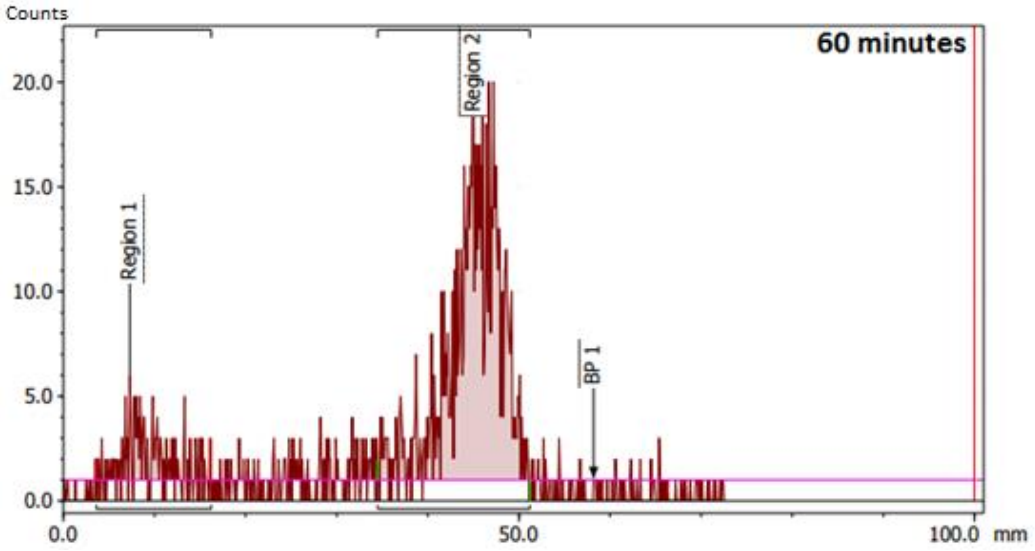
Counts
60 minutes
Region 1
Region 2
BP 1
20.0
15.0
10.0
5.0
0.0
0.0
50.0
100.0
mm

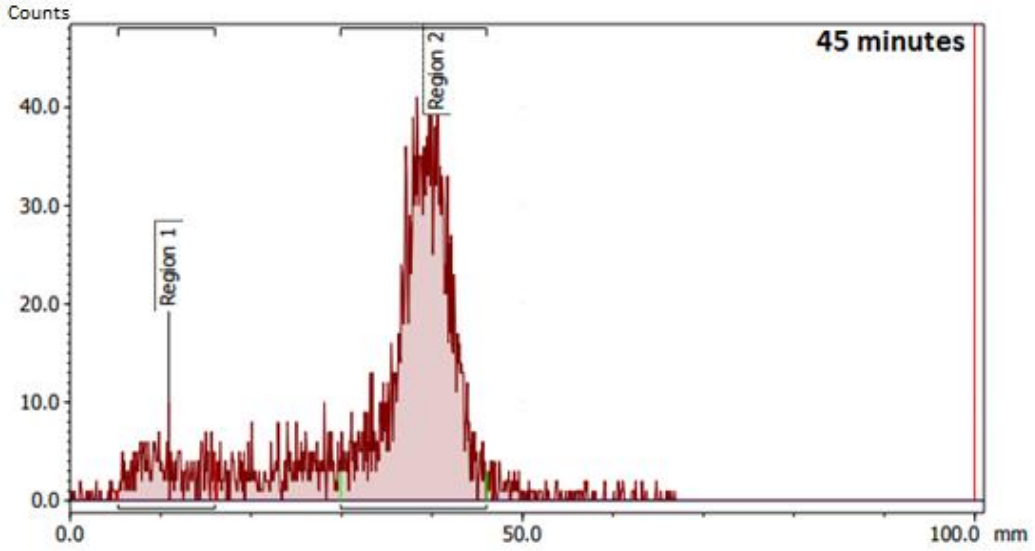
Counts
45 minutes
Region 1
Region 2
40.0
30.0
20.0
10.0
0.0
0.0
50.0
100.0
mm

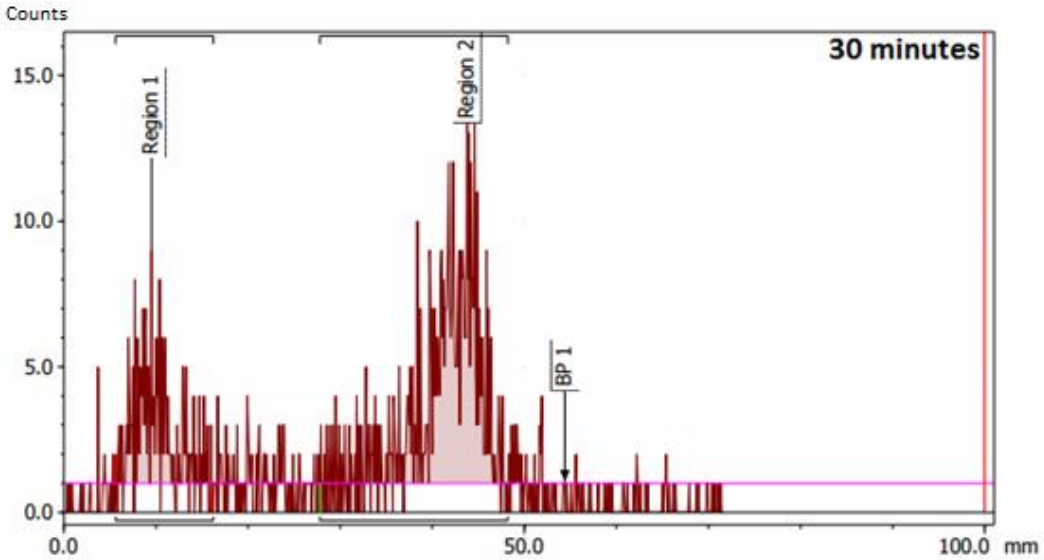
Counts
30 minutes
Region 1
Region 2
BP 1
15.0
10.0
5.0
0.0
0.0
50.0
100.0
mm

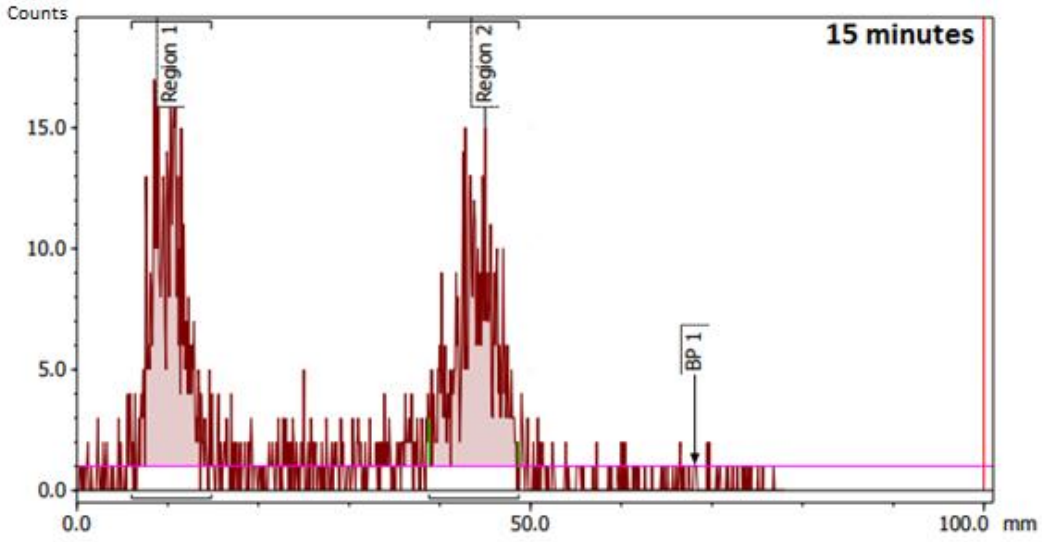

Figure 30 Chromatogram of radio-TLC of $[^{64}CuZn\mathbf{6}]^{4+}$ at concentration of 0.04 mM $[Zn_2\mathbf{6}]^{4+}$ (diluted 100 times) at different timepoint

In conclusion, important steps have been made toward the aim of radiolabelling a CXCR4 targeted macrocyclic ligand and data suggests that $[^{64}CuZn\mathbf{6}]^{4+}$ was successfully isolated but optimisation is needed to confirm the ideal reaction conditions.

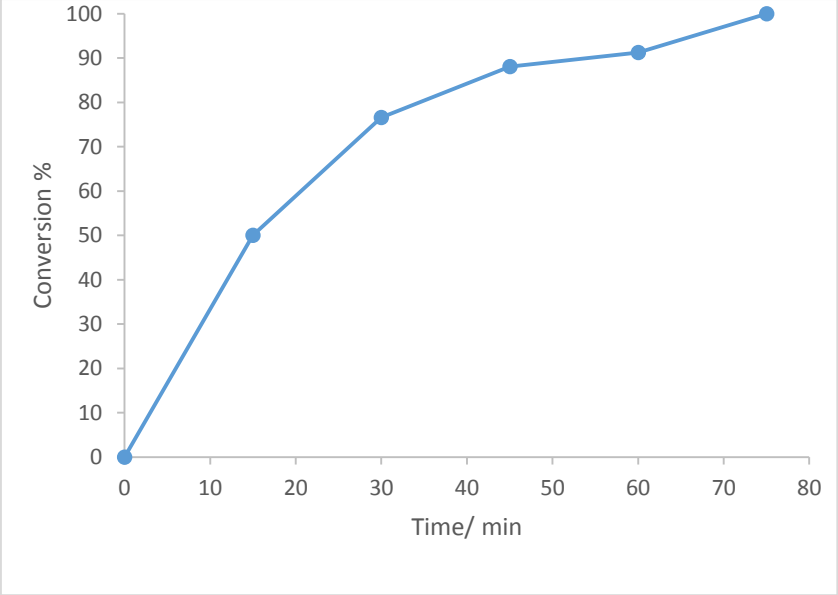

Figure 31Conversion of [CuZn**6**]$^{4+}$to [^{64}CuZn6]$^{4+}$ over time

3.3.2.2. Calculating the partition coefficient (LogP)

The partition coefficient (LogP) is a term used to describe how hydrophilic or hydrophobic a compound is.[184] As poor absorption and pharmacokinetics are the main reasons for drug candidates failing to progress in the drug development process, obtaining the physiochemical and pharmacokinetic drug properties as early as possible is highly advantageous.[185] Poor absorption is noted when drugs have a LogP of more than 5, solubility is known to be the limiting factor in terms of the absorption process which transports drugs across the gastrointestinal membrane in oral drugs.

LogP values were measured for [^{64}CuZn**6**]$^{4+}$ to determine whether this macrocyclic compound was hydrophilic or hydrophobic as this provides an insight into how the compound will behave *in vivo*.[184, 185] The general trend in LogP values of successfully launched oral drugs between 1965 and 2007 were between 1.5 to 3.5, what's more, between 1937 and 1997, the LogP value of approved drugs has not significantly changed.[186] A rationalisation for this is that when lipophilicity is too high, observed in compounds with high LogP values, the chances of non-specific binding, toxicity, poor solubility and metabolic clearance are higher.[184, 187-189] There

has been a general decline in the number of drugs released which have a molecular weight of less than 350 Da. A driving factor for this is that new biological targets are "less druggable" and require larger molecules to achieve high affinity binding, an example being antagonists for GPCRs. This contradicts the predictions of the rule of 5.[190, 191]

The rule of 5 was originally outlined by Lipinksi in 1997 and is a well-accepted method for predicting likely drug candidates that will have desirable absorption and permeability properties. The rules state that drugs should be less than 500 Da in molecular weight, have a LogP of less than 5, have less than 5 H-bond donors and less than 10 H-bond acceptors.[191] One well known exception to this rule is AMD3100 which has a molecular weight of 794 Da, which is well above the general trend for successful drugs. However, the difference between standard drugs and AMD3100 is that it is administered *via* injection into subcutaneous tissue rather than given orally. This difference may provide the reason for the success of AMD3100 which breaks multiple 'rule of 5' guidelines. It also provides strong evidence that other larger molecules which do not adhere to the rule of 5 can be developed as successful drugs.

The LogP value for $[^{64}CuZn\mathbf{6}]^{4+}$ was measured by making a solution of 0.5 MBq of the compound in 1 mL PBS:octanol 50:50. This mixture was then shaken for 5 min on a VV3 Vortex Mixer at 25ºC before being centrifuged for 5 min at 12,000 RPM at 25ºC. A small portion of each layer was sample and added to phosphate buffered saline (PBS) to give a final volume of 1 mL; 50 μL of the octanol layer and 5 μL of the PBS layer was taken, this was performed in triplicate. A larger volume of octanol was taken so that the instrument could detect a high enough reading of radioactivity because the hydrophilic nature of $[^{64}CuZn\mathbf{6}]^{4+}$ meant that the majority of the sample would be in the aqueous layer, this higher volume was corrected for when calculating the LogP values. The LogP values obtained for $[^{64}CuZn\mathbf{6}]^{4+}$ was 3.67. The LogP of $[^{64}CuAMD3100]^{2+}$ was 0.52 which is much higher than the LogP value of $[^{64}CuZn\mathbf{6}]$.[167] The low value for the AMD3100 labelled compound indicates that it would not be suitable to image CXCR4 expression beyond the blood-brain barrier because it is too hydrophilic. In conclusion, $[^{64}CuAMD3100]^{2+}$ has already been shown to have some potential as a PET imaging agent therefore the

[^{64}CuZn**6**]$^{4+}$ structure with some improved properties would be worthy of further investigation.

3.4. Conclusion

Targeting the chemokine receptor CXCR4 for positron emission tomography imaging could provide new tool for early diagnosis as well as treatment of cancer. This study aimed to develop novel a CXCR4 targeted agent that could be used in PET imaging. The initial focus was to further investigate the optimum configuration which cyclam (the main component of routinely used drug plerixafor/AMD3100) adopts once it is complexed with first row transition metals. This investigation was inspired by data that showed configurational restriction could increase the retention time at the CXCR4 receptor and optimise the binding interactions. A series of novel CXCR4 Cu(II), Zn(II) and Ni(II) complex antagonists that are restricted to either *trans II* or *trans IV* were evaluated in some biological assays. Their ability to effectively target the chemokine receptor CXCR4 was analysed using three different biological assays prior to investigation of radiolabelling with ^{64}Cu to determine whether potential use as a PET imaging agent was viable.

The first biological assay used was a displacement assay to investigate whether those complexes targeted CXCR4. The second method to assess them was an anti-HIV and toxicity essay which meant to find if those complexes could inhibit HIV infection using the CXCR4 receptor as well as their toxicity limits. The final method, was investigating whether those antagonists could block the downstream release of Ca^{2+} in the cell that is part of the natural biological signalling process. This study demonstrated that restriction of the cyclam macrocycle to the *trans IV* configuration was not optimal for targeting the chemokine receptor CXCR4. However, side bridge macrocycle restricted to *trans II* configuration has already shown promising results in *in vitro* analyses and a novel compound was made as a non-radioactive standard for a copper-64 radiolabelled derivative. Preliminary radiochemical experiments with copper-64 showed that the compound could be radiolabelled with $^{64}Cu^{2+}$ and the radiochemical yield (RCY) was recorded showing an efficient process could be carried out in good RCY in 75 mins.

Chapter Four

Development of CCR5 PET imaging agent

4. Development of CCR5 PET imaging agent

4.1. Aim

The aim of this chapter is to develop a novel CCR5 targeted PET imaging agent. Towards this goal, the synthesis of a carboxylic acid derivative of the known CCR5 antagonist TAK-779 was synthesised, followed by conjugation to the chelator DOTA. The conjugate was labelled with ^{68}Ga as a proof of principle for the formation of a potential CCR5 targeted PET imaging agent, see Figure 32 for a schematic of the compound. Finally, the synthesised molecules were assessed for their CCR5 binding affinity.

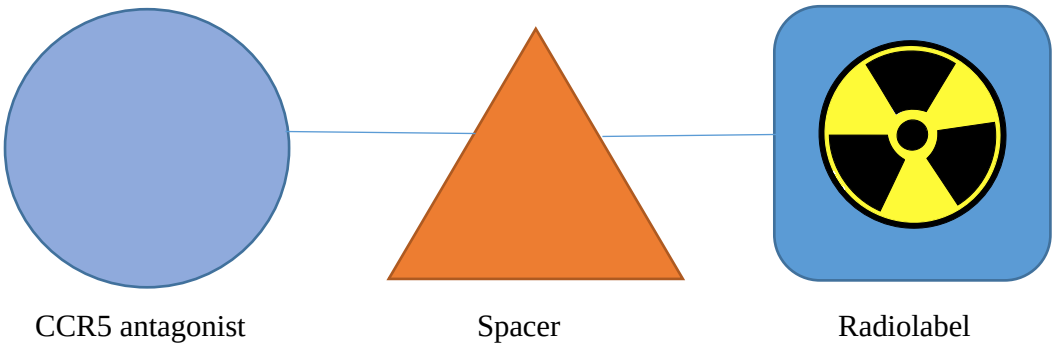

Figure 32 Schematic representation of developing CCR5 targeted PET imaging agent.

4.2. Introduction

4.2.1. CCR5 involvement in Cancer

CCR5 is a seven-transmembrane G-protein-coupled receptor, mediating diverse signalling cascades in response to its ligands. CCR5, a promiscuous receptor, binds with high affinity to CCL5, CCL3 (MIP-1a), and CCL4 (MIP-1b) and is the major co-receptor for HIV.[192] CCL5 belongs to the C-C chemokine family whose members also include CCL3 and CCL4.[193] The understanding of the roles played by CCR5 in tumour development and metastasis is currently under investigation. There is growing evidence indicating that CCR5 is strongly implicated in multiple

myeloma MM and breast cancer,[194, 195] and that the potential contribution to other cancers such as Hodgkin Lymphoma, melanoma, gastric, prostate, and ovarian and colon cancer deserves further study.[72]

In multiple myeloma (MM), the CCR5 ligand CCL3 is detected in MM cell lines and freshly isolated MM cells.[196-198] Several studies have evaluated the expression of CCR5 on MM cell lines and on cells derived from patients demonstrating that their activation contributes to MM cell survival and migration. MM cells migrate in the presence of CCL5 and the extent of migration depends on the CCR5 expression levels.[194, 199, 200]

Both CCR5 and its ligand CCL5 are also constitutively expressed by Hodgkin Lymphoma derived cell lines.[201, 202] The CCR5 receptor is shown to be functional since human recombinant CCL5 increases the growth of Hodgkin Lymphoma (HL) tumour cells. Neutralizing the signalling process using anti-CCL5 mAbs in these cells decrease the spontaneous growth, suggesting that CCL5 may represent an autocrine growth factor for HL cells.[203]

CCL5 plays a role in breast cancer development and/or progression, high expression of CCL5 by breast tumour cells at primary tumour sites and metastatic sites has been observed, indicating that increased CCL5 expression is associated with disease progression, relapse, and/or metastasis.[204-206] Lv *et al.* also found that, CCL5 expression is strongly associated with the progression of breast cancer, particularly triple-negative breast cancer (TNBC).[195]

In skin cancer, CCL5 and CCR5 are expressed by melanoma cells, primary melanomas, and cutaneous metastasis.[207] Mrowietz *et al.* indicated that, CCL5 is associated with enhanced tumour formation in nude mice.[208, 209] Kim *et al.* concluded that, CCL5 could serve as a predictor of metastasis in gastric cancer.[210] Based on a study analysing CCL5 circulating levels prior to anti gastric cancer treatment: CCL5 levels were found to be higher in patients than in healthy controls.[210, 211] The CCL5/CCR5 axis also plays a role in colon cancer as CCL5 and its receptors are overexpressed within primary tumours as well as liver and pulmonary metastases compared to healthy tissues.[212] CCL5 levels are higher in

ovarian cancer patients than in patients diagnosed with benign ovarian cysts and elevated in stages III-IV of ovarian cancer compared to stages I-II.[213]

In prostate cancer, CCR5 and its ligand CCL5 are involved in disease progression and both are expressed in human prostate cancer (PCa) cell lines, primary cultures of prostatic adenocarcinoma cells and PCa tissues were examined.[74] Maeda *et al.* discovered that, CCL5 stimulates PCa cell proliferation and invasion and both are inhibited by the chemokine receptor CCR5 antagonist TAK-779.[214]

4.2.2. Binding mode of TAK-779 to CCR5

The CCR5 binding pocket may bind to antagonists with different electrostatic nature and shape.[215] The shape and electrostatic properties of TAK-779 are shown in Figure 33. TAK-779 was developed by Takeda Inc. and can serve as a lead compound for the development of further other novel CCR5 antagonists.[216]

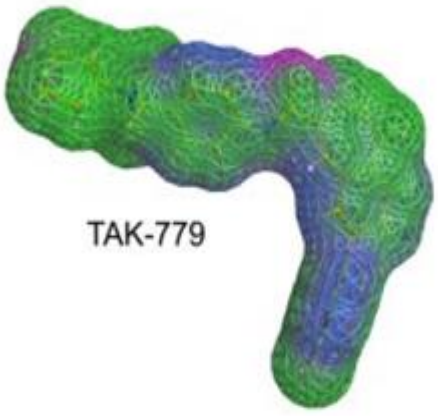

Figure 33 The electrostatic molecular grid that lines molecular volume is coloured according to the active lone pair formalism as implemented in MOE software. The green colour indicates the hydrophobic parts of the molecule, pink areas indicate the polar areas, and electropositive aromatic hydrogens are coloured blue. (Reproduced from Kondru *et al.*, 2008) [215]

The interactions between TAK-779 and two aromatic side chains of Tyr^{108} and Trp^{86} of CCR5 has been investigated see Figure 34. The antagonist TAK-779

may also interact with the binding sites of Thr[195], Ile[198], Phe[109], Trp[248], and Tyr[251] of CCR5 and these interactions are weak because of their hydrophobic nature, as suggested by the mutation data. The hydrophilic volume represented by Glu[283] is not fully utilised by TAK-779 offering a potential area for optimisation. This interaction with the quaternary ammonium ion does not offer the interaction strength predicted, which could be due to the increased salt bridge distance caused by methyl groups shielding the positive charge.[215, 217-219] Moreover, the mutation of Glu[283] to alanine strongly decreased the inhibitory effects of all small molecules with the exception of TAK-779. It is proposed that the negatively charged carboxylate of Glu[283] can interact with the positively charged nitrogen of the small molecule inhibitors. The lack of dependency of TAK-779 on this interaction could be explained by steric hindrance around the quaternary nitrogen of TAK-779.[73]

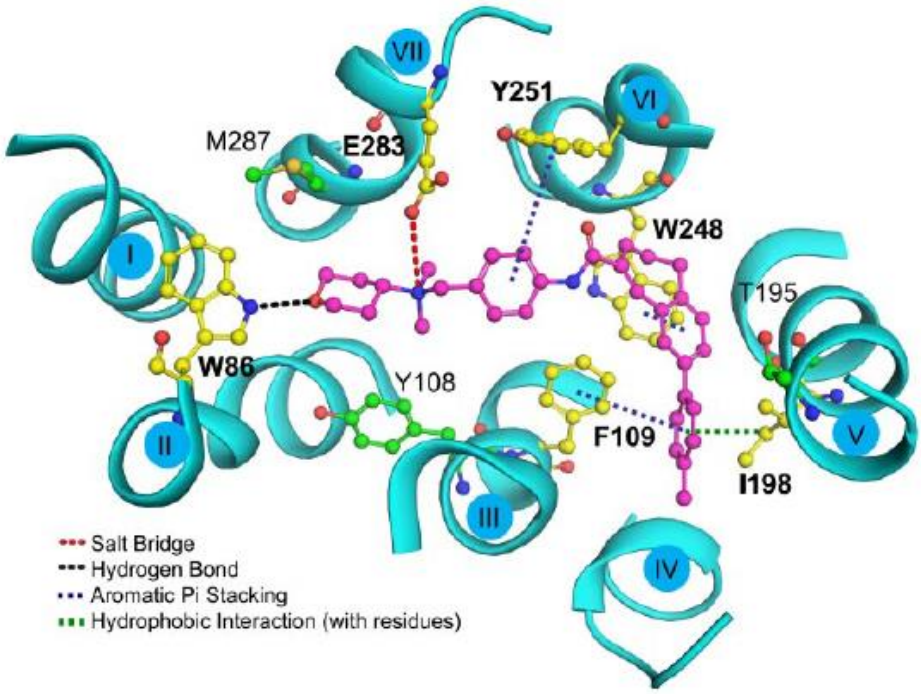

Figure 34 The binding mode for TAK-779 (pink), the key salt bridge interaction with Glu283 is indicated with red dotted lines. TAK-779 is predicted to have strong interactions with Trp86, Glu283, Phe109, Trp248, Tyr251, and Ile198 (shown in bold). The seven TM helices are labelled and shown in cyan. TAK-779 is the only CCR5 antagonist that interacts strongly with Trp248. The phenyl group of TAK-779 points toward TM4. The Tyr108 residue does not interact with TAK-779. (Reproduced from Kondru *et al.*, 2008) [215]

4.2.3. Imaging of CCR5

The current knowledge of involvement of CCR5 in cancer, leads to the suggestion that the chemokine receptor CCR5 and its ligand CCL5 formerly known as (RANTES) could be a potential therapeutic target in several cancers.[72] Zhagn *et al.* designed a probe with metal (silver) nanoparticles to find the expression and distribution of CCR5 receptor on the surface of cells using fluorescent imaging,[220] which can be a useful technique to detect the target molecules in the cells.[221] The emission from the single mAb–metal complexes could be distinctly identified from the cellular autofluorescence on the cell images.[222] The spatial distributions of CCR5 on the surface of cells were analysed and it was suggested that the high expression cells have dense clusters of CCR5 where as low-expression cells have the small clusters of CCR5 receptors on the cell surfaces.[220]

In addition, Luehmann and co-workers developed a CCR5 receptor targeted nanoparticle for the PET/CT imaging using apolipoprotein E knock-out (ApoE−/−) mouse model.[223] They used D-Ala1-peptide T-amide (DAPTA) peptide as a targeting ligand for the CCR5 receptor. The ^{64}Cu-DOTA-DAPTA tracer showed specific PET imaging of CCR5 with an extended blood signal. This tracer significantly accumulate high at the injury lesions, see Figure 35.[223]

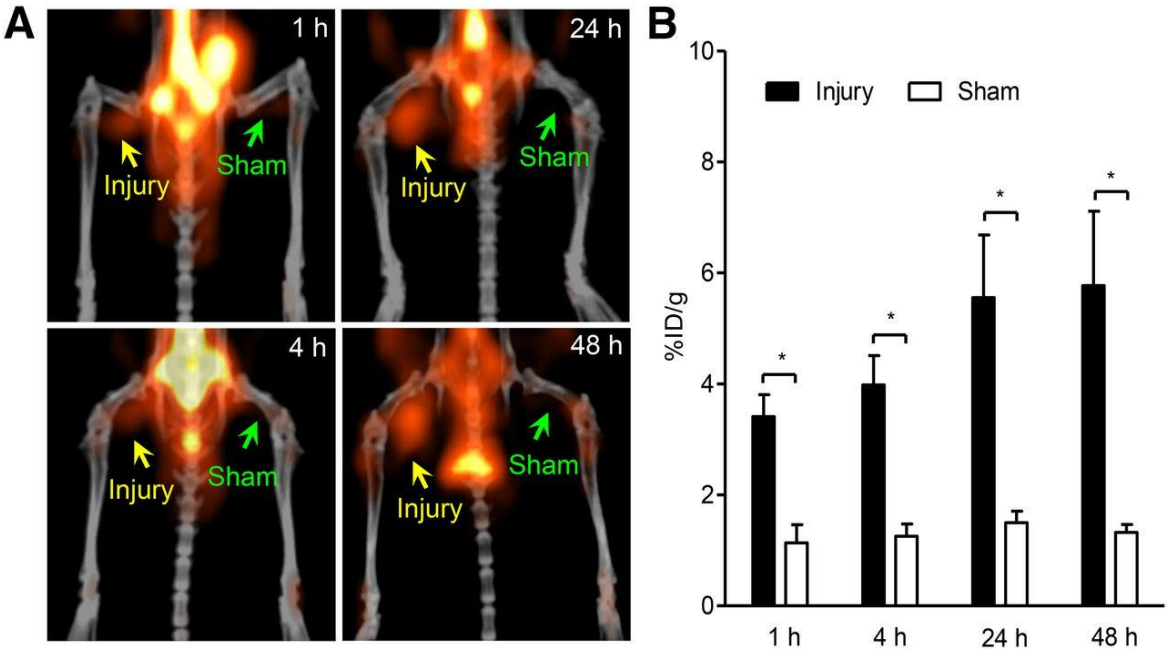

Figure 35 PET/CT images of ^{64}Cu-DOTA-DAPTA-comb in wire-injury–induced ApoE$^{-/-}$ mouse atherosclerosis model at 2 wk after injury. (A) Maximum-intensity-projection images showing accumulation of ^{64}Cu-DOTA-DAPTA-comb at injured lesion at various time points. (B) Uptake analysis of ^{64}Cu-DOTA-DAPTA-comb at injured and sham-operated sites (reproduced from Luehmann *et al*., 2014)[223]

The competitive PET receptor blocking studies confirmed the CCR5 receptor specific uptake. The assessment of ^{64}Cu-DOTA-DAPTA-comb in C57BL/6 mice and ^{64}Cu-DOTA-comb in ApoE−/− mice verified low nonspecific nanoparticle uptake with the upregulation of CCR5 in the progressive atherosclerosis model verified by other trechniques. The *in vivo* confirmation of the PET image results grants this nanoparticle significant potential as a non-invasive approach for further assessment of the pathologic functions of the CCR5 receptor in animal models.[223]

4.3. Synthesis of CCR5 antagonists

In the search for derivatives to target the chemokine receptor CCR5, the small-molecule non-peptide compounds synthesized by the Takeda chemists, showed highly potent activities.[224] TAK-779 was found to be effective when it was compared to some of the other known CCR5 antagonist such as maraviroc, vicriviroc, aplaviroc and TAK-220.[85, 215] TAK-779 showed high affinity to target the CCR5 with EC_{50} <2nM and, importantly, is relatively simple to synthesise.[225] As the aim of this work is to develop a CCR5 antagonist based on TAK-779 containing a carboxylic functional group to allow conjugation via formation of an amide bond with a chelator, such as DOTA, which will be radiolabelled with ^{68}Ga for potential use as a CCR5-PET imaging agent, as shown in Figure 36.

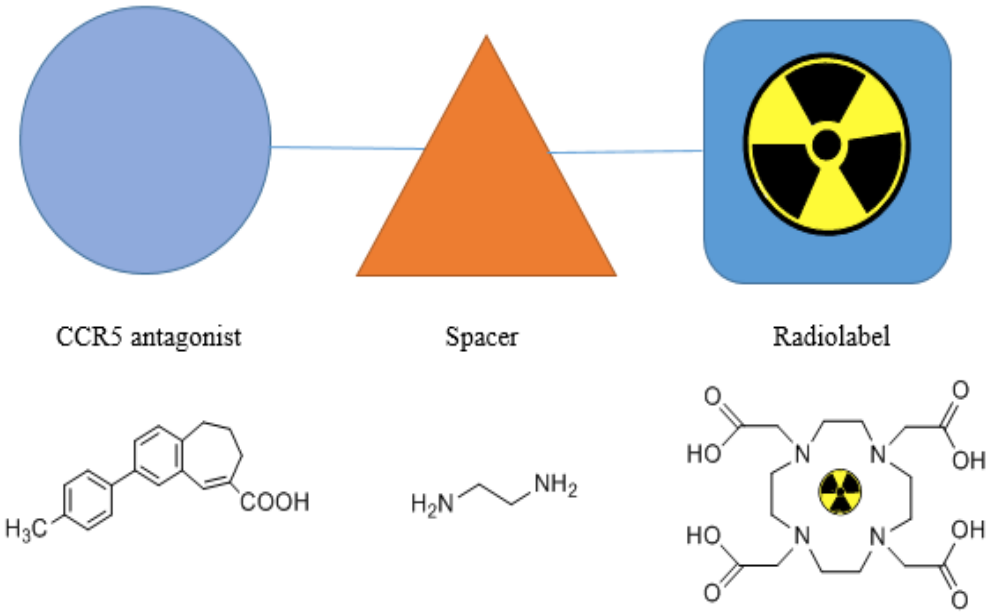

Figure 36 Schematic representation (2) of developing CCR5-PET imaging agent.

Two independent preparation routes for TAK-779 comprising the ammonium chloride moiety have been reported in the literature.[224, 225] One method

uses methylation of a tertiary amine followed by anion exchange,[224] and the other uses the reaction of benzyl chloride and tertiary amine.[225] The latter synthesis produced a high-quality product, since this treatment afforded only ammonium chloride without contamination by other counter ions. However, the original synthesis involved several limitations for example utilization of expensive reagents, requirement of a protection step, repeated time consuming chromatographic steps and lower yield. To avoid these limitations, compound **18** (small molecules TAK-779 derivative) was prepared following method proposed by Ikemoto *et al.* see Scheme 13, with some modifications (including HPLC monitoring of reaction progress) as will be discussed.[226]

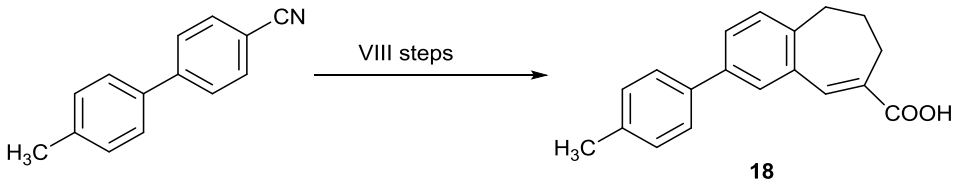

Scheme 13 synthetic pathway to obtain small molecules TAK-779 derivative

A method proposed by Ikemoto *et al.* for preparing TAK-779 that was designed for large scale production was followed.[226] A selective reduction of commercially available 4-(4-methylphenyl)benzonitrile was carried out to obtain **11**. Sodium bis(2-methoxyethoxy) aluminium hydride SBMEA in tetrahydrofuran THF at -20°C used as reducing agent to give 4'-methyl-[1,1'-biphenyl]-4-carbaldehyde in 90% yield. However, the use of SBMEA is comparable with $LiAlH_4$ but the most important differences are found in the reduction of nitriles, which are selectively reduced to aldehydes. The reducing power of SBMEA is close to that of lithium aluminum hydride.[226] An important advantage of this reagent is its stability to dry air (it does not ignite even in moist air or oxygen), and it is thermally stable up to 200°C unlike $LiAlH_4$, which can detonate at elevated temperatures. Perhaps the greatest utility of SBMEA is its solubility in aromatic hydrocarbon and ether solvents, which allows it to be conveniently used for applications that require inverse

addition of hydrides.[227, 228] NMR data confirmed the reduction of the nitrile group to aldehyde by the appearance of the distinctive peak at δ10.04 as well as the integration values of the peaks(12 protons in the correct ratios) with the expected splitting patterns.

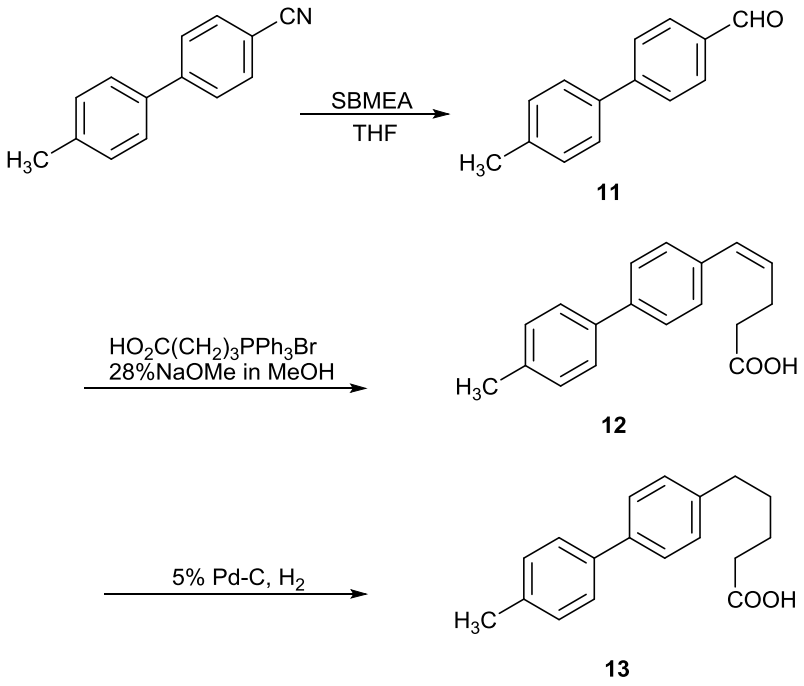

Scheme 14 Selective reduction of nitrile derivatives to form 4'-methyl-[1,1'-biphenyl]-4-carbaldehyde **11** then Wittig reaction conducted to form alkene **12** which was reduced to form alkanes **13**

The Wittig reaction was successfully utilised to form **12** in a 83% yield. The Wittig reaction belongs to a set of reactions, which add irreversibly to the carbon of the carbonyl-containing compounds such as aldehydes and ketones. The addition is to the carbon of the carbonyl group because there is a partial positive charge on that carbon. There are five steps in this reaction. The first step is to form a phosphonium ion. Phosphorus is a good nucleophile. In this reaction, the nucleophile is triphenylphosphine [$(C_6H_5)_3P$ or Ph_3P], which adds to the C of the RX forming phosphonium ion. In the second step, a base, such as sodium hydroxide (NaOH) or butyl lithium (BuLi) is used to deprotonate and forms the ylide (Wittig reagent). The ylide then acts as a nucleophile and adds to the carbonyl carbon. The resulting

alkoxide oxygen (-OR) adds to the phosphorus in an intramolecular closure reaction to form a four-membered ring, an oxaphosphetane which fragments to form triphenylphosphine oxide and the alkene. NMR and mass spectrometry (MS) data confirmed that the Wittig reaction had occurred due to the disappearance of the aldehyde peak and the appearance of the molecular mass ion at 266. Alkenes can be reduced to alkanes with H_2 in the presence of metal catalysts such as Pt, Pd, Ni or Rh. The alkene was hydrogenated in the presence of Pd/C to form compound **13** in 94% yield. The two new C-H bonds are formed simultaneously from H atoms absorbed into the metal surface Pd/C. The reaction is stereospecific giving only the *syn* addition product. ^{1}H NMR showed that hydrogenation was successful and the expected twenty protons were observed in the correct ratios with the expected splitting patterns. Mass spectrometry showed the mass ion of the desired product.

4.3.1. Developing HPLC method to monitor ring closure reaction by PPA

The route of cyclodehydration of the carboxylic acid **13** to form the ketone **14** was developed by Shiraishi *et al.* where a mixture of **13** and PPA (1:25) mass/mass was heated at 100°C for 12 hours and then the mixture was poured into ice and water to give a yield of 67% of the ketone **14**.[224] Ikemoto and co-workers, followed the same method suggested by Shiraishi *et al.* but as the preparation was on a larger scale they increased the ratio of the reactant to 1:30 mass/mass.[226] In addition, Junker *et al.* reported the ring closure of arylpentanoic acid **13** following Shiraishi and co-workers method.[229] However, in this work only 35% yield of ketone **14** resulted following the given reaction conditions. The yield even dropped to 25% after 23 h at 100 °C and neither an increase of the reaction temperature nor extension of the reaction time further increased the yield. Since all attempts to improve the yield by more forcing conditions failed, a PPA promoted cyclization under milder conditions was performed: the temperature during the conversion was kept at 80–95 °C, the amount of PPA was 300 g per 0.1 mol and the reaction was stopped after 30 min. This protocol led to the reproducible formation of **14** in 60% yield.[229]

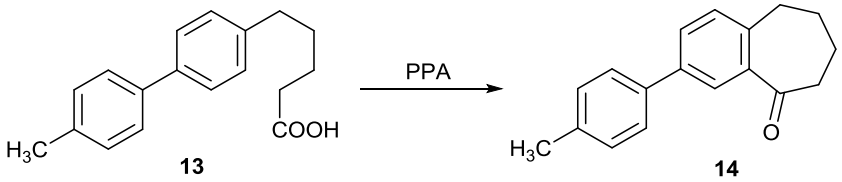

13 **14**

Scheme 15 Cyclisation of compound **13** using PPA to form compound **14**

In this work the cyclisation step to form compound **14,** has been performed using several different conditions in order to obtain the desired product. Temperature was varied from 25ºC to 300ºC and time of the reaction varied up to 3 days. Ratio (mass/mass) of the reactants also varied from 1:20 to 1:300 of polyphosphoric acid PPA, and that showed no improvement in obtaining good yields of the desired product. In most of these procedures the acid used was a polyphosphoric acid as acylation and cyclisation agent following the method of Ikemoto *et al*.[226] The PPA is a good solvent for many organic compounds especially in the synthesis of these organic compounds and very effective in alkylation, acid-catalyzed reactions as well as in acylation and cyclisation as previously mentioned. Furthermore, PPA can be used in other reactions such as dehydration, rearrangement and synthesis of nitrogen containing heterocycles and also in synthesis of polymers.[230] Strong acid has been tested such as sulphuric acid but the extraction was difficult to perform. Different conditions were applied to examine the effect on the result such as changing the temperature and heating time.

Microwave heating was used in an attempt to facilitate more rapid reaction and PPA used again with the temperature at 120ºC and TLC analysis was conducted every 30 minutes. In the first 30 minutes a light spot appeared in the middle of the TLC plate so temperature was increased to 200°C in an attempt to produce more of this compound (assumed to be product) but this high temperature caused degradation of the desired product.

Since all attempts to improve the yield by forcing conditions failed, the PPA promoted cyclization was monitored by high performance liquid chromatography (HPLC). To monitor this reaction a method of suitable solvents was developed as eleuent, MeCN/water (0.1% TFA). The temperature during the conversion was kept at 90–95 °C and the amount of PPA was 300 g per 0.1 g. This protocol led to the

reproducible formation of benzosuberone **14** in 78% yield, even on a large scale (up to 20 g) although monitoring of the reaction was necessary to select the optimum time to completion. The peak showing a retention time of 11 minutes corresponds to the starting material **13** that is consumed in the conversion to the desired product **14**.

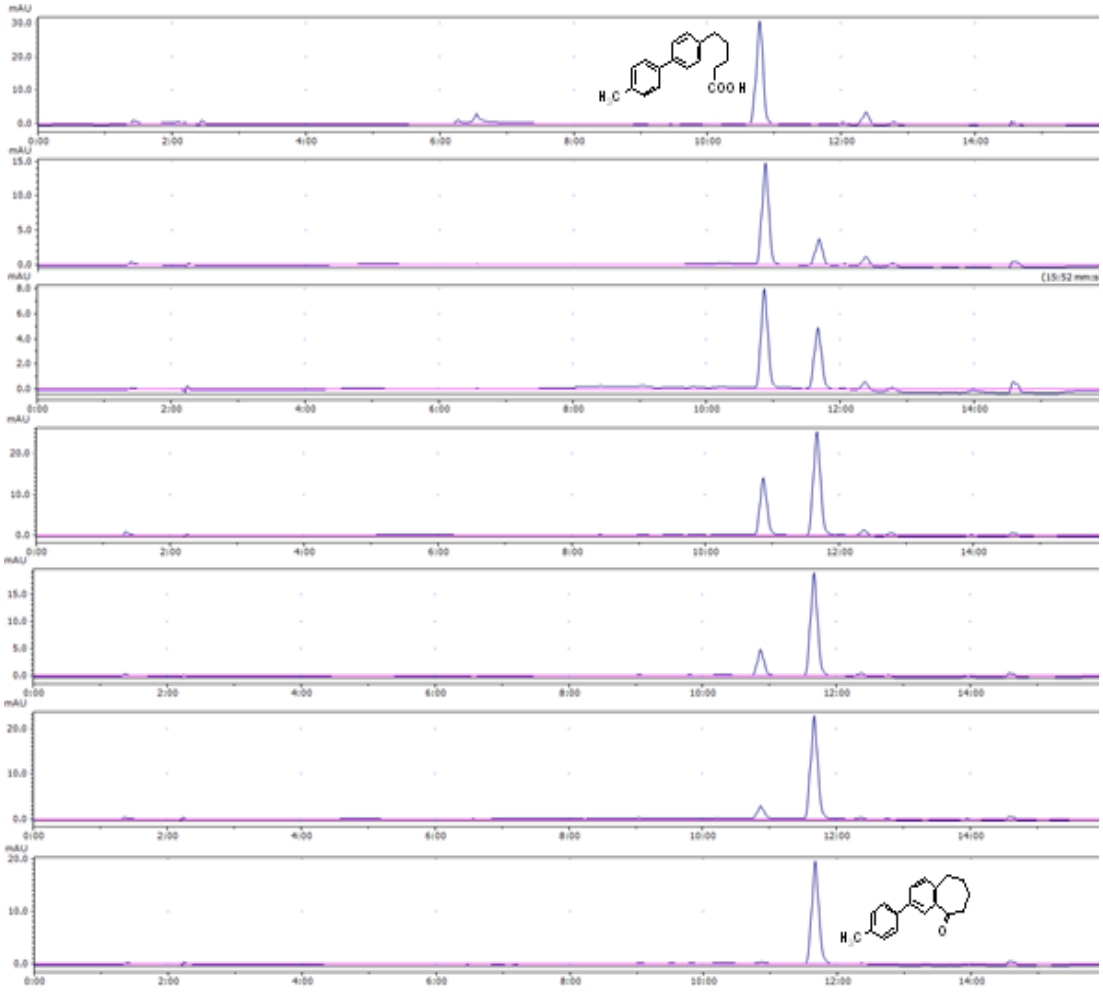

Figure 37 Formation of compound **14** shown using HPLC with eluent solvent system: MeCN/water (0.1% TFA)

Analysis of compound **14** using ^{1}H NMR and mass spectrometry have confirmed the closure of the ring forming cycloheptane ring derivative. Elemental analysis using CHN combustion analysis matched with the expected values.

4.3.2. Formation of compound 18

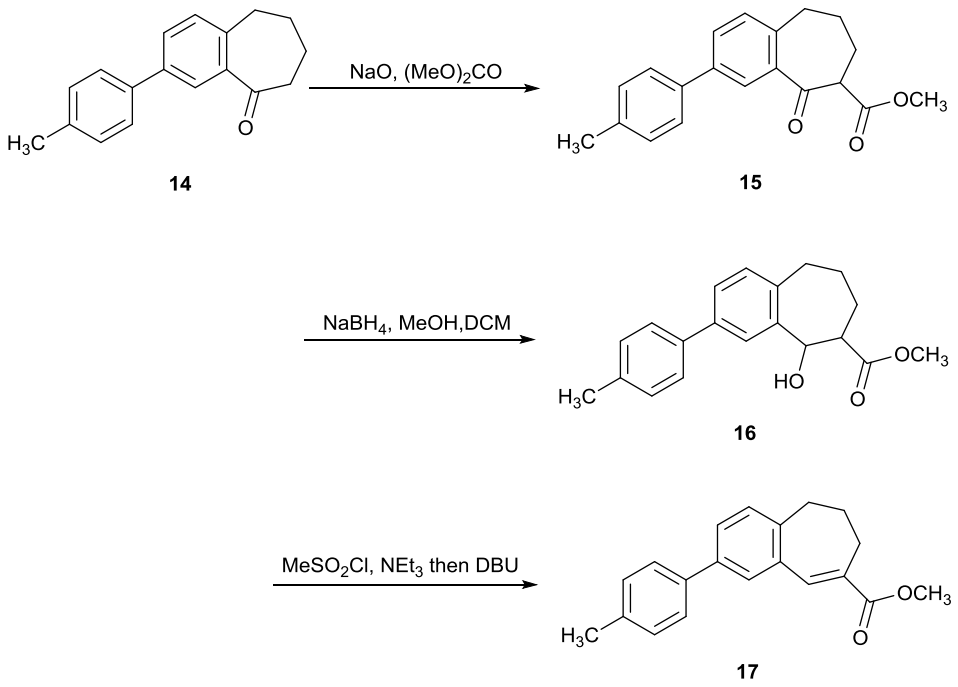

Scheme 16 Formation of compounds **15**, **16** and **17**

In the first reaction, Claisen ester condensation of ketone **14** with dimethyl carbonate and NaH led to the formation of the β-keto ester **15** in 80% yield. β-keto ester **15** was prepared using a suspension of **14** in dimethyl carbonate and heated to reflux under a nitrogen atmosphere. To obtain the pure product, the crude mixture of this reaction was purified through a flash/plug column. using petroleum ether: EtOAc (8:2) (R_f 0.26). Pure compound **15** was analysed using ^{1}H NMR and the additional methyl group in the product can be seen with the 3 protons in the alkyl region. Reduction of **15** was performed with $NaBH_4$ in MeOH at −20 °C to −10 °C which afforded a mixture of the desired product and some impurities.[231] Conditions for chromatographic purification were obtained via TLC which gave the best separation using hexane: ethyl acetate (8:2) (R_f 0.33), to give pure β-hydroxy ester **16** in 72% yield. Elimination of H_2O from secondary alcohol **16** by reaction with methane sulfonyl chloride and subsequent treatment with DBU gave α, β-unsaturated ester **17** in 68% yield. Analysis by ^{1}H NMR and MS for α, β-unsaturated ester **17** confirmed that elimination of H_2O had taken place to form the desired product **17**

which was hydrolysed using 5M NaOH and methanol. The reaction mixture was treated with concentrated HCl to precipitate the desired product **18**.

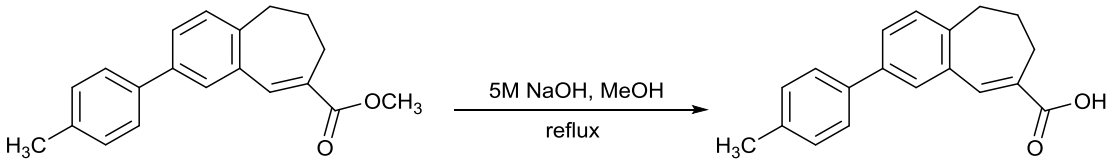

17 **18**

Scheme 17 Hydrolyses of compound **17** to form compound **18**

4.4. ^{68}Ga radiolabelling to form a potential CCR5 PET imaging agent

Having successfully synthesised a derivative of the chemokine receptor CCR5 antagonist TAK-779, it can now be modified for radiolabelling and its biological properties were evaluated. The next step in this research, is to attach the CCR5 targeting structure to one of the most common chelator for radiometal labelling, DOTA, in prior to be radiolabelled with ^{68}Ga to be investigated as a novel PET imaging agent for CCR5.

4.4.1. Conjugation to DOTA derivative

For ^{68}Ga complexation, cyclen (1,4,7,10-tetraazacyclododecane) based BFCs are a popular choice due to the widespread use of DOTA (1,4,7,10-tetraazacyclododecane-1,4,7,10-tetraacetic acid) based ligands in various applications from targeted MRI contrast agents to radio immunotherapy, dependent on metal ion selection, see Figure 38.[232] Bioconjugation of DOTA derivatives to different biomolecules, has been investigated by many groups worldwide; the simple variation of the stable metal to ^{68}Ga is a natural transition into PET radiochemistry.[233] However, complex formation is generally slow due to the preorganisation of DOTA means that usually conventional or microwave heat is required, limiting its use to non-heat sensitive biomolecules.[234, 235]

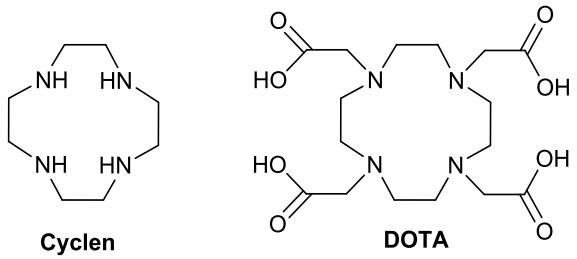

Figure 38 Chemical structure of cyclen and DOTA

The attachment of DOTA with a spacer included to the CCR5 antagonist TAK-779 derivative compound **18** will produce a functionalised ligand with targeting and diagnostic properties with high potential to be radiolabelled with ^{68}Ga.

Methods will focus on the formation of amide bonds for conjugation, a widely used functionality. The formation of an amide bond by reacting an amine and a carboxylic acid (initially forming a salt) is a common feature in both many synthetic and natural molecules. This reaction has been used in many areas of organic, bioinorganic and medicinal chemistry but most notably in peptide synthesis. The formation of amide bonds usually relies on activation of the acidic moiety, achieved with a wide variety of coupling reagents, followed by aminolysis with the amine functionality. The scope of methods involving amide bond formation is large and a thorough review of the topic was carried out by Montalbetti *et al.*[236]

To form the amide bond to obtain compound **19** see Scheme 18, reaction has been carried out in anhydrous DMF where compound **18** was dissolved together with carbonyldimidazole CDI as the coupling agent. The mixture was heated at 60^{o}C for 10 min and then cooled to room temperature. After that, the mixture was set under vacuum for 10 min. DO3A with the spacer ethyl amine (synthesised and supplied by Alicja Kownacka) was dissolved in DMF and added rapidly to the mixture. The reaction was allowed to stir for 24h at room temperature then DMF was removed under reduced pressure and the resulting solid was extracted in DCM to yield the desired product **19**.

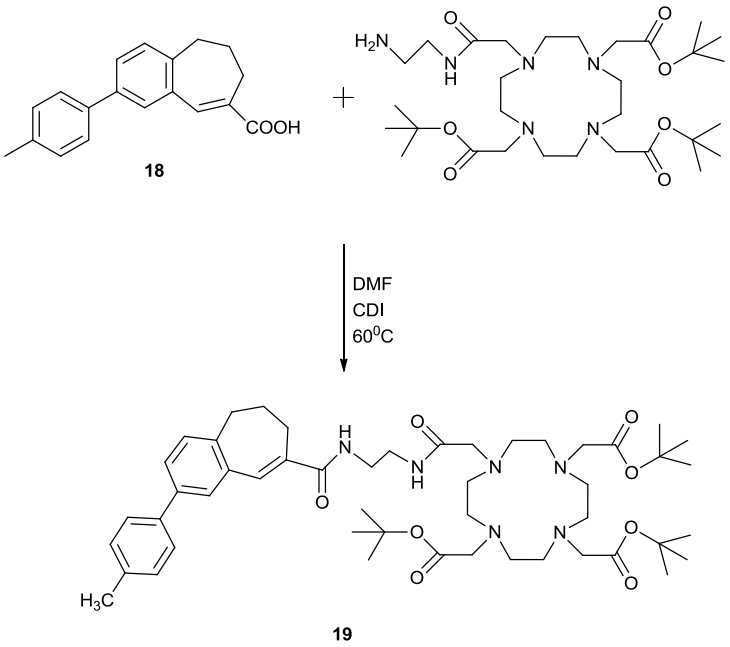

Scheme 18 Amide formation between DO3A with spacer arm and compound **18** to form compound **19**

For compound **19**, analysis of high resolution mass spectrum HRMS confirmed the formation of amide bond and isolation of the desired product. Deprotection of **19** was initially carried out by dissolving the compound in DCM and TFA which was added dropwise to the mixture, stirred overnight, and the solvents were then removed under reduced pressure. Finally, the product was dissolved in a minimal amount of methanol and added dropwise to diethyl ether where white crystals precipitated. The white powder was collected by centrifugation, re-dissolved in water for transfer and then freeze dried to give the desired product **20**, see Scheme 19.

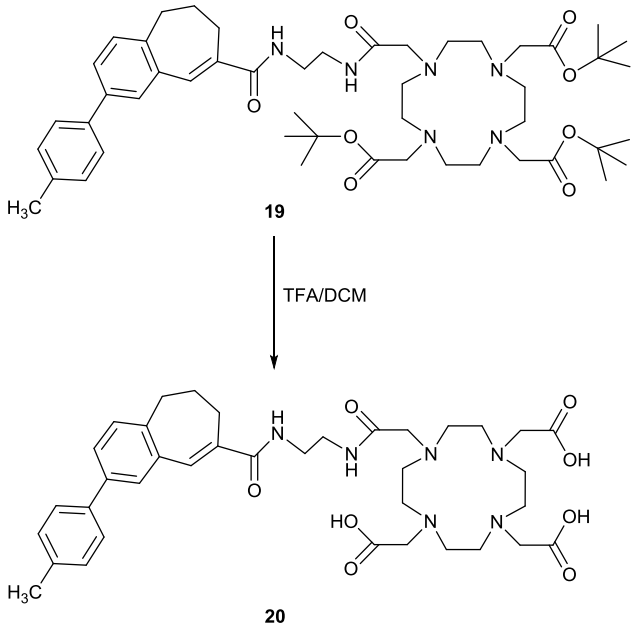

Scheme 19 Deprotection reaction to form ligand **20**

HPLC showed that this reaction yielded about 65% of the desired product. As it can be seen from the following chart see Figure 39, that the product was not pure. The four regions appeared in HPLC chart were analysed by mass spectrometry and was found that region 3 corresponded to the molecular weight of the desired product. Hence, isolation of the compound appearing in region 3 was carried out using semi-prep HPLC with acetonitrile: 0.2M Acetate buffer pH=5.0 as eluent using a gradient of acetonitrile: 30-50% for 30 min, to give single pure product as shown in Figure 40. The isolated pure product has a retention time of about 12.35 minutes that will be

compared with retention time of the complex formed between **20** Ga^{3+} to determine conditions for purification of the radiolabelled compound.

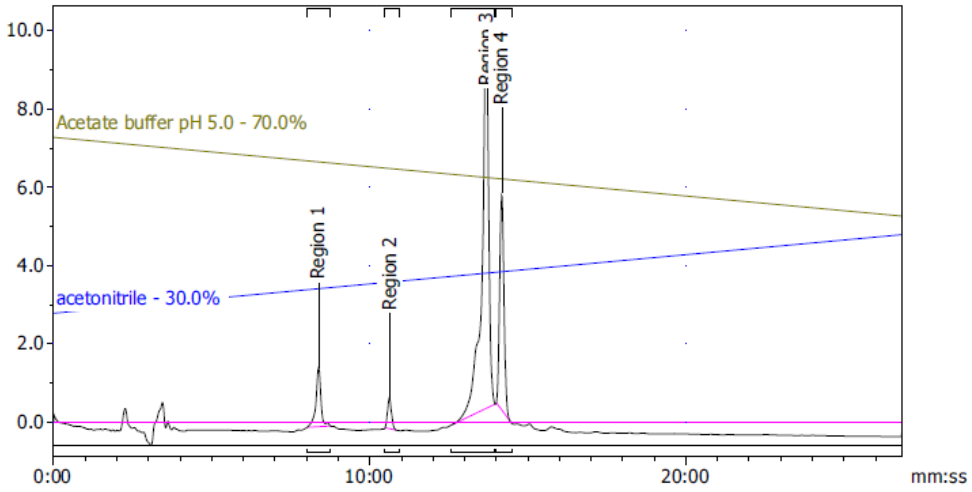

Regions: DA-B@254nm Detector:

Name	Start (mm:ss)	End (mm:ss)	Retention (mm:ss)	Area (mAU·s)	%ROI (%)	%Total (%)
Region 1	8:01	8:46	8:23	16.5	7.47	N/A
Region 2	10:29	10:55	10:38	6.9	3.13	N/A
Region 3	12:35	13:58	13:41	144.1	65.36	N/A
Region 4	14:00	14:29	14:11	53.0	24.04	N/A
4 Peaks				220.4	100.00	N/A

Figure 39 HPLC chart of compound **20** with some impurity

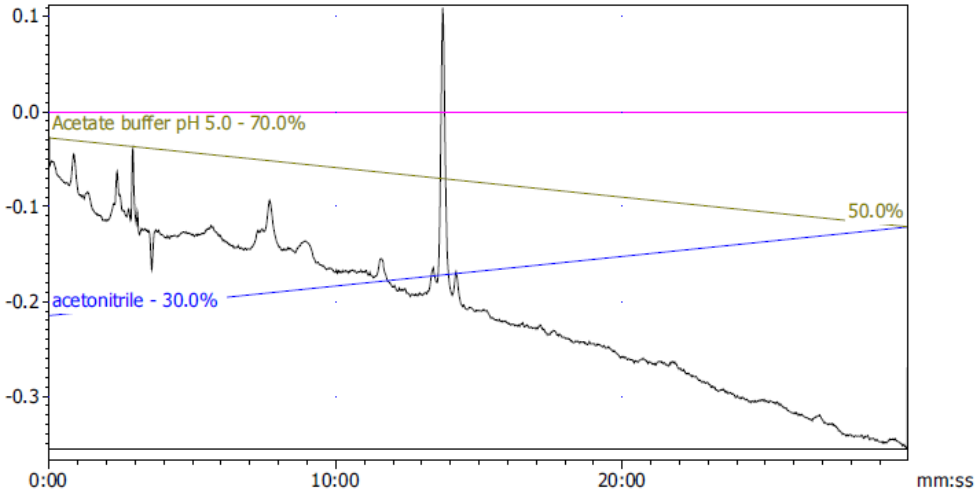

Figure 40 HPLC chart of isolated pure compound **20**

Compound **20** was complexed with $^{69/71}$Ga (cold standard) which can be useful for two reasons. The first is to determine the conditions for the formation of $^{69/71}$Ga complex that can be translated to ^{68}Ga radiolabelling. The secondly is to provide cold standards of $^{69/71}$Ga complexes are needed for HPLC identification of radiolabelled species.

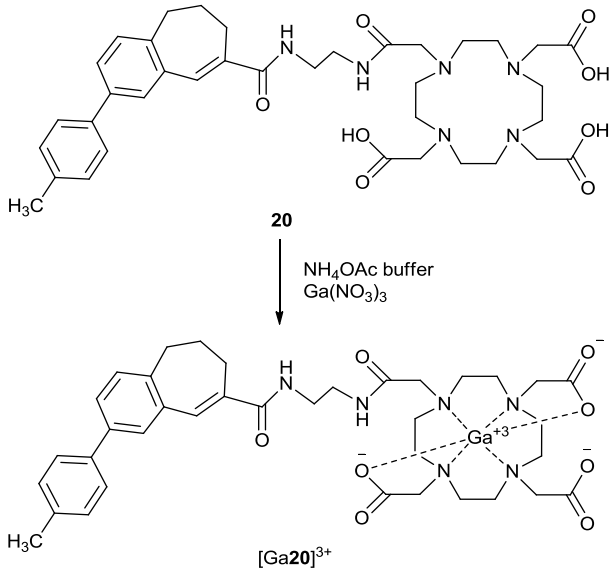

Scheme 20 Formation of $^{69/71}$Ga complex with ligand **20**

The reaction to produce the $^{69/71}$Ga complex [Ga**20**] $^{3+}$ was carried out using gallium(III) nitrate hydrate in ratio (1:1.05) ligand to $Ga(NO_3)_3.H_2O$, see Scheme 20. The reaction proceeded for 2 h at 95ºC and the formation of [Ga**20**] $^{3+}$ was determined using HPLC. Comparison of the HPLC chart of the ligand **20** with the complex [Ga**20**]$^{3+}$ gives the cold standard for radiochemistry, with a shift of the product peak retention time from 12.35 minutes for **20** to 2.12 minutes for [Ga**20**]$^{3+}$ as show in Figure 41. HPLC of the cold standard confirms that, the reaction is complete because the starting material has disappeared. However, any HPLC conditions attempted gave the product at the solvent front. This is the same retention time as 'free' gallium-68. This means that these conditions are not ideal for analysis of the radiochemistry by HPLC and it was instead carried out by radio-TLC.

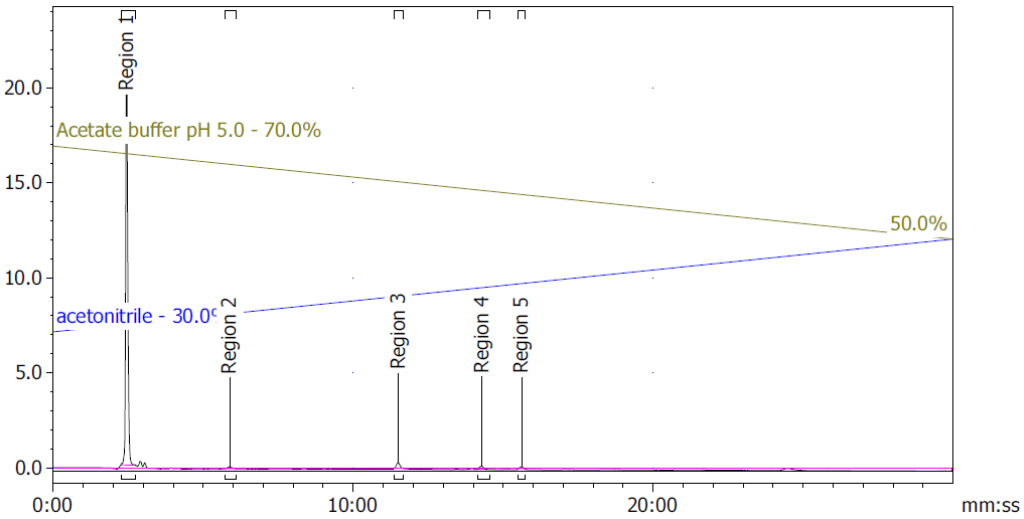

Figure 41 HPLC chart of cold standard product [Ga**20**]$^{3+}$

4.4.1. ^{68}Ga radiolabelling of compound 20

Once the cold standards had been successfully synthesised, the ligand **20** could be radiolabelled and analysed. The comparatively short half-life (68 minutes) and its production by radioactive decay of a parent isotope, have made ^{68}Ga unusual as a metallic PET radioisotope.[87] As a parent isotope, ^{68}Ge has ideal characteristics for generator production, with a half-life of 271 days, ^{68}Ge decays to ^{68}Ga to give a daily supply of the isotope from the generator.[95]

Literature reports of ^{68}Ga radiolabelling of DOTA type chelators gives some general indications of the best conditions for successful synthesis. When testing and comparing a new chelator, Blower *et al.* performed the radiolabelling reaction with a series of different concentrations for both the novel chelator and as a comparison also investigated the labelling of standard chelators under the same conditions.[237] This work demonstrated that DOTA could be radiolabelled at 100 ºC at pH 5 for 30 minutes at 10 µM ligand concentration. However, lowering the concentration to 1 µM gave yields lower than 10% in their work.

Ferreira *et al*. performed a similar study to determine optimal conditions for radiolabelling a range of chelators.[238] Showing that a C-functionalised DOTA

derivative is radiolabelled at more than 90% yield at 80ºC for 5 minutes at 10 µM ligand concentration, room temperature for 30 minutes gave similar yields of 88%. Similar conditions to those reported were selected for initial labelling reactions. The crude mixture of ligand **20** (65% pure), see Figure 39, was radiolabelled with ^{68}Ga as a proof of principle before moving on to purify the starting material and radiolabel the pure material, see Scheme 21.

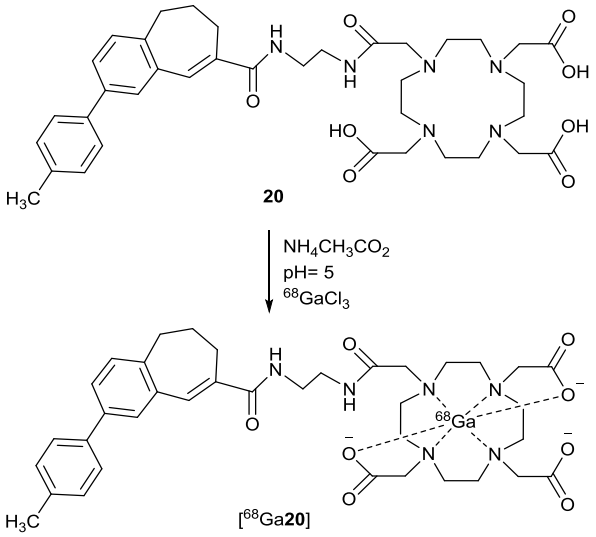

Scheme 21 ^{68}Ga radiolabelling of **20** to form [^{68}Ga**20**]

Gallium-68 was eluted from ^{68}Ge/^{68}Ga generator to give activity of 321 MBq. The radioactivity was collected in 3mL which was diluted in 15 mL of water and filtered through a purification cartridge to remove the impurities (such as ^{68}Ge and other metals). The trapped activity from the cartridge was transferred to the HPLC vial with in a volume of 1 mL using a mixture of acetone:HCl (98:2). The 1 mL of activity was split per two HPLC vials and the solvents were dried under argon flow. Then, 200uL of each of the two stock solutions of **20** (concentration 1mg/mL and 0.5mg/mL) were added to the vials with the activity. Radiochemical complexation reactions were analysed by radio-TLC, eluting with 0.2 M citric acid, free ^{68}Ga forms gallium citrate and is expected to appear in the solvent front (on the right of the TLC scan trace) and the product(s) come near baseline, see Figure 42, indicating that, successful complex formation has occurred to give [^{68}Ga**20**] . Based on the

chromatogram presented below, we can clearly see that that all free gallium-68 has been consumed.

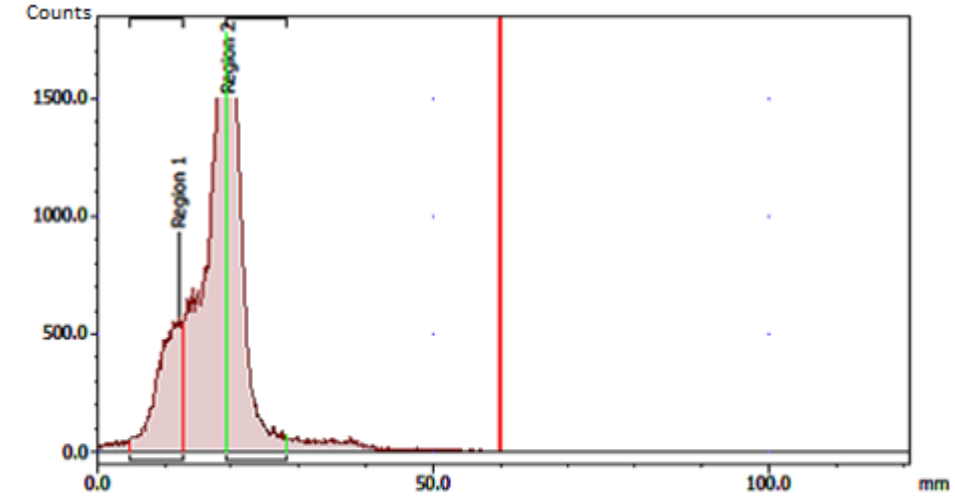

Regions: Ga-68

Name	Start (mm)	End (mm)	Retention (RF)	Area (Counts)	%ROI (%)	%Total (%)
Region 1	4.8	12.8	0.203	11850.4	31.91	16.41
Region 2	19.2	28.0	0.327	25281.7	68.09	35.01
2 Peaks				37132.0	100.00	51.42

Figure 42 Example of radio-TLC used to analyse [^{68}Ga**20**]

Compound **20** radiolabelled with ^{68}Ga at 90 ^{o}C was studied for stability under conditions relevant to *in vivo* applications. The experiments were conducted in PBS and in competition with a protein species which can complex gallium(III), transferrin.[225] The experiments were carried out at physiological temperature (37 ^{o}C) and were performed on the longest timescale that still gave informative data by radio-TLC (3 hours).The stability study on [^{68}Ga**20**] showed no dissociation of gallium from first until third hour of incubation in either PBS and transferrin at two different concentrations of [^{68}Ga**20**].

4.5. Biological evaluation of compounds of CCR5 antagonist

The synthesized CCR5 antagonist, the derivatives of TAK-779 (**11-14 & 18**) and ligand **20** were tested for their cytotoxicity, calcium signalling and anti-HIV properties. These experiments were carried out by the group of Prof Dominique Scholas at the Rega Institute for Medical Research, Katholieke Universiteit in Leuven, Belgium. Further data is still awaited at the time of thesis submission hence full conclusions cannot yet be drawn on the biological properties and potential for targeting the CCR5 chemokine receptor *in vivo* using this series of compounds.

The TZM-bl cell line (HeLa-cell derivatives that express high levels of CD4 and both co-receptors CXCR4 and CCR5)[85] was used to investigate the cytotoxicity and calcium signalling assay. For anti-HIV assay, they again used the TZM-bl cell line and strain, HIV-1 Bal. Here, the assay results were compared with the published value of the known and medicinal applicable CCR5 antagonist, maraviroc.

The CC_{50} and EC_{50} values of the selected compounds of TAK-779 derivatives (**11-14, 18**), ligand **20** and maraviroc are summarised in Table 5. The compounds **11-14, 18** are less effective than maraviroc with **13** the only compound that achieved a reasonable potency at target. The data for the conjugate compound and the cold standard compound containing the gallium ion have not yet been obtained although there is some concern that the modification of the TAK779 has disrupted the receptor binding. The full set of data is required before conclusions can be drawn from this data and further targets for investigation determined.

Sample	Cytotoxicity CC_{50} [a] (nM)	Anti-HIV EC_{50} [b] (nM)	Calcium signalling IC_{50} [c]
11	43000	>43000	AD
12	3750	3500	AD
13	1710	300	AD
14	63000	>63000	AD
18	1760	28000	AD
20	AD	AD	AD
maraviroc	>1000	0.0039	AD

Table 5 Cytotoxicity, Anti-HIV activity and calcium signalling for TAK-779 derivatives in TZM-bl cells., [a] (CC_{50}) is average concentration required to have a cytotoxic effect reducing TZM-bl cell viability by 50%. [b] (EC_{50}) average effective concentration to reduce the HIV-induced cytopathic effect by 50% in TZM-bl cells.). [c] IC_{50} (calcium signalling) concentration required to reduce the level of Ca^{2+} ions observed during a 'normal' signalling process by 50%. AD awaiting data

4.6. Conclusion

A modified synthetic pathway was developed to obtain a derivative of small molecule CCR5 antagonist, TAK-779, containing carboxylic acid group including an HPLC method to monitor the formation of compound **14**. Compound **18** containing the carboxylic acid functional group, has been successfully synthesised and fully characterised.

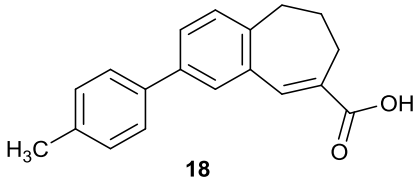

18

In the next stage of the work, compound **18** was successfully attached to a DOTA macrocycle via a bisamino spacer group through a formation of amide bond and the isolation of that compound was confirmed by mass spectrometry showing formation of **19**. Complex formation of **19** with Ga^{3+} (cold standard) was developed and the product characterised by mass spectrometry with the purity of [Ga**20**] determined by HPLC. **19** was then radiolabelled with $^{68}Ga^{3+}$ and its stability in PBS and a solution of transferrin investigated. Finally, biological assays including cytotoxicity, anti-HIV and calsium signalling were evaluated for compounds **11**, **12**, **13**, **14**, **18**, and **20**. Unfortunately the complete data set is not yet available but only compound **13** showed submicromolar potency in any of the assays investigated. This indicates that further work may be required to modify the TAK779 conjugate structure to increase CCR5 receptor affinity.

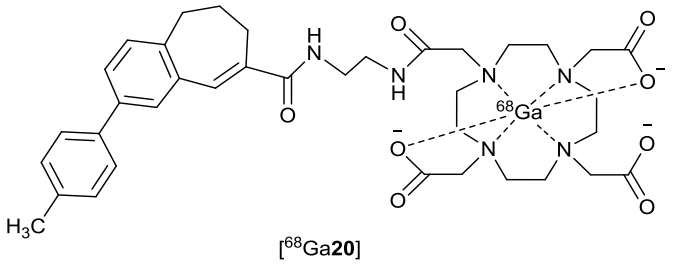

[^{68}Ga**20**]

Chapter Five

Conclusions and Future Work

5. Conclusions and Future Work

5.1 Main achievements

The development of molecular medical imaging agents has received considerable attention in recent years for a wide range of diagnostic applications and to monitor therapeutic response, particularly for cancer. Targeting the chemokine receptors CXCR4 and CCR5 could provide new tools for early diagnosis as well as validating potential new routes to treat cancer. This study aimed to develop novel CXCR4 and CCR5 imaging agents for application in positron emission tomography imaging. Macrocyclic chelators feature extensively in the literature for molecular targeting of the chemokine receptor CXCR4. However, one of the main issues limiting the application of the metal complexes is their stability. The structural reinforcement present in the compounds discussed in this work can counteract this limitation and also offer additional advantages in optimising the coordination interaction with the protein target.

This work reports the development of a synthetic route to obtain a configurationally restricted analogue of the licenced CXCR4 antagonist, AMD3100. Cyclam is a key main component of AMD3100. It has been demonstrated that, cyclam can adopt six different configurations when it is bound to a first row transition metal ion. Moreover, the configurations (or a subset of them) are in equilibrium in solution. The hypothesis that configurational fixing would optimise target receptor binding is an extension of work within the Archibald group which established that fixing the configuration to *trans II* or *cis V* enhances both the binding affinity and the residence time of the macrocyclic compounds to the CXCR4 receptor relative to AMD3100. In addition, metal complexes of the macrocyclic chelators showed enhanced stability.

Synthetic pathways to obtain series of novel metal complexes (copper(II), zinc(II) and nickel(II)) of mono and bismacrocycles fixed to an alternate configuration (*trans IV*) were developed. As indicated, restriction of the configuration of the macrocyclic compounds is important because it ensures that the binding to the receptor in a single configuration so the most biologically active configuration can be identified and used for receptor targeting.

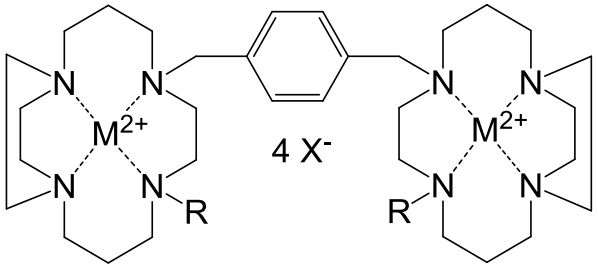

Figure 43 Chemical structure of novel *trans IV* metal bicyclam complex produced in this work

A novel mixed metal $[ZnCu\mathbf{6}]^{4+}$ complex fixed to *trans II* configuration (expanding on the previous work with homo dinuclear metal complexes of this chelator) was successfully synthesised in an 85% yield, see Figure 44

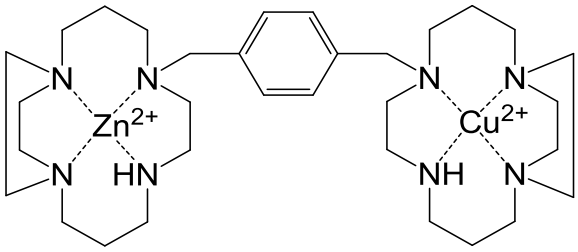

Figure 44 Chemical structure of novel *trans II* mixed metals bicyclam complex produced in this work

The research reported in chapter three was towards the development of a novel radiolabelled CXCR4 compoundto be used as a PET imaging agent. Novel CXCR4 targeting copper(II), zinc(II) and nickel(II) complexes restricted to either *trans II* or *trans IV* configurations were evaluated using *in vitro* biological assays. Their ability to target the chemokine receptor CXCR4 was analysed using a series of assays to determine the compound that would be selected for radiolabelling with the ^{64}Cu isotope for subsequent assessment of its potential to be used as a PET imaging agent. The assays included a displacement assay with an anti-CXCR4 antibody, and anti-HIV infection assay, cytotoxicity assessment and the potential to Ca^{2+} flux on signalling using the natural ligand CXCL12. The *trans IV* complexes $[Zn_2\mathbf{9}]^{4+}$ and $[Zn_2\mathbf{10}]^{4+}$ have EC_{50} values of 516 and 247 nM respectively in the anti-viral assay and showed low toxicity in MT-4 cell line tested with CC_{50} values of 42800 and

39600 nM respectively. The novel mixed metal *trans II* complex $[ZnCu\mathbf{6}]^{4+}$ showed higher binding affinity than the *trans IV* complexes with an EC_{50} value of 3 nM in the anti-viral assay, four times more potent than AMD3100 with low cytotoxicity (CC_{50} of 102178 nM). This data indicates that the *trans IV* configuration is not the optimum configuration to bind to the chemokine receptor CXCR4. The high affinity $[ZnCu\mathbf{6}]^{4+}$ complex was successfully radiolabelled with ^{64}Cu *via* transmetallation using $[Zn_2\mathbf{6}]^{4+}$ see Figure 45. A crude radiochemical yield (crude-RCY) of 92% was achieved for the formation of $[^{64}CuZn\mathbf{6}]^{4+}$.

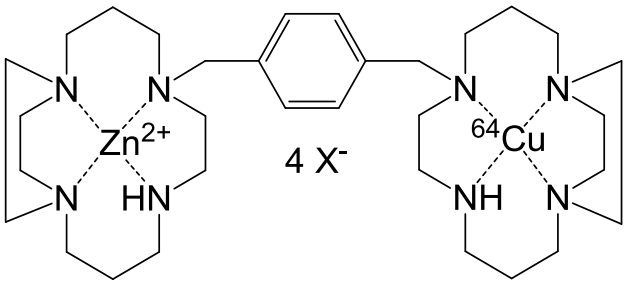

Figure 45 Chemical structure of novel ^{64}Cu radiolabel *trans II* $[^{64}CuZn\mathbf{6}]^{4+}$

Overall, a series of *trans IV* compounds were synthesised (using a reproducible route to produce the compound in good yields), see Figure 43, with a varying degree of steric bulk and demonstrated to have lower affinity for the CXCR4 chemokine receptor than the previously synthesised *trans II* and *cis V* complexes. Whilst this aspect of the research work has not identified any novel lead compounds for targeting the CXCR4 chemokine receptor it clearly supports the hypothesis that configurational fixing has significant impact on the binding process. It also gives further insight into the key structure activity relationships that are important for design and optimisation of this compound class.

The research presented in chapter four is towards the development of an imaging agent for targeted imaging of the chemokine receptor CCR5. A modified synthetic pathway was used to obtain a derivative of known small molecule CCR5 antagonist, TAK-779, containing a carboxylic acid functional group. An HPLC method was developed to monitor the formation of compound **14** which was highly

problematic to synthesise as the reaction time is variable and the product decomposes as it forms. Compound **18** was successfully synthesised for conjugation to a chelator for radiolabelling with gallium-68. A derivative of DO3A with a spacer group that has primary amine terminal group (tri-tert-butyl 2,2',2''-(10-(2-((2-aminoethyl)amino)-2-oxoethyl)-1,4,7,10-tetraazacyclododecane-1,4,7-triyl)triacetate), was successfully conjugated to compound **18** forming **20** with the two components linked *via* an amide bond. Complex formation of **20** with Ga^{3+} (to form a cold standard) was developed and the HPLC retention time of [Ga**20**]$^{3+}$ was determined. Radiolabelling of **20** with ^{68}Ga was successfully carried and the product identified by analogy with the cold standard, see Figure 46. A crude radiochemical yield (crude RCY) of ca, 100% was achieved for [^{68}Ga**20**]$^{3+}$ and it was demonstrated that the compound is stable in competition with transferrin over four hours. The initial biological assay studies indicated that there are potential issues with the disruption of the binding interactions in the molecular design of the conjugate. Affinity of the new compounds for the CCR5 receptor is considerably lower than the parent structure of TAK779. This would need to be addressed through optimised molecular design before the construct could be taken further into PET imaging studies. Further biological characterisation is also required to determine impact of the chelator moiety on the targeting and surface interactions with the protein.

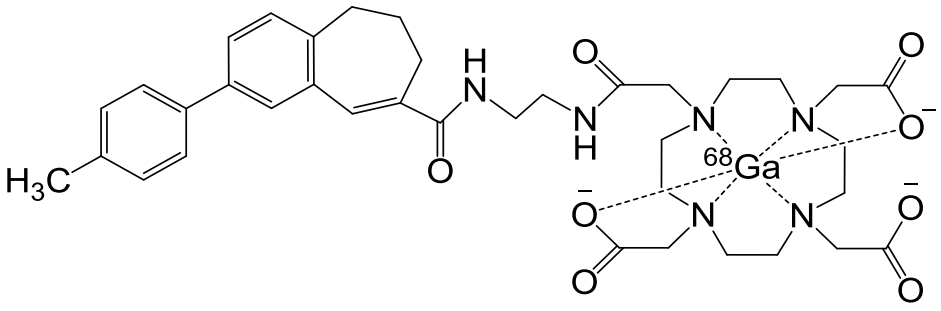

Figure 46 Chemical structure of novel PET-CCR5 imaging agent [^{68}Ga**20**]$^{3+}$

5.2 Future work

1. Developing a synthetic route to obtain *trans I* and *trans III* configurationally restricted macrocyclic transition metal complexes. Evaluation of their biological activity of binding to the chemokine receptor CXCR4 to further elucidate structure activity relationships.

2. Developing asynthetic pathway to obtain mixed configuration macrocyclic compounds as shown in Figure 47. This approach can be used to evaluate whether each binding group (assuming one protein residue interaction for each macrocyclic complex unit) has a different optimal configuration.

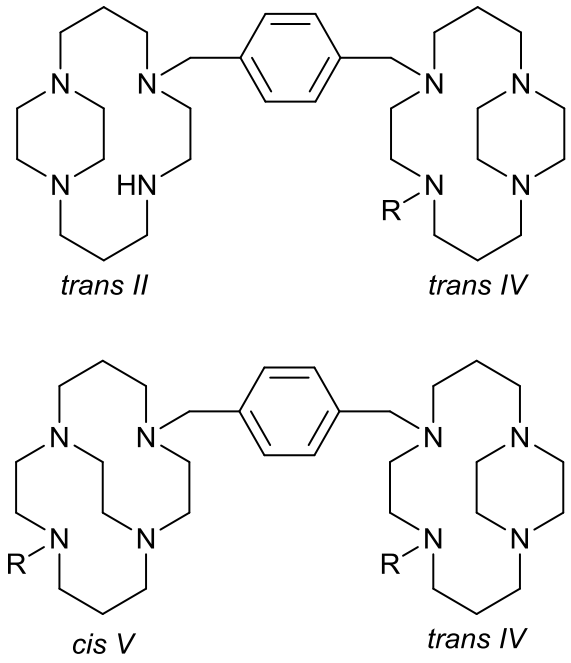

Figure 47 Two examples of proposed asymmetrical bis-macrocyclic compounds

3. As the macrocyclic transition metal complexes lack oral bioavailability, improving delivery of them could be achieved by encapsulating them into liposomal or biomaterial derived delivery vehicles such as viral nanoparticles or sporopollenin exines. This would be ideal for therapeutic applications rather than diagnostic applications but could be optimised using radiolabelled derivatives.

4. Development of a CXCR4/CCR5 dual antagonist could be achieved by combining components derived from TAK779 (small molecule cycloheptane derivatives) as a CCR5 antagonist, with CXCR4 binding macrocyclic derivatives to give compounds of the type shown in Figure 48. Improved binding of the CCR5 component would need to be achieved for this strategy to be successful and multiple macrocyclic ring components could be attached to improve CXCR4 binding. Biological assays would allow structure activity optimisation. There is significant interest in cancer imaging in more general profiling of the chemokine receptor expression which could be achieved with these molecules.

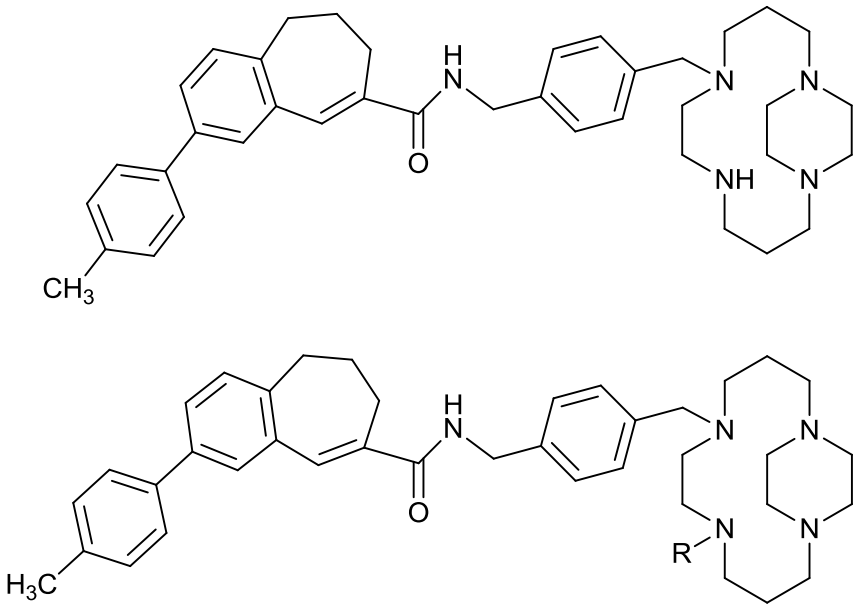

Figure 48 Two examples of proposed CXCR4/CCR5 dual antagonist

Chapter Six

Experimental

6. Experimental

6.1. General methods for synthetic experiments

6.1.1. General Methods

Bulk solvent was removed by rotary evaporation under reduced pressure and trace solvent was removed by a vacuum pump. Reactions were run at room temperature (RT) unless otherwise stated. All metal containing compounds were purified *via* size exclusion chromatography through Sephadex LH20, which was pre-soaked in methanol for over three hours. The complexes were dissolved in the minimum amount of methanol then added onto the column containing the pre-soaked Sephadex LH20.

6.1.2. Instrumentation

6.1.2.1. NMR spectroscopy

^{1}H NMR and ^{13}C NMR were obtained using a Jeol JNMLA400 spectrometer at 400 MHz for ^{1}H NMR and 100 MHz for ^{13}C NMR referenced against standard internal TMS or residual non deuterated solvent signal. Splitting patterns are designated as *s* (singlet), *d* (doublet), *t* (triplet), *q* (quartet), *quin* (quintet), *m* (multiplet), *dt* (double triplet) and *br* (broad). Chemical shifts (δ) are quoted in parts per million (ppm). Deuterated solvents were purchased from either Goss chemicals Ltd or Cambridge Isotopes Ltd.

6.1.2.2. MS

Electrospray mass spectra were rerecorded at the University of Hull using Finnigan MAT 900 XLT using electrospray ionisation (ESI). Accurate mass spectrometry measurements (HRMS) were recorded at the EPSRC National Mass Spectrometry Service Centre at the University of Swansea using a LQT Orbitrap XL.

6.1.2.3. CHN

CHN analysis was performed using a CHN analyser EA1108 (Carlo Erba). Most compounds were within the limit of 0.4% of the expected ratios.

6.1.3. Materials

Solvents were used as received, apart from when dry solvents were required. Solvents Solvents were dried over activated (oven dried at 300 °C for 18 hours) 3 Å molecular sieves following literature method outlined by Bradley and co-workers.[239] Acetonitrile (MeCN), dichloromethane (DCM) tetrahydrofuran (THF) and methanol (MeOH) were dried over molecular sieves, following activation at 300ºC for 18 h. Chemicals were used as purchased from Sigma-Aldrich, Fisher, Acros, Novabiochem, CheMatech, Goss and Strem. Chemicals were used as received without further purification.

6.2. High performance liquid chromatography (HPLC)

High performance liquid chromatography was carried out using either an Agilent 1200 series or an Agilent 1100 series using a Phenomenex Gemini 5 µ C18 110 Å, 150 x 4.60 mm column at 1 ml/min. Both equipped with a UV detector (series G1314A) and a NaI radiodetector. Data was recorded using Lablogic Laura (version 4.1.13.91).

6.2.1 Standard HPLC methods

Method 1: (a) acetonitrile 0.1% TFA (b) ammonium acetate buffer (0.2 M, pH 5); Gradient from 100% (b) to 0% (b) over 30 minutes.

Method 2: (a) acetonitrile (b) ammonium acetate buffer (0.2 M, pH 5); Gradient from 30% (a) to 50% (a) over 30 minutes.

6.3. Radio-thin layer chromatography (radio-TLC)

Radio-TLCs were run on ‘neutral alumina sheets’ (Merck USA), eluting with H_2O : MeOH (95:5) saturated with NaCl. Radio-TLC was carried out using a Lablogic Scan-Ram, equipped with a NaI detector at a scanning speed of 10mm/min. Data was recorded using Lablogic Laura (version 4.1.7.70).

6.4. Experimental Section

6.4.1. Synthesis of 1,4,8,11-Tetraazacyclotetradodecane (Cyclam)[137]

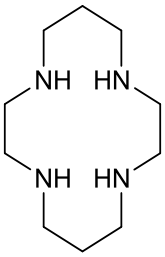

1

First reported by Barefield *et al.*[137] Amounts used: 1,5,8,12-tetrazadodecane (26.0 g, 0.15 mol), nickel(II) perchlorate (54.7 g, 0.15 mol) in water (400 ml), gyloxal (40% w/w, 25 ml, 0.15 mol). Sodium borohydride (11.0 g, 0.30 mol), sodium cyanide (29.0 g, 0.60 mol), sodium hydroxide (15.0 g, 0.38 mol), chloroform (200 ml), water (300 ml) chloroform (3 x 100 ml) chloroform (5 x 50 ml). (Na_2SO_4), chlorobenzene (150 ml), ether (50 ml) to yield white needles (13.23 g, 46%). ^1H NMR, ^{13}C NMR and MS are consistent with the published data.

6.4.2. Synthesis of Cis-3a,5a,8a,10a-tetraazaperhydropyrene (bridged cyclam)[127]

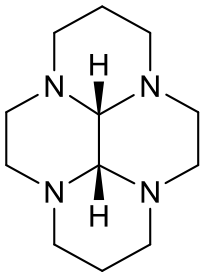

2

First reported by Le Baccon *et al.*[127] Amounts used: Cyclam **1** (12 g, 47.5 mmol), MeOH (200 ml) –10˚C. Solution of glyoxal (40% w/w, 8.7 g, 149.8 mmol), ether (100 ml), ($MgSO_4$), to yield a white solid (9.65 g, 91%). ^1H NMR, ^{13}C NMR and MS are consistent with the published data.

6.4.3. Synthesis of 3a-benzyldodecahydro-1H-3a,5a,8a,10a-tetraazapyren-3a-ium bromide[63]

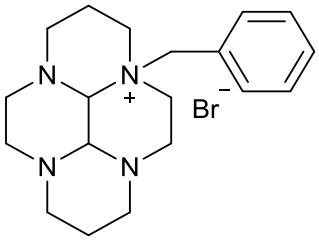

3

First reported by McRobbie *et al.*[63] Amounts used: bridged cyclam **2** (4 g, 18 mmol), dry MeCN (120 ml), benzyl bromide (12.24 g, 8.5 ml, 71.5 mmol), diethyl ether (5 x 50 ml) to yield a white powder (5.7 g, 81%). ^{1}H NMR and MS are consistent with the published data.

6.4.4. Synthesis of 3a,3a''-(1,4-phenylenebis(methylene))bis(dodecahydro-6H-3a,5a,8a,10a-tetraazapyren-3a-ium)

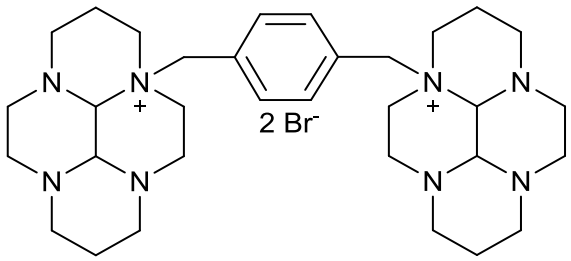

4

First reported by Valks *et al.*[62] Amounts used: Dodecahydro-3a,5a,8a,10a-tetraazapyrene **2** (4 g, 18 mmol), para-xylene dibromide (2.38 g, 9 mmol), dry MeCN (100 ml), MeCN (50 ml) THF (200 ml), to yield a white powder (5.52 g, 87%). ^{1}H NMR and MS are consistent with the published data.

6.4.5. Synthesis of 5-benzyl-1,5,8,12-tetraazabicyclo[10.2.2]hexadecane

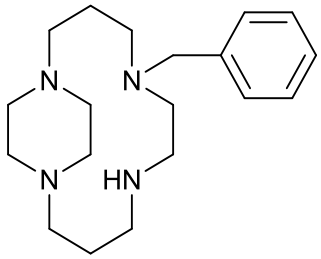

5

This compound was synthesised following a modified method based on the preparation of related compounds by Kolinski *et al.*[134] To a stirred solution of 3a-benzyldodecahydro-1H-3a,5a,8a,10a-tetraazapyren-3a-ium bromide **3** (2.5 g, 6.3 mmol) in ethanol (150 ml), was added slowly sodium borohydride (7 g, 185 mmol), and the solution was stirred at RT for 30 min before being heated to reflux for 2 h. The solution was left to cool to RT, excess $NaBH_4$ was decomposed with water (40 ml), and solvents were removed. Water (100 ml) was added to the residue, the solution was made basic (KOH, pH 14), and extracted with DCM (4 × 50 ml). Organic extracts were combined, dried, and the solvent was removed to yield a colourless oil (1.99 g, 93 %). ^{1}H NMR ($CDCl_3$): δ 7.48-7.28 (*m*, 5H, H(Ar)), 4.90 (*s*, 2H, CH_2-Ar), 4.69 (*m*, 2H, CH_2-N), 4.26 (*m*, 2H, CH_2- N), 4.24-4.18 (*m*, 2H, CH_2-N), 3.65 (*t*, 1H, CH_2-N), 3.20-3.08 (*m*, 2H, CH_2-N), 2.98 (*s*, 2H, CH_2-N), 2.69-2.48 (*m*, 5H, CH_2-N), 2.29-2.11 (*m*, 5H, CH_2-N), 1.81-1.64 (*m*, 2H, CH_2-β-N), 1.31 (*m*, 2H, CH_2-β-N). MS: (ESI) m/z 317.4 ($[M+H]^+$)

6.4.6. Synthesis of 5-benzyl-1,5,8,12-tetraazabicyclo[10.2.2]hexadecane $[Ni4]^{2+}$

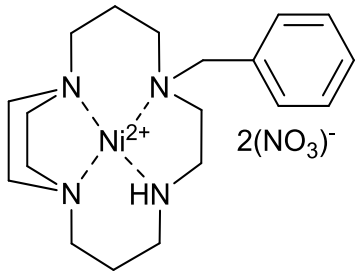

$[Ni\mathbf{5}]^{2+}$

This complex was synthesised using a modified method of that reported by Valks *et al.* for related metal complexes.[62] 5-Benzyl-1,5,8,12-tetraazabicyclo[10.2.2]hexadecane **5** (1.1 g, 3.47 mmol) was dissolved in degassed anhydrous MeOH (25 ml), an anhydrous methanolic (10 ml) solution of nickel(II) nitrate hexahydrate (1.11 g, 3.82 mmol) was added dropwise and the mixture was refluxed under argon for 12 h. Solvent was removed *in vacuo* then the macrocycle complex was purified *via* size exclusion chromatography (Sephadex LH20) in MeOH to yield bright orange crystals (1.51 g, 87%) Anal. calcd. for $C_{19}H_{32}N_4Ni.2NO_3$: C, 45.72; H, 6.46; N, 16.84. Found: C, 45.51; H, 6.77; N, 16.65. MS: (ESI) m/z 436.19 ($[M- NO_3^-]^+$)

6.4.7. Synthesis of 1,4-bis((1,5,8,12-tetraazabicyclo[10.2.2]hexadecan-5-yl)methyl)benzene

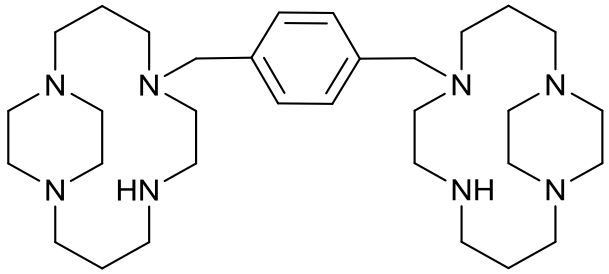

6

First ported by McRobbie *et al*.[63] Amounts used: 3a,3a'-[1,4-Phenylenebis(methylene)]-bis(decahydro-3a,5a,8a,10a-tetraazapyrenium) dibromide **4** (5.00 g, 7 mmol), ethanol (100 ml), sodium borohydride (12 g, 318 mmol), water (50 ml), (KOH pellets) pH= 14, DCM (5 × 50 ml), ($MgSO_4$). To yield a clear oil (3.59 g, 93%). ^{1}H NMR, MS and CHN are consistent with the published data.

6.4.8. Synthesis of 1,4-bis((1,5,8,12-tetraazabicyclo[10.2.2]hexadecan-5-yl)methyl)benzene $[Zn_2\mathbf{6}]^{4+}$ [63]

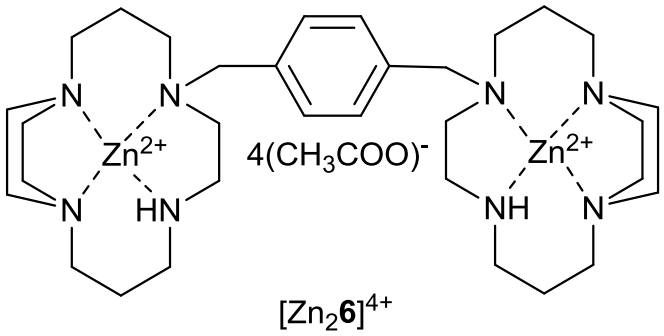

$[Zn_2\mathbf{6}]^{4+}$

First reported by McRobbie *et al.*[63] Amounts used: 1,4-bis((1,5,8,12-tetraazabicyclo[10.2.2]hexadecan-5-yl)methyl)benzene **6** (1.0 g, 1.8 mmol), MeOH (25 ml), solution of zinc(II) acetate dihydrate $Zn(CH_3COO)_2.2H_2O$ (0.88 g, 3.96 mmol) in anhydrous methanolic (10 ml), to yield yellow crystals (1.55 g, 94%) Anal. calcd for $C_{32}H_{58}N_8Zn_2.4CH_3CO_2.0.3CH_3OH.0.2H_2O$: C, 51.97; H, 7.75; N, 12.12. Found: C, 51.91; H, 7.69; N, 12.10. MS: (ESI) m/z 860.37 ($[M-CH_3CO_2^-]^+$)

6.4.9. Synthesis of 1,4-bis((1,5,8,12-tetraazabicyclo[10.2.2]hexadecan-5-yl)methyl)benzene [Zn**8**]$^{2+}$

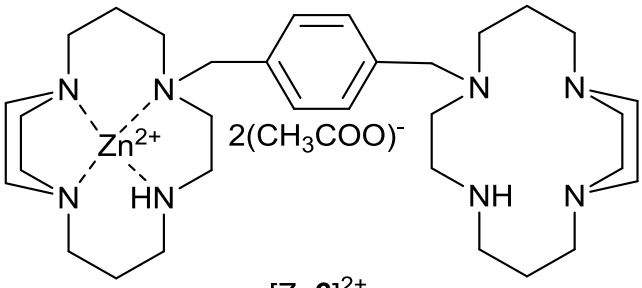

[Zn**6**]$^{2+}$

1,4-bis((1,5,8,12-tetraazabicyclo[10.2.2]hexadecan-5-yl)methyl)benzene **6** (1.2 g, 2.2 mmol) was dissolved in degassed anhydrous MeOH (30 ml), an anhydrous methanolic (10 ml) solution of zinc(II) acetate dihydrate $Zn(CH_3COO)_2.2H_2O$ (0.6 g, 2.64 mmol) was added dropwise and the mixture was refluxed under argon for 24 h. Solvent was removed *in vacuo* then the compound was purified *via* size exclusion chromatography (Sephadex LH20) in MeOH, to yield yellow crystals (1.8 g, 92%) Anal. calcd. for $C_{32}H_{58}N_8Zn.2CH_3CO_2.1.2CH_3OH.0.4H_2O$: C, 56.99; H, 8.95; N, 14.29. Found: C, 56.81; H, 8.89; N, 14.27. MS: (ESI) m/z 677.42 ($[M-CH_3CO_2^-]^+$)

6.4.10. Synthesis of 1,4-bis((1,5,8,12-tetraazabicyclo[10.2.2]hexadecan-5-yl)methyl)benzene [ZnCu6]$^{4+}$

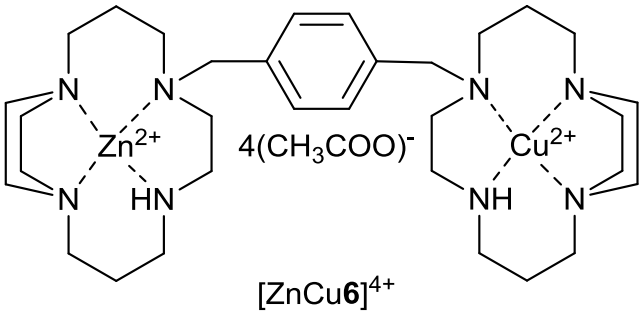

[ZnCu**6**]$^{4+}$

1,4-bis((1,5,8,12-tetraazabicyclo[10.2.2]hexadecan-5-yl)methyl)benzene [Zn**6**]$^{2+}$ (1.4 g, 1.1 mmol) was dissolved in degassed anhydrous MeOH (25 ml), an anhydrous methanolic (10 ml) solution of copper(II) acetate monohydrate $Cu(CH_3COO)_2.H_2O$ (0.3 g, 1.32 mmol) was added dropwise and the mixture was refluxed under argon for 24 h. Solvent was removed *in vacuo* then the compound was purified *via* size exclusion chromatography (Sephadex LH20) in MeOH, to yield blue crystals (0.92 g, 90%) Anal. calcd. for $C_{32}H_{58}N_8ZnCu.4CH_3CO_2.0.8CH_3OH.0.9H_2O$: C, 50.95; H, 7.86; N, 11.65. Found: C, 50.88; H, 7.79; N, 11.63. MS: (ESI) m/z 858.38 ([M− $CH_3CO_2^-$]$^+$)

6.4.11. Transmetalation of 1,4-bis((1,5,8,12-tetraazabicyclo[10.2.2]hexadecan-5-yl)methyl)benzene zinc(II) acetate $[Zn_2\mathbf{6}]^{4+}$ with 64-copper(II) acetate $[^{64}CuZn\mathbf{6}]^{4+}$

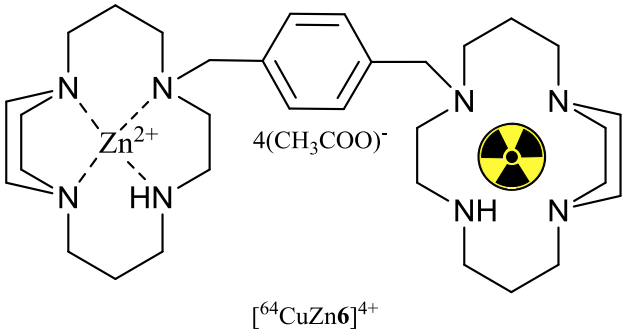

$[^{64}CuZn\mathbf{6}]^{4+}$

General procedure:

Ammonium acetate buffer was added to 64-copper(II) chloride and incubated for 10 min at 60 °C. A stock solution of the macrocycle was made by dissolving it in ammonium acetate buffer. A portion of the macrocycle ammonium acetate buffer solution was added to the 64-copper(II) chloride ammonium acetate buffer solution and incubated at 90 °C for up to 75 min.

6.4.11.1. Transmetalation of 1,4-bis((1,5,8,12-tetraazabicyclo[10.2.2]hexadecan-5-yl)methyl)benzene zinc(II) acetate $[Zn_2\mathbf{6}]^{4+}$ with 64-copper(II) acetate $[^{64}CuZn\mathbf{6}]^{4+}$

Amounts: ammonium acetate buffer (400 mM, pH 5.5, 230 µL), 64-copper(II) chloride (3 MBq), 1,4-bis((1,5,8,12-tetraazabicyclo[10.2.2]hexadecan-5-yl)methyl)benzene zinc(II) acetate $[Zn_2\mathbf{6}]^{4+}$ (1.00 mg, 0.71 µmol), ammonium acetate buffer (400 mM, pH 5.5, 250 µL), 1,4-bis((1,5,8,12-tetraazabicyclo[10.2.2]hexadecan-5-yl)methyl)benzene zinc(II) acetate $[Zn_2\mathbf{6}]^{4+}$ ammonium acetate buffer solution (2.8 mM, 12.5 µL). Crude RCY: 82%

6.4.12. Synthesis of 1,4-bis((1,5,8,12-tetraazabicyclo[10.2.2]hexadecan-5-yl)methyl)benzene [Ni6]$^{2+}$ [121]

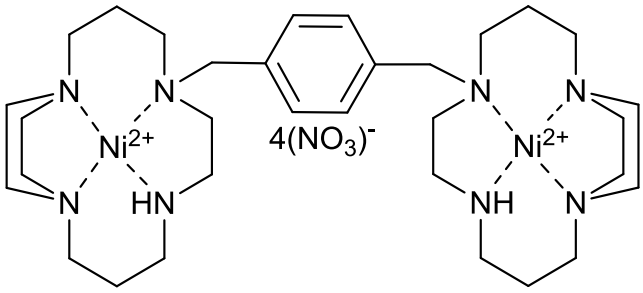

$[Ni_2\mathbf{6}]^{4+}$

First reported by Smith *et al.*[121] Amounts used: 1,4-bis((1,5,8,12-tetraazabicyclo[10.2.2]hexadecan-5-yl)methyl)benzene **6** (3.3 g, 5.95 mmol) in dry MeOH (50 ml), an anhydrous methanolic (20 ml) solution of nickel(II) nitrate hexahydrate (3.80 g, 13.08 mmol). To yield bright orange crystals (4.91 g, 90%) Anal. calcd. for $C_{32}H_{58}N_8Ni_2.4NO_3.2CH_3OH.0.5H_2O$: C, 41.11; H, 6.80; N, 16.92. Found: C, 41.07; H, 6.77; N, 16.98. MS: (ESI) m/z 857.40 ($[M- NO_3^-]^+$)

6.4.13. Synthesis of nickel (II) 5-benzyl-8-methyl-1,5,8,12-tetraazabicyclo [10.2.2] hexadecane di(hexafluorophosphate)

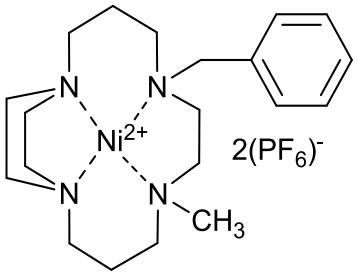

[Ni**7**]$^{2+}$

A route was designed based on modification of the synthetic work reported by Kaden *et al.*[124] Nickel(II) 5-(4-phenylmethyl benzoate)-1,5,8,12-tetraazabicyclo-[10.2.2]hexadecane nitrate [Ni**5**]$^{2+}$ (1.2 g, 2.4 mmol) bright orange colour, was dissolved in dry DMSO (15 ml) and stirred *in vacuo* for 1 h. The orange solution was purged with argon for 10 minutes. Then, n-butyl lithium 2.5M in hexane (0.4 ml, 4.8 mmol, 2 eq.) was added dropwise over 30 minutes. A blue colour developed, and the mixture was stirred at RT for 30 minutes. Methyl iodide (1.36 g, 9.6 mmol, 4eq.) was added dropwise and an orange solution reappeared which was stirred at room temperature for 1 h. The solution was stirred under vacuum again to remove hexanes and excess methyl iodide. The DMSO solution was added dropwise to a saturated solution of ammonium hexafluorophosphate (40 eq.) in ethanol (40 ml). The orange precipitate which formed was filtered off and washed with ether (100 ml). The orange solid was dissolved in acetonitrile and evaporated *in vacuo* to yield an orange crystalline solid (1.5 g, 92%) Anal. calcd. for $C_{20}H_{34}N_4Ni.2PF_6.1.8H_2O$: C, 33.76; H, 5.33; N, 7.87. Found: C, 33.71; H, 5.70; N, 8.01. MS: (ESI) m/z 533.19 ([M-PF_6^-]$^+$)

6.4.14. Synthesis of 5-benzyl-8-methyl-1,5,8,12-tetraazabicyclo [10.2.2] hexadecane

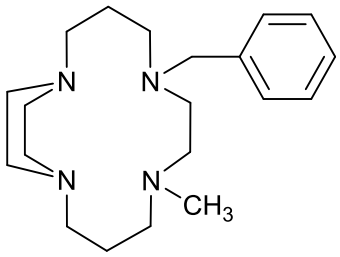

7

Nickel(II) 5-benzyl-8-methyl-1,5,8,12-tetraazabicyclo[10.2.2]hexadecane di(hexafluorophosphate) $[Ni\mathbf{7}]^{2+}$ (1.4 g, 2.06 mmol) was dissolved in a mixture of water and MeCN (90 : 10) (10 ml) to form bright orange solution and sodium cyanide (400 mg, 8.24 mmol) was added to the orange solution in one portion, the mixture became less intense and was heated at 80 °C for 24 h. The resulting mixture was cooled in RT and then in an ice bath, it was filtered to remove the nickel cyanide salt and the filtrate was concentrated *in vacuo* to remove MeCN. KOH was added to aqueous residue to adjust pH=14 and extracted with DCM (5 x 40 ml). The combined organic layer was dried over $MgSO_4$, filtered and concentrated *in vacuo* to yield colourless oil which was dried using a Schlenk line overnight to yield colourless solid (622 mg, 91%). ^{1}H NMR ($CDCl_3$): δ 7.45-7.23 (*m*, 5H, H(Ar)), 4.87 (*s*, 2H, CH_2-Ar), 4.33 (*s*, 4H, CH_2- N), 4.24-4.18 (*m*, 2H, CH_2-N), 3.12-3.01 (*m*, 2H, CH_2-N), 2.86 (*s*, 2H, CH_2-N), 2.70-2.58 (*m*, 5H, CH_2-N), 2.43-2.19 (*m*, 5H, CH_2-N), 1.81(s, 3H, CH_3), 1.54 (*m*, 2H, CH_2- -N), 1.48 (*m*, 2H, CH_2- -N). ^{13}C NMR ($CDCl_3$): δ 23.51 (N- -CH_2), 25.62 (N- -CH_2), 44.88 (N-CH_3), 48.19 (N-CH_2), 50.21 (N-CH_2), 55.32 (N-CH_2), 55.71 (N-CH_2), 56.46 (N-CH_2), 56.91 (N-CH_2), 61.11 (CH_2-Ar), 124.32 (Ar C), 129.51 (Ar CH), 129.82 (Ar CH), 143.22 (Ar C). Anal. calcd. for $C_{20}H_{34}N_4.2.3H_2O$: C, 64.58; H, 10.46; N, 15.06. Found: C, 64.20; H, 10.37; N, 10.19. MS: (ESI) m/z 331.2 ($[M+H]^+$)

6.4.15. Synthesis of metal mono macrocyclic methyl trans *IV* complexes

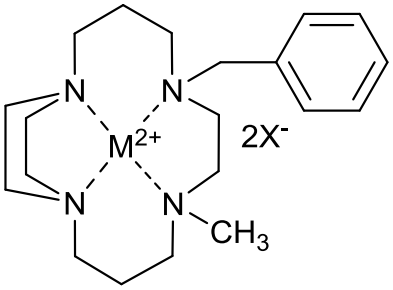

$[Cu\mathbf{7}]^{2+}$ $M^{2+}= Cu^{2+}$ $X^{-}= CH_3CO_2^{-}$

$[Zn\mathbf{7}]^{2+}$ $M^{2+}= Zn^{2+}$ $X^{-}= CH_3CO_2^{-}$

$[Ni\mathbf{7}]^{2+}$ $M^{2+}= Ni^{2+}$ $X^{-}= NO_3^{-}$

6.4.15.1. General method

5-Benzyl-8-methyl-1,5,8,12-tetraazabicyclo[10.2.2]hexadecane **7** was dissolved in degassed anhydrous MeOH (15-20 ml), an anhydrous methanolic (10 ml) solution of inorganic salt was added dropwise and the mixture was refluxed under argon for 24 h. Solvent was removed *in vacuo* and purified *via* size exclusion chromatography (Sephadex LH20) then solvent removed to yield the product.

6.4.15.1.1. Synthesis of $[Cu7]^{2+}$

Amounts: 5-benzyl-8-methyl-1,5,8,12-tetraazabicyclo[10.2.2]hexadecane **7** (200 mg, 0.6 mmol) in anhydrous MeOH (10ml). Copper(II) acetate monohydrate $Cu(CH_3COO)_2.H_2O$ (132 mg, 0.66 mmol) in anhydrous MeOH (5 ml) was added dropwise to the mixture at 80 °C. The mixture was heated to reflux for 24 h. Solvent was removed *in vacuo* to 1 ml and the complex purified *via* size exclusion chromatography (Sephadex LH20) then solvent removed to yield the desired compound as green bluish solid (290 mg, 94%). Anal. calcd. for $C_{20}H_{34}N_4Cu.2(OAc)1.9H_2O.1CH_3OH$: C, 51.23; H, 8.53; N, 9.23. Found: C, 50.92; H, 8.47; N, 9.18. MS: (ESI) *m/z* 452.22 $[M\text{-}CH_3CO_2^{-}]^{+}$. HRMS: calcd. for $C_{20}H_{34}N_4Cu^{2+}.(CH_3CO_2)^{-}$ 452.2217; Found 452.2221. UV-vis: (H_2O) λ_{max} 533 nm

6.4.15.1.2. Synthesis of $[Zn7]^{2+}$

Amounts: 5-benzyl-8-methyl-1,5,8,12-tetraazabicyclo[10.2.2]hexadecane **7** (200 mg, 0.6 mmol) in anhydrous MeOH (10 ml). Zinc(II) acetate dihydrate $Zn(CH_3COO)_2.2H_2O$ (145 mg, 0.66 mmol) in anhydrous MeOH (5 ml) was added dropwise to the mixture at 80 °C. The mixture was heated to reflux for 24 h. Solvent was removed in *vacuo* to 1 ml and the complex was purified *via* size exclusion chromatography (Sephadex LH20). The solvent removed to yield the desired compound as yellow solid (285 mg, 92%). ^{1}H NMR (DMSO-d_6): δ 7.56-7.23 (*br m*, 5H), 3.50-3.25 (*br m*, 20H), 3.23-3.11 (*br m*, 5H), 3.08-2.90 (*br m*, 5H), 1.94-1.67 (*br m*, 5H). Anal. calcd. for $C_{20}H_{34}N_4Zn(OAc)_2.2.2H_2O.1.2CH_3OH$: C, 51.12; H, 8.38; N, 9.46. Found: C, 50.99; H, 8.43; N, 9.52. MS: (ESI) *m/z* 453.22 $[M\text{-}CH_3CO_2^-]^+$. HRMS: calcd. for $C_{20}H_{34}N_4Cu^{2+}.(CH_3CO_2)^-$ 453.2219; Found 453.2222. UV-vis: (H_2O) λ_{max} 526 nm

6.4.15.1.3. Synthesis of $[Ni7]^{2+}$

Amounts: 5-benzyl-8-methyl-1,5,8,12-tetraazabicyclo[10.2.2]hexadecane **7** (200 mg, 0.6 mmol) in anhydrous MeOH (10 ml). Anhydrous nickel nitrate (120 mg, 0.66 mmol) in anhydrous MeOH (5 ml) was added dropwise to the mixture at 80 °C. The mixture was heated to reflux for 24 h. Solvent was removed in *vacuo* to 1ml and the complex purified *via* size exclusion chromatography (Sephadex LH20). The solvent removed to yield the desired complex as bright green solid (310 mg, 92%). ^{1}H NMR (CD_3CN): δ 8.19-7.29 (*br m*, 5H), 3.69-3.00 (*br m*, 14H), 2.98-2.59 (*br m*, 10H), 1.44-1.39 (*br m*, 5H). Anal. calcd. for $C_{20}H_{34}N_4Ni(NO_3)_2.2H_2O$ $0.8CH_3OH$: C, 43.46; H, 7.22; N, 14.62. Found: C, 43.40; H, 7.33; N, 14.41. MS: (ESI) *m/z* 450.20 $[M\text{-}\ NO_3^-]^+$. HRMS: calcd. for $C_{20}H_{34}N_4Ni^{2+}.(NO_3)^-$ 450.2019; Found 450.2020. UV-vis: (H_2O) λ_{max} 490 nm

6.4.16. Synthesis of Nickel (II) 5,8-dibenzyl-1,5,8,12-tetraazabicyclo[10.2.2]hexadecane di(hexafluorophosphate)

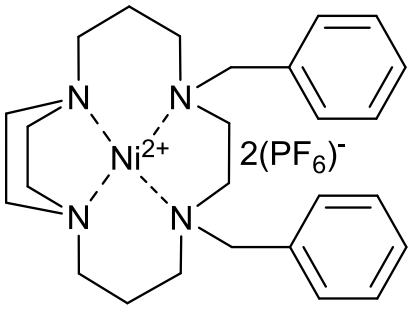

[Ni**8**]$^{2+}$

Nickel (II) 5-(4-phenylmethyl benzoate)-1,5,8,12-tetraazabicyclo-[10.2.2]hexadecane Nitrate [Ni**5**]$^{2+}$ (1.2 g, 2.4 mmol) bright orange colour, was dissolved in dry DMSO (15 ml) and stirred *in vacuo* for 1 h. The orange solution was purged with argon for 10 minutes. Then, n-butyl lithium 2.5M in hexane (0.4 ml, 0.3 g, 4.8 mmol, 2 eq.) was added dropwise over 30 minutes. A blue colour developed, and the reaction mixture was stirred RT for 30 minutes. Benzyl bromide (1.64 g, 9.6 mmol, 4 eq.) was added dropwise and an orange solution reappeared which was stirred at room temperature for 1 h. The solution was stirred under *vacuum* again to remove hexanes and excess benzyl bromide. The DMSO solution was added dropwise to a saturated solution of ammonium hexafluorophosphate (40 eq.) in ethanol (40 ml). The orange precipitate which formed was filtered off and washed with ether (100 ml). The orange solid was dissolved in acetonitrile and evaporated *in vacuo* to yield an orange crystalline solid (1.6 g, 88%) Anal. calcd. for $C_{26}H_{38}N_4Ni.2PF_6.1.6H_2O$: C, 39.83; H, 5.30; N, 7.15. Found: C, 39.67; H, 5.63; N, 7.2. MS: (ESI) m/z 609.12 ([M-PF_6^-]$^+$)

6.4.17. Synthesis of 5,8-dibenzyl-1,5,8,12-tetraazabicyclo[10.2.2]hexadecane

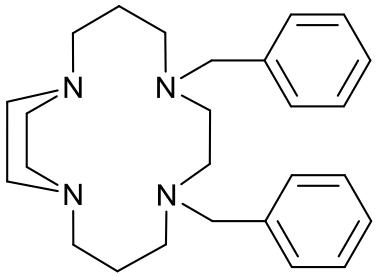

8

Nickel (II) 5-benzyl-8-methyl-1,5,8,12-tetraazabicyclo[10.2.2]hexadecane di(hexafluorophosphate) [Ni**8**]$^{2+}$ (1.4 g, 1.85 mmol) was dissolved in a mixture of water and MeCN (90 : 10) (20 ml) to form bright orange solution and sodium cyanide (365 mg, 7.42 mmol) was added to the orange solution in one portion, the mixture became less intense and was heated at 80°C for 24 h. The resulting mixture was cooled in RT and then in an ice bath, filtered to remove the residue of nickel cyanide salt and the filtrate was concentrated to remove MeCN, KOH was added to aqueous residue to adjust pH=14 and extracted with DCM (5 x 40 ml). The combined organic layer was dried over $MgSO_4$, filtered and concentrated in *vacuo* to yield colourless oil which was dried using a Schlenk line over night to yield a colourless solid (680 mg, 91%) ^{1}H NMR ($CDCl_3$): δ 7.40-7.18 (*m*, 10H, H(Ar)), 4.01 (*s*, 4H, CH_2-Ar), 3.88 (*s*, 4H, CH_2- N), 3.66-3.51 (*m*, 2H, CH_2-N), 3.12-3.01 (*m*, 2H, CH_2-N), 2.86 (*s*, 2H, CH_2-N), 2.70-2.58 (*m*, 5H, CH_2-N), 2.43-2.19 (*m*, 5H, CH_2-N), 1.54 (*m*, 2H, CH_2- -N), 1.48 (*m*, 2H, CH_2- -N). ^{13}C NMR ($CDCl_3$): δ 23.18 (N- -CH_2), 25.36 (N- -CH_2), 48.22 (N-CH_2), 50.21 (N-CH_2), 55.18 (N-CH_2), 55.71 (N-CH_2), 63.06 (CH_2-Ar), 119.32 (Ar C), 125.26 (Ar CH), 125.38 (Ar CH), 141.32 (Ar C). Anal. calcd. for $C_{20}H_{38}N_4.1.8H_2O$: C, 71.13; H, 9.55; N, 12.76. Found: C, 70.96; H, 9.47; N, 12.62. MS: (ESI) m/z 406.13 ([M+H]$^+$)

6.4.18. Synthesis of metal mono macrocyclic benzyl trans *IV*complexes

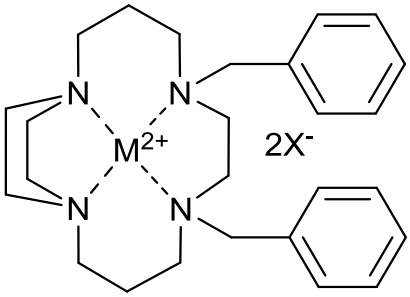

$[Cu\mathbf{8}]^{2+}$ $M^{2+}= Cu^{2+}$ $X^{-}= CH_3CO_2^{-}$

$[Zn\mathbf{8}]^{2+}$ $M^{2+}= Zn^{2+}$ $X^{-}= CH_3CO_2^{-}$

$[Ni\mathbf{8}]^{2+}$ $M^{2+}= Ni^{2+}$ $X^{-}= NO_3^{-}$

6.4.18.1. General method

5,8-Dibenzyl-1,5,8,12-tetraazabicyclo[10.2.2]hexadecane **8** was dissolved in degassed anhydrous MeOH (15-20 ml). An anhydrous methanolic (10 ml) solution of inorganic salt was added dropwise and the mixture was refluxed under argon for 24 h. Solvent was removed *in vacuo* and purified *via* size exclusion chromatography (sephadex LH20) to yield the desired product.

6.4.18.1.1. Synthesis of $[Cu\mathbf{8}]^{2+}$

Amounts: 5,8-dibenzyl-1,5,8,12-tetraazabicyclo[10.2.2]hexadecane **8** (200 mg, 0.5 mmol) in anhydrous MeOH (10 ml). Copper(II) acetate monohydrate $Cu(CH_3COO)_2.H_2O$ (110 mg, 0.55 mmol) in anhydrous MeOH (5 ml) was added dropwise to the mixture at 80 °C. The mixture was heated to reflux for 24 h. Solvent was removed in *vacuo* to 1 ml and the complex was purified *via* size exclusion chromatography (Sephadex LH20) to yield the desired product as green bluish solid (270 mg, 80%) Anal. calcd. for $C_{26}H_{38}N_4Cu.2(OAc)1.2H_2O.1.3CH_3OH$: C, 57.70; H, 7.98; N, 8.60. Found: C, 57.65; H, 8..08; N, 8.52. MS: (ESI) *m/z* 528.25 $[M\text{-}CH_3CO_2^{-}]^{+}$. HRMS: calcd. for $C_{26}H_{38}N_4Cu^{2+}.(CH_3CO_2)^{-}$ 528.2520; Found 528.2521. UV-vis: (H_2O) λ_{max} 517 nm

6.4.18.1.2. Synthesis of $[Zn8]^{2+}$

Amounts: 5,8-dibenzyl-1,5,8,12-tetraazabicyclo[10.2.2]hexadecane **8** (200 mg, 0.5 mmol) in anhydrous MeOH (10 ml). Zinc(II) acetate dihydrate $Zn(CH_3COO)_2.2H_2O$ (120 mg, 0.55 mmol) in anhydrous MeOH (5 ml) was added dropwise to the mixture at 80 °C. The mixture was heated to reflux for 24 h. Solvent was removed in *vacuo* to 1 ml and the compound was purified *via* size exclusion chromatography (Sephadex LH20) to yield the desired product as yellow solid (255 mg, 79%) Anal. calcd. for $C_{26}H_{38}N_4Zn(OAc)_2.1.2H_2O.1CH_3OH$: C, 57.84; H, 7.89; N, 8.70. Found: C, 57.90; H, 7.82; N, 8.68. MS: (ESI) *m/z* 529.25 $[M\text{-}CH_3CO_2^-]^+$. HRMS: calcd. for $C_{26}H_{38}N_4Cu^{2+}.(CH_3CO_2)^-$ 529.2519; Found 529.2525. UV-vis: (H_2O) λ_{max} 506 nm

6.4.18.1.3. Synthesis of $[Ni8]^{2+}$

Amounts: 5,8-dibenzyl-1,5,8,12-tetraazabicyclo[10.2.2]hexadecane **8** (200 mg, 0.5 mmol) in anhydrous MeOH (10 ml). Anhydrous nickel nitrate (100 mg, 0.55 mmol) in (5 ml) anhydrous MeOH was added dropwise to the mixture at 80 °C. The mixture was heated to reflux for 24 h. Solvent was removed in *vacuo* to 1 ml and the complex was purified *via* size exclusion chromatography (Sephadex LH20) to yield the desired product as a bright green solid (285 mg, 88%) Anal. calcd. for $C_{26}H_{38}N_4Ni(NO_3)_2.1.6H_2O$ $0.7CH_3OH$: C, 50.06; H, 6.92; N, 13.12. Found: C, 50.10; H, 7.03; N, 13.11. MS: (ESI) *m/z* 526.23 $[M\text{-}NO_3^-]^+$. HRMS: calcd. for $C_{26}H_{38}N_4Ni^{2+}.(NO_3)^-$ 526.2308; Found 526.2310. UV-vis: (H_2O) λ_{max} 481 nm

6.4.19. Synthesis of Di Nickel (II) 1,4-bis ((8-methyl-1,5,8,12-tetraazabicyclo [10.2.2]hexadecan-5-yl) methyl) benzene di (hexafluorophosphate)

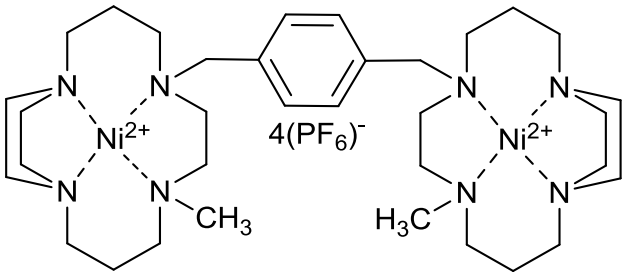

$[Ni_2\mathbf{9}]^{4+}$

Following a modified method from route reported by Kaden *et al.*[124] Di-Nickel (II) 1,4-bis((1,5,8,12-tetraazabicyclo[10.2.2]hexadecan-5-yl)methyl)benzene Di-nitrate $[Ni\mathbf{6}]^{2+}$ (1.5 g, 1.63 mmol) which is bright orange in colour, was dissolved in dry DMSO (15 ml) and stirred *in vacuo* for 1 h. The orange solution was purged with argon for 10 min. n-Butyl lithium 2.5M in hexane (0.6 ml, 6.52 mmol, 4 eq.) was added dropwise over 30 minutes. A blue colour developed, and the resulting solution was stirred at RT for 30 min. Methyl iodide (1.85 g, 13.04 mmol, 8 eq.) was added dropwise and an orange solution reappeared which was stirred at RT for 1 h. The solution was stirred under *vacuum* again to remove hexanes and excess methyl iodide. The DMSO solution was added dropwise to a saturated solution of ammonium hexafluorophosphate (60 eq.) in ethanol (60 ml). The orange precipitate which formed was filtered off and washed with ether (100 ml). The orange solid was dissolved in acetonitrile and evaporated *in vacuo* to yield an orange crystalline solid (1.88 g, 90%) Anal. calcd. for $C_{34}H_{62}N_8Ni_2.4PF_6.2.4H_2O$: C, 30.86; H, 5.09; N, 8.47. Found: C, 30.80; H, 5.12; N, 8.61. MS: (ESI) m/z 991.08 ($[M\text{-}2PF_6^-]^{2+}$)

6.4.20. Synthesis of 1,4-bis((8-methyl-1,5,8,12-tetraazabicyclo[10.2.2]hexadecan-5-yl) methyl) benzene

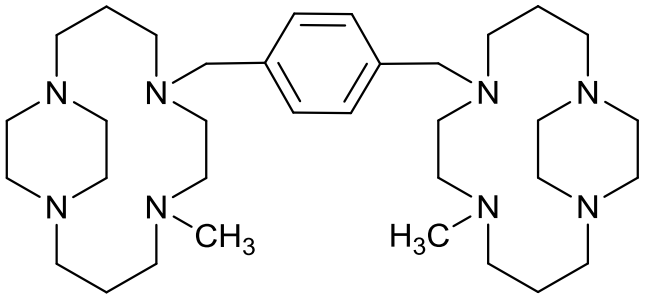

9

Dinickel(II) 1,4-bis ((8-methyl-1,5,8,12-tetraazabicyclo[10.2.2]hexadecan-5-yl) methyl) benzene di-(hexafluorophosphate) $[Ni_2\mathbf{9}]^{4+}$ (1.8 g, 1.40 mmol) was dissolved in a mixture of water and MeCN (90 : 10) (20 ml) to form bright orange solution and sodium cyanide (700 mg, 14 mmol) was added to the orange solution in one portion, the mixture became less intense and was heated at 80° C for 24 h. The resulting mixture was cooled in RT and then in an ice bath, filtered to remove residue of nickel cyanide salt and. The filtrate was concentrated to remove MeCN. Solid KOH was added to the aqueous residue to adjust the pH to 14 and then extracted with DCM (5 x 40 ml). The combined organic layer was dried over $MgSO_4$, filtered and concentrated *in vacuo* to yield a colourless oil which was dried on the Schlenk line under *vacuum* overnight to yield a white solid (770mg, 94%). ^{1}H NMR ($CDCl_3$): δ 7.20 (*s*, 4H, CHAr), 3.63 (*s*, 4H, NCH_2Ar), 3.22 (*m*, 4H, NCH_2), 3.01 (*m*, 4H, NCH_2), 2.82 (*m*, 4H, NCH_2), 2.61 (*m*, 4H, NCH_2), 2.52 (*m*, 8H, NCH_2), 2.44 (*m*, 12H, NCH_2), 2.14 (*m*, 4H, NCH_2), 2.01 (s, 6H, CH_3), 1.75 (*m*, 4H, NCH_2), 1.66 (*m*, 4H, NCH_2). ^{13}C NMR ($CDCl_3$): δ 19.51 (N- -CH_2), 20.45 (N- -CH_2), 41.12 (N-CH_3), 44.73 (N-CH_2), 49.13 (N-CH_2), 51.02 (N-CH_2), 54.21 (N-CH_2), 57.43 (N-CH_2), 59.31 (N-CH_2), 63.55(N-CH_2-Ar), 122.82 (Ar CH), 141.22 (Ar C). Anal. Calcd. for $C_{34}H_{62}N_8.1.35H_2O$: C, 67.25; H, 10.74; N, 18.45. Found: C, 67.18; H, 10.59; N, 18.63. MS: (ESI) m/z 583.5 ($[M+H]^+$)

6.4.21. Synthesis of metal bis macrocyclic methyl *trans IV* complexes

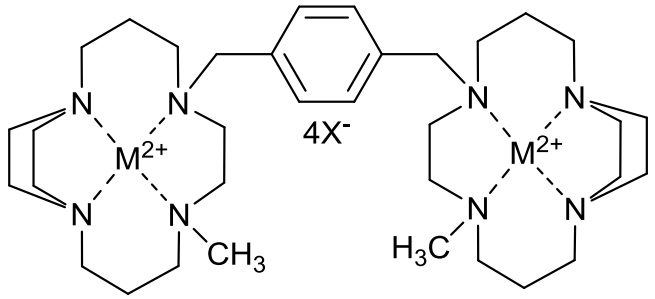

$[Cu_2\mathbf{9}]^{4+}$ $M^{2+}= Cu^{2+}$ $X^-= CH_3CO_2^-$

$[Zn_2\mathbf{9}]^{4+}$ $M^{2+}= Zn^{2+}$ $X^-= CH_3CO_2^-$

$[Ni_2\mathbf{9}]^{4+}$ $M^{2+}= Ni^{2+}$ $X^-= NO_3^-$

6.4.21.1. General method

1,4-Bis((8-methyl-1,5,8,12-tetraazabicyclo[10.2.2]hexadecan-5-yl) methyl) benzene **9** was dissolved in degassed anhydrous MeOH (15-20 ml). An anhydrous methanolic (10 ml) solution of inorganic salt was added dropwise and the mixture was refluxed under argon for 24 h. Solvent was removed *in vacuo* and the compound purified *via* size exclusion chromatography (Sephadex LH20). The solvent was then removed to yield the desired product.

6.4.21.1.1. Synthesis of $[Cu_2\mathbf{9}]^{4+}$

Amounts: 1,4-bis((8-methyl-1,5,8,12-tetraazabicyclo[10.2.2]hexadecan-5-yl) methyl) benzene **9** (200 mg, 0.34 mmol) in anhydrous MeOH (10ml). Copper(II) acetate monohydrate $Cu(CH_3COO)_2.H_2O$ (150 mg, 0.75 mmol) in anhydrous MeOH (5 ml) was added dropwise to the mixture at 80 °C. The mixture was heated to reflux for 24 h. Solvent was removed *in vacuo* to 1 ml and purified *via* size exclusion chromatography (Sephadex LH20) then solvent was removed to yield the desired product as purple bluish solid (300 mg, 93%) Anal. calcd. for $C_{34}H_{62}N_8Cu_2.4(OAc)1.2H_2O.1CH_3OH$: C, 51.65; H, 8.11; N, 11.21. Found: C, 51.62; H, 8.17; N, 11.25. MS: (ESI) *m/z* 415.2 $[M\text{-}2(CH_3CO_2)^-]^{2+}$. HRMS: calcd. For $C_{34}H_{62}N_8Cu_2.(CH_3CO_2)_4$ 452.2217; Found 452.2221. UV-vis: (H_2O) λ_{max} 518 nm

6.4.21.1.2. Synthesis of $[Zn_2\mathbf{9}]^{4+}$

Amounts: 1,4-bis((8-methyl-1,5,8,12-tetraazabicyclo[10.2.2]hexadecan-5-yl) methyl) benzene **9** (200 mg, 0.34 mmol) in anhydrous MeOH (10 ml). Zinc(II) acetate dihydrate $Zn(CH_3COO)_2.2H_2O$ (137 mg, 0.75 mmol) in anhydrous MeOH (5 ml) was added dropwise to the mixture at 80 °C. The mixture was heated to reflux for 24 h. Solvent was removed *in vacuo* to 1 ml and purified *via* size exclusion chromatography (Sephadex LH20). The solvent was then removed to yield the desired product as a yellow powder (270 mg, 92%). ^{1}H NMR (DMSO-d_6): δ 7.42-7.18 (*br m*, 5H), 3.69-3.45 (*br m*, 10H), 3.43-3.21 (*br m*, 6H), 3.16-2.95 (*br m*, 4H), 2.92-2.68 (*br m*, 10H), 2.60-2.43 (*br m*, 18H), 2.40-2.24 (*br m*, 10H), 2.14-1.95 (*br m*, 6H), 1.62-1.48 (*br m*, 6H). Anal. calcd. for $C_{34}H_{62}N_8Zn_2(OAc)_4.2H_2O.0.8CH_3OH$: C, 50.82; H, 8.09; N, 11.08. Found: C, 50.89; H, 8.03; N, 11.18. MS: (ESI) *m/z* 415.20 $[M\text{-}2(CH_3CO_2)^-]^{2+}$. HRMS: calcd. for $C_{34}H_{62}N_8Zn_2.2(OAc)^-$ 415.2019; Found 415.2022. UV-vis: (H_2O) λ_{max} 536 nm

6.4.21.1.3. Synthesis of $[Ni_2\mathbf{9}]^{4+}$

Amounts: 1,4-bis((8-methyl-1,5,8,12-tetraazabicyclo[10.2.2]hexadecan-5-yl) methyl) benzene **9** (200 mg, 0.34 mmol) in anhydrous MeOH (10 ml). Anhydrous nickel nitrate (136 mg, 0.75 mmol) in (5 ml) anhydrous MeOH was added dropwise to the mixture at 80 °C. The mixture was heated to reflux for 24 h. Solvent was removed *in vacuo* to 1 ml and purified *via* size exclusion chromatography (Sephadex LH20). The solvent was then removed to yield the desired product as a bright green powder (260 mg, 80%) Anal. calcd. for $C_{34}H_{62}N_8Ni_2(NO_3)_4.2H_2O$ $0.8CH_3OH$: C, 41.38; H, 6.19; N, 16.64. Found: C, 41.40; H, 6.20; N, 16.70. MS: (ESI) *m/z* 884.34 $[M\text{-}2(NO_3)^-]^{2+}$. HRMS: calcd. for $C_{34}H_{62}N_8Ni_2{}^{4+}.3(NO_3)^-$ 884.3418; Found 884.3420. UV-vis: (H_2O) λ_{max} 488 nm

6.4.22. Synthesis of di(nickel(II)) 1,4-bis((8-benzyl-1,5,8,12-tetraazabicyclo [10.2.2]hexadecan-5-yl)methyl)benzene di-(hexafluorophosphate)

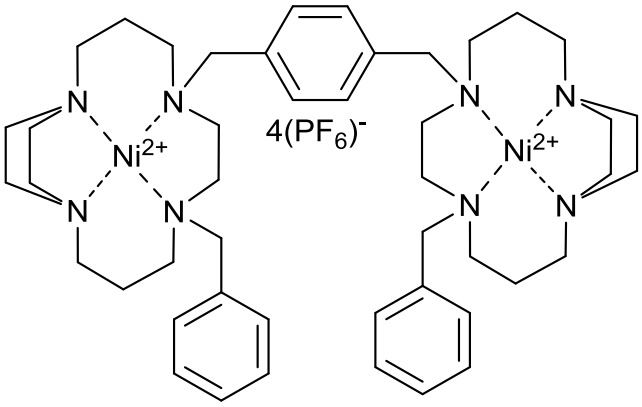

$[Ni_2\mathbf{10}]^{4+}$

Following a modified method from route reported by Kaden *et al.*[124] di-nickel(II) 1,4-bis((1,5,8,12-tetraazabicyclo[10.2.2]hexadecan-5-yl)methyl)benzene di-nitrate [Ni**8**]$^{2+}$ (1.2 g, 1.30 mmol) bright orange colour, was dissolved in dry DMSO (15 ml) and stirred *in vacuo* for 1 h. The orange solution was purged with argon for 10 minutes. Then, n-butyl lithium 2.5M in hexane (0.5 ml, 0.33 g, 5.22 mmol, 4 eq.) was added dropwise over 30 minutes. A blue colour developed, and the reaction mixture was tehn stirred at room temperature for 30 minutes. Benzyl bromide (1.78g, 10.4 mmol, 8eq.) was added dropwise and an orange solution reappeared which was stirred at room temperature for 1 h. The solution was stirred under *vacuum* again to remove hexanes and excess benzyl bromide. The DMSO solution was added dropwise to a saturated solution of ammonium hexafluorophosphate (60eq.) in ethanol (60 ml). An orange precipitate which formed was filtered off and washed with ether (100 ml). The orange solid was dissolved in acetonitrile and evaporated *in vacuo* to yield an orange crystalline solid (1.01 g, 85%) Anal. calcd. for $C_{46}H_{70}N_8Ni_2.4PF_6.1.4H_2O$: C, 37.91; H, 5.03; N, 7.69. Found: C, 37.88; H, 5.02; N, 7.60. MS: (ESI) m/z 570.19 ($[M\text{-}2PF_6^-]^{2+}$)

6.4.23. Synthesis of 1,4-bis((8-benzyl-1,5,8,12-tetraazabicyclo[10.2.2]hexadecan-5-yl)methyl)benzene

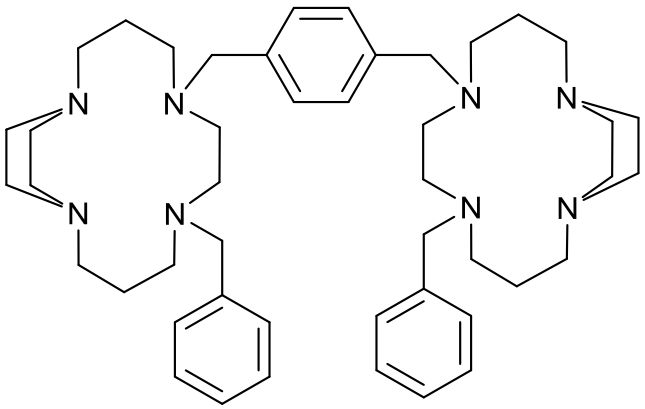

10

Following a modified route from a method reported by Barefield *et al.*[137], dinickel(II) 1,4-bis ((8-methyl-1,5,8,12-tetraazabicyclo[10.2.2]hexadecan-5-yl) methyl) benzene di-(hexafluorophosphate) $[Ni_2\mathbf{10}]^{4+}$ (1 g, 0.7 mmol) was dissolved in a mixture of water and MeCN (90 : 10) (20 ml) to form bright orange solution and sodium cyanide (350 mg, 7 mmol) was added to the orange solution in one portion; the mixture became less intense and was heated at 80 °C for 24 h. The resulting mixture was cooled at RT and then ice bath, filtered to remove residue of nickel cyanide salt and the filtrate was concentrated to remove MeCN, KOH was added to aqueous residue to adjust pH=14 and extracted with DCM (5 x 40 ml). The combined organic layer was dried over $MgSO_4$, filtered and concentrated *in vacuo* to yield colourless oil which was dried in Schlenk line overnight to yield a white solid (465 mg, 90%). ^{1}H NMR ($CDCl_3$): δ 7.20-7.37 (*s*, 14H, CHAr), 3.61 (*s*, 8H, NCH_2Ar), 3.15 (*m*, 4H, NCH_2), 2.97 (*m*, 4H, NCH_2), 2.79 (*m*, 4H, NCH_2), 2.57 (*m*, 4H, NCH_2), 2.46 (*m*, 8H, NCH_2), 2.24 (*m*, 12H, NCH_2), 2.04 (*m*, 4H, NCH_2), 1.69 (*m*, 4H, NCH_2), 1.62 (*m*, 4H, NCH_2). ^{13}C NMR ($CDCl_3$): δ 22.53 (N- -CH_2), 23.47 (N- -CH_2), 47.12 (N-CH_2), 49.11 (N-CH_2), 57.73 (N-CH_2), 59.28 (N-CH_2), 66.12(N-CH_2-Ar), 67.19(N-CH_2-Ar),118.44 (Ar CH), 130.07 (Ar CH), 131.94 (Ar CH), 133.44 (Ar CH), 141.22 (Ar C), 144.18 (Ar C). Anal. calcd. for $C_{46}H_{70}N_8.0.8H_2O$: C, 73.71; H, 9.63; N, 14.95. Found: C, 73.70; H, 9.52; N, 14.79. MS: (ESI) m/z 735.58 ($[M+H]^+$)

6.4.24. Synthesis of metal mono macrocyclic benzyl *trans IV* complexes

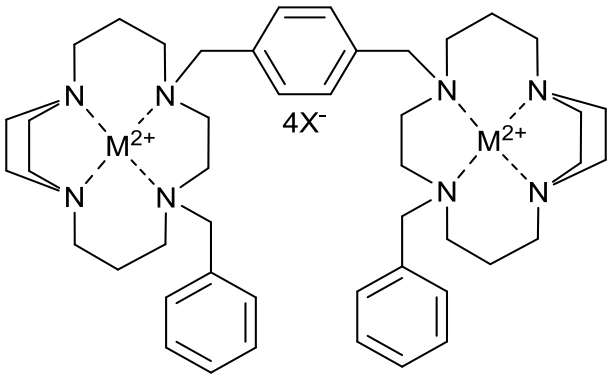

$[Cu_2\mathbf{10}]^{4+}$ $M^{2+}= Cu^{2+}$ $X^-= CH_3CO_2^-$

$[Zn_2\mathbf{10}]^{4+}$ $M^{2+}= Zn^{2+}$ $X^-= CH_3CO_2^-$

$[Ni_2\mathbf{10}]^{4+}$ $M^{2+}= Ni^{2+}$ $X^-= NO_3^-$

6.4.24.1. General method

1,4-Bis((8-benzyl-1,5,8,12-tetraazabicyclo[10.2.2]hexadecan-5-yl)methyl)benzene **10** was dissolved in degassed anhydrous MeOH (15-20 ml), an anhydrous methanolic (10 ml) solution of inorganic salt was added dropwise and the mixture was refluxed under argon for 24 h. Solvent was removed *in vacuo* and the compound was then purified *via* size exclusion chromatography (Sephadex LH20). The resulting solution was then concentrated to yield the desired product as a powder.

6.4.24.1.1. Synthesis of $[Cu_2\mathbf{10}]^{4+}$

Amounts: 1,4-bis((8-benzyl-1,5,8,12-tetraazabicyclo[10.2.2]hexadecan-5-yl)methyl)benzene **10** (100 mg, 0.14 mmol) in anhydrous MeOH (6 ml). Copper(II) acetate monohydrate $Cu(CH_3COO)_2.H_2O$ (62 mg, 0.31 mmol) in anhydrous MeOH (2 ml) was added dropwise to the mixture at 80 °C. The mixture was heated to reflux for 24 h. Solvent was removed *in vacuo* to 1 ml and purified *via* size exclusion chromatography (Sephadex LH20) to yield the desired product as purple blue solid (125 mg, 82%) Anal. calcd. for $C_{46}H_{70}N_8Cu_2.(OAc)_4.0.8H_2O.0.7CH_3OH$: C, 57.87; H, 7.67; N, 9.87. Found: C, 57.80; H, 7.65; N, 9.83. MS: (ESI) *m/z* 489.23 $[M-2(CH_3CO_2)^-]^{2+}$. HRMS: calcd. for $C_{46}H_{70}N_8Cu_2.2(CH_3CO_2)^-$ 489.2317; Found 489.2319. UV-vis: (H_2O) λ_{max} 502 nm

6.4.24.1.2. Synthesis of $[Zn_2\mathbf{10}]^{4+}$

Amounts: 1,4-bis((8-benzyl-1,5,8,12-tetraazabicyclo[10.2.2]hexadecan-5-yl)methyl)benzene **10** (100 mg, 0.14 mmol) in anhydrous MeOH (6 ml). Zinc(II) acetate dihydrate $Zn(CH_3COO)_2.2H_2O$ (68 mg, 0.31 mmol) in anhydrous MeOH (2 ml) was added dropwise to the mixture at 80 °C. The mixture was heated to reflux for 24 h. Solvent was removed *in vacuo* to 1 ml and purified *via* size exclusion chromatography (Sephadex LH20) to yield the desired product as a yellow solid (120 mg, 78%). ^{1}H NMR (CD_3CN): δ 7.52-7.21 (*br m*, 14H), 4.62-4.01 (*br m*, 4H), 3.81-3.38 (*br m*, 8H), 3.31-2.13 (*br m*, 4H), 2.99-2.81 (*br m*, 6H), 2.71-2.55 (*br m*, 18H), 2.07-1.94 (*br m*, 20H), 1.83-1.68 (*br m*, 8H). Anal. calcd. for $C_{46}H_{70}N_8Zn_2(OAc)_4.0.9H_2O.0.7CH_3OH$: C, 57.60; H, 7.65; N, 9.82. Found: C, 57.58; H, 7.62; N, 9.80. MS: (ESI) *m/z* 491.23 $[M-2(CH_3CO_2)^-]^{2+}$. HRMS: calcd. for $C_{46}H_{70}N_8Zn_2.2(CH_3CO_2)^-$ 491.2319; Found 491.2322. UV-vis: (H_2O) λ_{max} 535 nm

6.4.24.1.3. Synthesis of $[Ni_2\mathbf{10}]^{4+}$

Amounts: 1,4-bis((8-benzyl-1,5,8,12-tetraazabicyclo[10.2.2]hexadecan-5-yl)methyl)benzene **10** (100 mg, 0.14 mmol) in anhydrous MeOH (6 ml). Anhydrous nickel(II) nitrate (57 mg, 0.31 mmol) in anhydrous MeOH (2 ml) was added dropwise to the mixture at 80 °C. The mixture was heated to reflux for 24 h. Solvent was removed *in vacuo* to 1 ml and purified *via* size exclusion chromatography (Sephadex LH20) to yield the desired product as bright green (117 mg, 76%) Anal. calcd. for $C_{46}H_{70}N_8Ni_2(NO_3)_4.1.2H_2O$ $0.6CH_3OH$: C, 49.04; H, 6.61; N, 14.73. Found: C, 49.00; H, 6.59; N, 14.71. MS: (ESI) *m/z* 487.21 $[M-2(NO_3)^-]^{2+}$. HRMS: Calcd. for $C_{46}H_{70}N_8Ni_2.2(NO_3)^-$ 487.2117; Found 487.2122. UV-vis: (H_2O) λ_{max} 483 nm

6.4.25. Synthesis of 4-(4-methylphenyl)benzaldehyde[226]

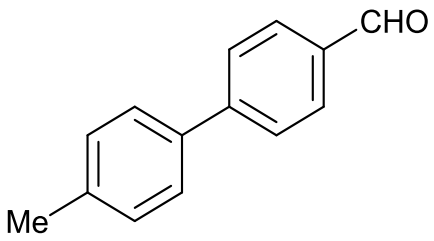

11

First reported by Ikemoto *et al.*[226] Amounts: A solution of 70% (w/v) sodium bis(2-methoxyethoxy)aluminum hydride in toluene SBMEA (33 g, 31.85 ml, 163 mmol), 4-(4- methylphenyl)benzonitrile (22 g, 113 mmol) in THF (220 ml), conc. H_2SO_4 (72 g, 132.5 ml) in water (150 ml), water (500 ml) and ethyl acetate (500 ml), THF (100 ml) and ethyl acetate (300 ml) 1:3. 5% NaCl solution (110 ml) and 7% $NaHCO_3$ solution (110 ml), 2-propanol (50 ml). Cold 2-propanol (300 ml). Dried to give **11** 4-(4-methylphenyl)benzaldehyde (19.90 g, 90%) as a white crystalline powder. Anal. calcd. for $C_{14}H_{12}O$: C, 85.68; H, 6.16. Found: C, 85.61; H, 6.01, ^1H NMR and MS are consistent with the published data.

6.4.26. Synthesis of 5-[4-(4-methylphenyl)phenyl]-4-pentenoic acid[226]

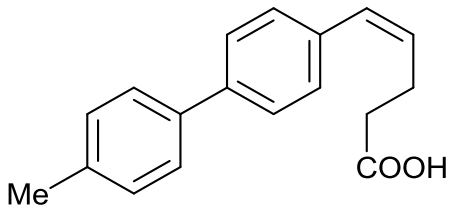

12

First reported by Ikemoto *et al.*[226] Amounts used: A solution of 28% NaOMe in MeOH (160 ml), solution of **11** 4-(4-methylphenyl)benzaldehyde (19 g, 96.8 mmol) in THF (60 ml), (3-carboxypropyl)triphenylphosphonium bromide (52.3 g, 123 mmol) in THF (530 ml), a solution of KOH (13.76 g) and water (150 ml), diisopropyl ether (130 ml), a solution of KOH (10g) in water (200 ml), THF (300 ml) and ethyl acetate (300 ml), pH= 1.5 with 6 N HCl, 10% NaCl solution (300 ml), ethanol (160 ml) and water (80 ml), mixture of ethanol (35 ml) and water (15 ml) 2 : 1. Dried under reduced pressure to give 5-[4-(4-methylphenyl)phenyl]-4-pentenoic acid **12** (21.29 g, 83%) as a white crystalline powder. Anal. calcd. for $C_{18}H_{18}O_2$: C, 81.17; H, 6.81. Found: C, 81.20; H, 6.68. ^{1}H NMR and MS are consistent with the published data.

6.4.27. Synthesis of 5-[4-(4-methylphenyl)phenyl]-4-pentanoic Acid[226]

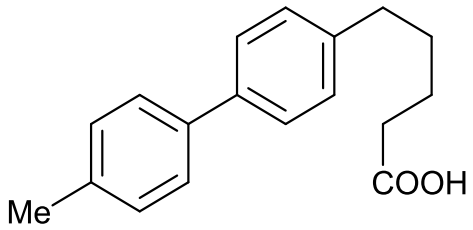

13

First reported by Ikemoto *et al.*[226] Amounts used: a solution of 5-[4-(4-methylphenyl)phenyl]-4-pentenoic acid **12** (20.0 g, 75 mmol) in THF (231 ml), 5% Pd-C (wet, 0.2 g), THF (230 ml), diisopropyl ether (46 ml), di-isopropyl ether (23 ml). Dried under reduced pressure at to give 5-[4-(4-methylphenyl)phenyl]-4-pentanoic acid **13** (19.0 g, 94%) as a white crystalline powder. Anal. calcd. for $C_{18}H_{20}O_2$: C, 80.56; H, 7.51.found: C, 80.67; H, 7.41. ^{1}H NMR and MS are consistent with the published data.

6.4.28. Synthesis of 3-(p-tolyl)-6,7,8,9-tetrahydro-5H-benzo[7]annulen-5-one

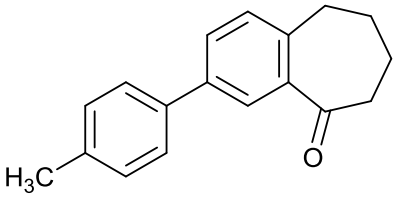

14

5-[4-(4-Methylphenyl)phenyl]-4-pentanoic acid **13** (7.08 g, 26.4 mmol) was added to polyphosphoric acid (140 g, 1.4 mol) at 130 ºC to 140 ºC and stirred together. The reaction was followed using HPLC (95% Acetonitrile, 5% 0.2 M trifluoroacetic acid in H_2O), and when the reaction was complete (as shown by the disappearance of the peak for 5-[4-(4-methylphenyl)phenyl]-4-pentanoic acid **13**), ice was then added to the reaction mixture for rapid cooling. The reaction mixture was then stirred for 1 h with the temperature between 45ºC to 70ºC. The reaction was then cooled to between 30ºC to 45ºC, DCM (80 ml) was added and the reaction mixture was allowed to stand whilst the layers separated. The aqueous layer washed with DCM (3 x 50 ml), the organic layers were combined, dried (Na_2SO_4) and evaporated *in vacuo* to produce crude produce as a yellow oil (6.8 g), which was purified using flash chromatography (hexane : ethyl acetate 9:1). This resulted in a pure yellow oil of 3-(p-tolyl)-6,7,8,9-tetrahydro-5H-benzo[7]annulen-5-one **14** (5.41g, 82%). ^{1}H NMR ($CDCl_3$) : δ 7.97 (*d*, 1H, CH-Ar), 7.65 (*dd*, 1H, CH-Ar), 7.51-7.53 (*m*, 2H, CH-Ar), 7.24-7.27 (*m*, 3H, CH-Ar), 2.97-2.98 (*m*, 2H, CH_2), 2.78 (*m*, 2H CH_2), 2.39 (*s*, 3H, CH_3), 1.84-1.93 (*m*, 4H, CH_2). MS: (ESI) m/z 250.14 ($[M+H]^+$)

6.4.29. Synthesis of methyl 5-oxo-3-(p-tolyl)-6,7,8,9-tetrahydro-5H-benzo[7]annulene-6-carboxylate[224]

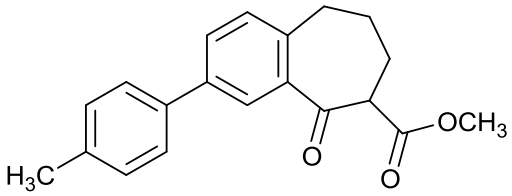

15

First reported by Shiraishi *et al.*[224] A suspension of sodium hydride in mineral oil was washed three times with diethyl ether and filtered. Sodium hydride (4.74 g, 0.197 mol) was suspended in dimethyl carbonate (90 ml) and the mixture heated to 80 ºC for 30 min. A solution of 3-(p-tolyl)-6,7,8,9-tetrahydro-5H-benzo[7]annulen-5-one **14** (4.94 g, 19.4 mmol) in dimethyl carbonate (90 ml) was added to the suspension, the mixture was heated to reflux for 3 h under a nitrogen atmosphere. The resulting solution diluted with MeOH (150 ml) and added to 1 M HCl (200 ml) under ice cooling. The aqueous solution was concentrated *in vacuo* and extracted with ethyl acetate (2 x 200 ml). The combined organic layers were washed successively with water (200 ml) and brine (200 ml), dried over Na_2SO_4 and evaporated *in vacuo* to give an orange oil which was purified by flash chromatography (petroleum-ether/ethyl acetate (8 : 2)) R_f: 0.26 to yield methyl 5-oxo-3-(p-tolyl)-6,7,8,9-tetrahydro-5H-benzo[7]annulene-6-carboxylate **15** (5.1 g, 80%). ^{1}H NMR ($CDCl_3$) : δ 7.84-7.98 (*m*, 1H, CH_2), 7.50-7.50 (*m*, 3H, CH-Ar), 7.24-7.29 (*m*, 4H, CH-Ar), 3.83-3.84 (*m*, 3H, OCH_3), 2.65-2.68 (*m*, 2H, CH_2), 2.39 (*s*, 3H, CH_3), 2.08-2.19 (*m*, 4H, CH_2).

6.4.30. Synthesis of methyl 5-hydroxy-3-(p-tolyl)-6,7,8,9-tetrahydro-5H-benzo[7] annulene-6-carboxylate[224]

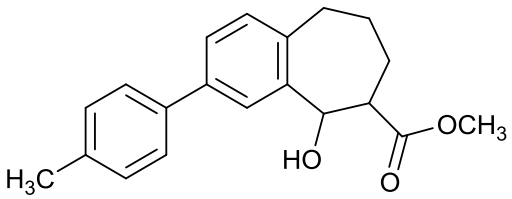

16

First reported by Shiraishi *et al.*[224] A solution of methyl 5-oxo-3-(p-tolyl)-6,7,8,9-tetrahydro-5H-benzo[7]annulene-6-carboxylate **15** (3.30 g, 11.2 mmol) in DCM (150 ml) was cooled to -20 ºC and sodium borohydride (560 mg, 15.5 mmol, 1.5eq.) and absolute MeOH (2 ml) were added. The solution was stirred for 1 h at -10 ºC and the mixture was poured into water (100 ml) and acidified with 1 M HCl. The organic layer was separated and the aqueous layer extracted with DCM (3 x 100 ml). The combined organic layers were washed first with water (100 ml), then with brine (100 ml), dried over Na_2SO_4 and the solvents removed *in vacuo* to give a crude yellow oil (2.8g). Purified using flash column chromatography (hexane : ethyl acetate (8 : 2)) to give pure 5-hydroxy-3-(p-tolyl)-6,7,8,9-tetrahydro-5H-benzo[7]annulene-6-carboxylate **16** (2.6 g, 72%). ^{1}H-NMR ($CDCl_3$) : δ 7.51 - 7.53 (*m*, 1H, CH), 7.46- 7.48 (*m*, 2H, CH-Ar), 7.36 - 7.41 (*m*, 1H, CH-Ar), 7.22 - 7.24 (*d*, 2H, CH-Ar), 7.14 - 7.16 (*d*, 1H, CH-Ar), 5.14 - 5.20 (*m*, 2H, CH_2), 3.68 - 3.75 (*m*, 3H, OCH_3), 3.19 - 3.25 (*m*, 1H, CH), 2.66 -2.87 (*m*, 2H, CH_2), 2.38 (*s*, 3H, CH_3), 1.99 - 2.05 (*m*, 2H, CH_2), 1.60 - 1.61 (*m*, 1H, CH_2), 1.21 - 1.28 (*m*, 1H, CH_2). MS : m/z $[M+Na^+]^+$ = 332.3

6.4.31. Synthesis of methyl 2-(p-tolyl)-6,7-dihydro-5H-benzo[7]annulene-8-carboxylate[224]

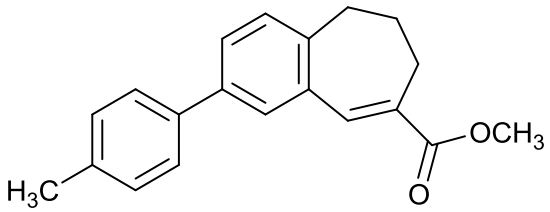

17

First reported by Shiraishi *et al*.[224] Methanesulfonyl chloride (1.89 g, 16.6 mmol, 2eq.) was added to a solution of 5-hydroxy-3-(p-tolyl)-6,7,8,9-tetrahydro-5H-benzo[7]annulene-6-carboxylate **16** (2.2 g, 8.1 mmol) and triethylamine (2.94 g, 3.5eq.) in DCM (50 ml) under ice cooling. The resulting mixture was stirred overnight at room temperature. 1,8-Diazabicyclo[5.4.0]undec-7-ene DBU (5.68 g, 37.35 mmol, 4.5eq.) was added drop wise under ice cooling and the resulting mixture was stirred for 1h at RT, and poured into water, 1 M HCl was added to acidify the solution pH= 3 and the mixture was extracted using DCM (2 x 100 ml). The combined organic layers were extracted washed first with water (100 ml), brine (100 ml), dried over Na_2SO_4 and evaporated *in vacuo* to give the crude product, which was purified using plug column (flash column) (hexane : ethyl acetate (7:3)) to yield methyl 2-(p-tolyl)-6,7-dihydro-5H-benzo[7]annulene-8-carboxylate **17** as a pure white solid (1.52 g, 68%). MS: m/z [M^+] = 291

6.4.32. Synthesis of 2-(p-tolyl)-6,7-dihydro-5H-benzo[7]annulene-8-carboxylic acid[224]

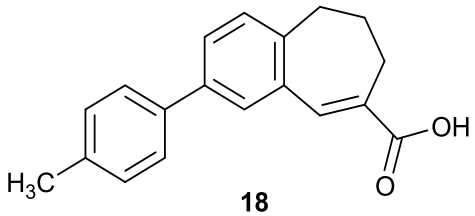

18

First reported by Shiraishi *et al*.[224] In a round bottom flask, methyl 2-(p-tolyl)-6,7-dihydro-5H-benzo[7]annulene-8-carboxylate **17** (1.45 g, 5 mmol) was dissolved in MeOH (50 ml) and 5 M sodium hydroxide solution (50 ml) was added. The mixture was headed to reflux for 3 h and after cooling to RT the solution was concentrated *in vacuo* and acidified with conc. HCl in order to form a precipitate. The solution was cooled in an ice bath to complete the precipitation and the solid was filtered off, washed with 1 M HCl and dried overnight to give 2-(p-tolyl)-6,7-dihydro-5H-benzo[7]annulene-8-carboxylic acid **18** as a colourless solid (1.2 g, 87%). ^{1}H-NMR (DMSO) : δ 10.02 (*brs*, OH), 7.67 - 7.72 (*m*, 2H, CH-Ar), 7.58 - 7.60 (*m*, 2H, CH-Ar), 7.51 - 7.53 (*m*, 1H, CH-Ar), 7.25 - 7.28 (*m*, 3H, CH-Ar), 2.80 - 2.83 (*m*, 2H, CH_2), 2.56 - 2.58 (*m*, 2H, CH_2), 2.34 (*s*, 3H, CH_3), 1.94 - 1.96 (*m*, 2H, CH_2). MS: m/z $[M]^-$ = 278

6.4.33. Synthesis of tri-tert-butyl 2,2',2''-(10-(2-oxo-2-((2-(2-(p-tolyl)-6,7-dihydro-5H-benzo[7]annulene-8-carboxamido)ethyl)amino)ethyl)-1,4,7,10-tetraazacyclododecane-1,4,7-triyl)triacetate

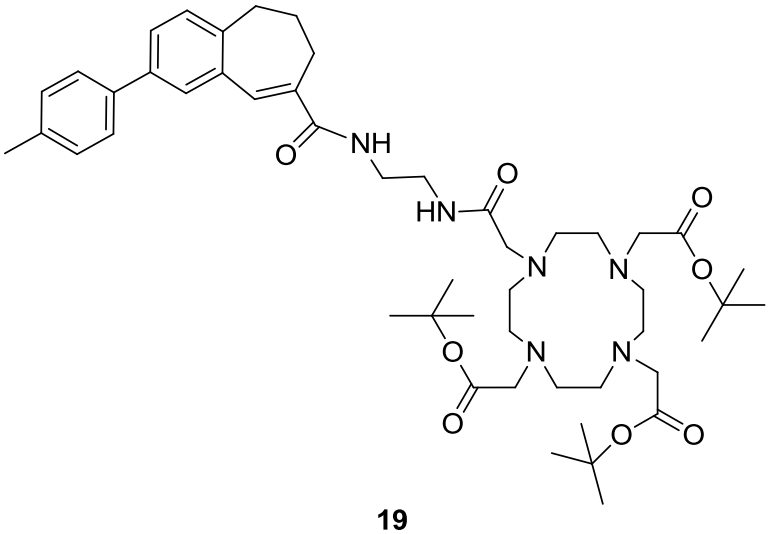

19

Carboxylic acid **18** (15 mg, 0,036 mmol) was dissolved together with carbonyldimidazole (CDI) (12 mg, 0.072 mmol) in anhydrous DMF (2 ml); the mixture was heated at 60 ^{o}C for 10 min and cooled down. The mixture was set under vacuum to remove formed carbon dioxide for next 10 min. Tri-tert-butyl 2,2',2''-(10-(2-((2-aminoethyl)amino)-2-oxoethyl)-1,4,7,10-tetraazacyclododecane-1,4,7-triyl)triacetate (21 mg, 0.034 mmol) was dissolved in DMF (1 ml) and added quickly to the carboxylic acid and CDI mixture. The reaction was stirred for 24 h at room temperature. Afterwards, DMF was removed under reduced pressure and extracted DCM to isolate compound **19** (22 mg, 76%)

6.4.34. Synthesis of 2,2',2''-(10-(2-oxo-2-((2-(2-(p-tolyl)-6,7-dihydro-5H-benzo[7]annulene-8-carboxamido)ethyl)amino)ethyl)-1,4,7,10-tetraazacyclododecane-1,4,7-triyl)triacetic acid

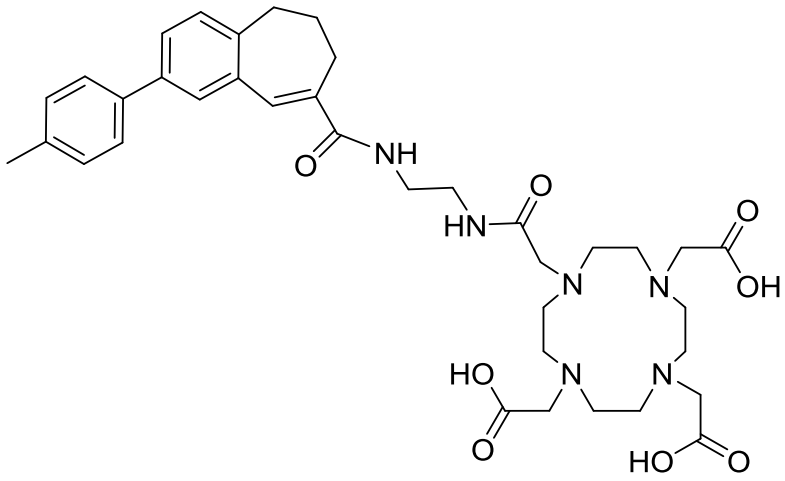

20

Tri-tert-butyl-2,2',2''-(10-(2-oxo-2-((2-(2-(p-tolyl)-6,7-dihydro-5H-benzo [7]annulene-8-carboxamido)ethyl)amino)ethyl)-1,4,7,10-tetraazacyclododecane-1,4,7-triyl)triacetate **19** (20 mg, 0.023 mmol) was dissolved in DCM (2 ml) and TFA (2 ml) was added dropwise to the mixture. The product was stirred overnight, and the solvents were removed under reduced pressure. Finally, the product was dissolved in minimal amount of methanol (HPLC grade) and added dropwise to (20 ml) of diethyl ether where white crystals crashed out. A white powder was collected by centrifugation and re-dissolved in water and freeze dried (18.7 mg). HPLC (method 2) was performed to check purity of the sample and it was found to be 65% pure. The pure product was isolated by semi-preparative HPLC (MeCN 30%- Acetate buffer pH 5.00 70%), analysed by mass spectrometry and used in the complex formation reaction. MS: m/z $[M\text{-}H^+]^-$ = 705.5

6.4.35. Synthesis of gallium (III) 2,2',2''-(10-(2-oxo-2-((2-(2-(p-tolyl)-6,7-dihydro-5H-benzo[7]annulene-8-carboxamido)ethyl)amino)ethyl)-1,4,7,10-tetraazacyclododecane-1,4,7-triyl)triacetic acid complex

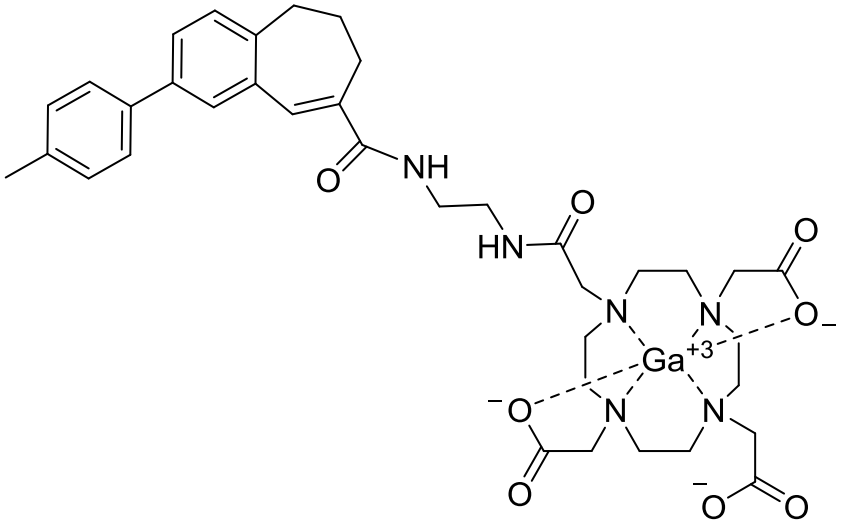

[Ga**20**]$^{+3}$

Complexation with gallium(III); used gallium(III) nitrate hydrate (ca. 2 mg) in ammonium acetate buto form a standard of the gallium(III) complex with 2,2',2''-(10-(2-oxo-2-((2-(2-(p-tolyl)-6,7-dihydro-5H-benzo[7]annulene-8-carboxamido)ethyl)amino)ethyl)-1,4,7,10-tetraazacyclododecane-1,4,7-triyl)triacetic acid **20**. The HPLC vial was shaken at 90 ^{o}C for 2h before HPLC analysis was carried out to show the retention time of the product (2.12 minutes).

6.4.36. Synthesis of ^{68}Ga- 2,2',2''-(10-(2-oxo-2-((2-(2-(p-tolyl)-6,7-dihydro-5H-benzo[7]annulene-8-carboxamido)ethyl)amino)ethyl)-1,4,7,10-tetraazacyclododecane-1,4,7-triyl)triacetic acid complex

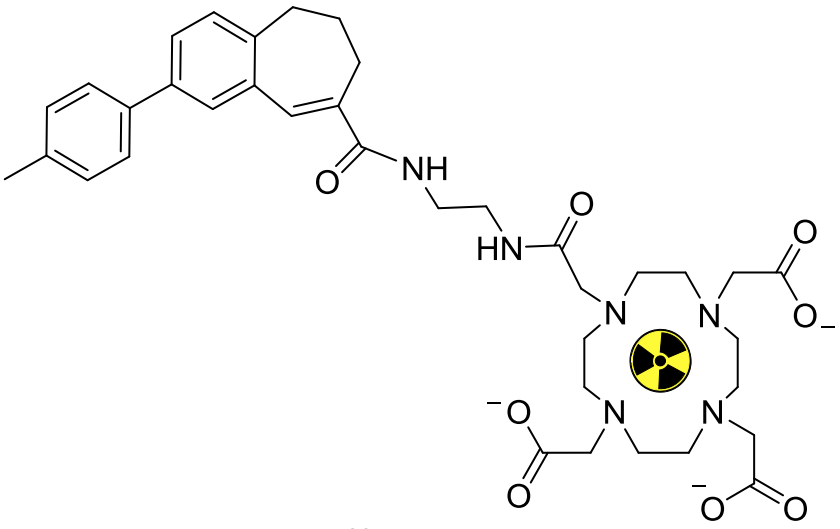

[^{68}Ga**20**]

To (200 µl, 1mg/ml) of 2,2',2''-(10-(2-oxo-2-((2-(2-(p-tolyl)-6,7-dihydro-5H-benzo[7]annulene-8-carboxamido)ethyl)amino)ethyl)-1,4,7,10-tetraazacyclododecane-1,4,7-triyl)triacetic acid **20** in ammonium acetate buffer (0.2 M, pH 5) was added to formulated $^{68}GaCl_3$ (231 MBq) and the reaction was mixed at 90 ºC for 15 minutes. RCY (radio-TLC): 100%.

7. References

1. J. Lichty, S. M. Allen, A. I. Grillo, S. J. Archibald and T. J. Hubin, *Inorg. Chim. Acta*, 2004, **357**, 615-618.
2. H. Holtmann and K. Resch, *Naturwissenschaften*, 1995, **82**, 178-187.
3. B. A. Teicher and S. P. Fricker, *Clin. Cancer. Res.*, 2010, **16**, 2927-2931.
4. J.-M. Zhang and J. An, *Int. Anesthesiol. Clin.*, 2007, **45**, 27-37.
5. A. Zlotnik and O. Yoshie, *Immunity*, 2012, **36**, 705-716.
6. M. Baggiolini, B. Dewald and B. Moser, *Annu. Rev. Immunol.*, 1997, **15**, 675-705.
7. A. Khan, J. Greenman and S. J. Archibald, *Curr. Med. Chem.*, 2007, **14**, 2257-2277.
8. J. J. Onuffer and R. Horuk, *Trends Pharmacol. Sci.*, 2002, **23**, 459-467.
9. A. P. Vicari and C. Caux, *Cytokine Growth Factor Rev.*, 2002, **13**, 143-154.
10. J. Panse, K. Friedrichs, A. Marx, Y. Hildebrandt, T. Luetkens, K. Bartels, C. Horn, T. Stahl, Y. Cao, K. Milde-Langosch, A. Niendorf, N. Kroeger, S. Wenzel, R. Leuwer, C. Bokemeyer, S. Hegewisch-Becker and D. Atanackovic, *Br. J. Cancer*, 2008, **99**, 930-938.
11. M. O'Hayre, C. L. Salanga, T. M. Handel and D. J. Hamel, *Expert Opin Drug Discov.* , 2010, **5**, 1109-1122.
12. C. J. Hutchings, M. Koglin and F. H. Marshall, *Mabs*, 2010, **2**, 594-606.
13. C. Murdoch and A. Finn, *Blood*, 2000, **95**, 3032-3043.
14. T. J. Hubin, J. M. McCormick, S. R. Collinson, N. W. Alcock and D. H. Busch, *Chem. Commun.*, 1998, DOI: 10.1039/a802060d, 1675-1676.
15. L. O. Gerlach, R. T. Skerlj, G. J. Bridger and T. W. Schwartz, *J. Biol. Chem.*, 2001, **276**, 14153-14160.
16. A. Muller, B. Homey, H. Soto, N. F. Ge, D. Catron, M. E. Buchanan, T. McClanahan, E. Murphy, W. Yuan, S. N. Wagner, J. L. Barrera, A. Mohar, E. Verastegui and A. Zlotnik, *Nature*, 2001, **410**, 50-56.
17. B. A. Teicher and S. P. Fricker, *Clinical Cancer Research*, 2010, **16**, 2927-2931.
18. H. Tamamura and N. Fujii, *Expert Opin. Ther. Targets*, 2005, **9**, 1267-1282.
19. J. Wang, K. A. Reiss, R. Khatri, E. Jaffee and D. Laheru, *J. Clin. Oncol.*, 2015, **33**, 1745-53.
20. S. Chatterjee, B. B. Azad and S. Nimmagadda, in *Emerging Applications of Molecular Imaging to Oncology*, eds. M. G. Pomper and P. B. Fisher, 2014, vol. 124, pp. 31-82.

21. M. R. Kuhne, T. Mulvey, B. Belanger, S. Chen, C. Pan, C. Chong, F. Cao, W. Niekro, T. Kempe, K. A. Henning, L. J. Cohen, A. J. Korman and P. M. Cardarelli, *Clin. Cancer. Res.*, 2013, **19**, 357-366.
22. H. Tamamura, Y. O. Xu, T. Hattori, X. Y. Zhang, R. Arakaki, K. Kanbara, A. Omagari, A. Otaka, T. Ibuka, N. Yamamoto, H. Nakashima and N. Fujii, *Biochem. Biophys. Res. Commun.*, 1998, **253**, 877-882.
23. H. Tamamura, A. Omagari, K. Hiramatsu, K. Gotoh, T. Kanamoto, Y. N. Xu, E. Kodama, M. Matsuoka, T. Hattori, N. Yamamoto, H. Nakashima, A. Otaka and N. Fujii, *Bioorg. Med. Chem. Lett.*, 2001, **11**, 1897-1902.
24. H. Tamamura, H. Tsutsumi, H. Masuno, S. Mizokami, K. Hiramatsu, Z. Wang, J. O. Trent, H. Nakashima, N. Yamamoto, S. C. Peiper and N. Fujii, *Org. Biomol. Chem.*, 2006, **4**, 2354-2357.
25. D. Schols, *Curr. Top. Med. Chem.*, 2004, **4**, 883-893.
26. M. Sumnersmith, Y. Zheng, Y. P. Zhang, E. M. Twist and S. C. Climie, *Drugs Exp. Clin. Res.*, 1995, **21**, 1-6.
27. B. J. Doranz, L. G. Filion, F. Diaz-Mitoma, D. S. Sitar, J. Sahai, F. D. Baribaud, M. J. Orsini, J. L. Benovic, W. Cameron and R. W. Doms, *AIDS Res. Hum. Retroviruses*, 2001, **17**, 475-486.
28. K. Ichiyama, S. Yokoyama-Kumakura, Y. Tanaka, R. Tanaka, K. Hirose, K. Bannai, T. Edamatsu, M. Yanaka, Y. Niitani, N. Miyano-Kurosaki, H. Takaku, Y. Koyanagi and N. Yamamoto, *Proc. Natl. Acad. Sci. U. S. A.*, 2003, **100**, 4185-4190.
29. W. M. Kazmierski, T. P. Kenakin and K. S. Gudmundsson, *Chem. Biol. Drug Des.*, 2006, **67**, 13-26.
30. T. Murakami, S. Kumakura, T. Yamazaki, R. Tanaka, M. Hamatake, K. Okuma, W. Huang, J. Toma, J. Komano, M. Yanaka, Y. Tanaka and N. Yamamoto, *Antimicrob. Agents Chemother.*, 2009, **53**, 2940-2948.
31. D. Schols, S. Claes, S. Hatse, K. Princen, K. Vermeire, E. De Clercq, R. Skerlj, G. Bridger and G. Calandra, *Antiviral Res.*, 2003, **57**, A39-A39.
32. K. Princen, S. Hatse, K. Vermeire, S. Aquaro, E. De Clercq, L. O. Gerlach, M. Rosenkilde, T. W. Schwartz, R. Skerlj, G. Bridger and D. Schols, *J. Virol.*, 2004, **78**, 12996-13006.
33. N. A. Piro, J. R. Robinson, P. J. Walsh and E. J. Schelter, *Coord. Chem. Rev.*, 2014, **260**, 21-36.
34. S.-G. Kang, Y.-T. Lee, H. Chun and K. Kim, *Inorg. Chim. Acta*, 2014, **409**, 315-319.
35. H. Khoshro, H. R. Zare, A. Gorji and M. Namazian, *Electrochim. Acta*, 2014, **117**, 62-67.

36. S. Hatse, K. Princen, E. De Clercq, M. M. Rosenkilde, T. W. Schwartz, P. E. Hernandez-Abad, R. T. Skerlj, G. J. Bridger and D. Schols, *Biochem. Pharmacol.*, 2005, **70**, 752-761.
37. G. J. Bridger, R. T. Skerlj, P. E. Hernandez-Abad, D. E. Bogucki, Z. Wang, Y. Zhou, S. Nan, E. M. Boehringer, T. Wilson, J. Crawford, M. Metz, S. Hatse, K. Princen, E. De Clercq and D. Schols, *J. Med. Chem.*, 2010, **53**, 1250-1260.
38. E. De Clercq, *Nat. Rev. Drug Discov.*, 2003, **2**, 581-587.
39. J. Dessolin, P. Galea, P. Vlieghe, J. C. Chermann and J. L. Kraus, *J. Med. Chem.*, 1999, **42**, 229-241.
40. P. Zhan and X. Liu, *Curr. Med. Chem.*, 2013, **20**, 1743-1758.
41. E. De Clercq, *Biochem. Pharmacol.*, 2009, **77**, 1655-1664.
42. K. L. Arnolds and J. V. Spencer, *Infect. Genet. Evol.*, 2014, **25**, 146-156.
43. M. Ciampolini, L. Fabbrizzi, A. Perotti, A. Poggi, B. Seghi and F. Zanobini, *Inorg. Chem.*, 1987, **26**, 3527-3533.
44. G. J. Bridger, R. T. Skerlj, D. Thornton, S. Padmanabhan, S. A. Martellucci, G. W. Henson, M. J. Abrams, N. Yamamoto, K. Devreese, R. Pauwels and E. Declercq, *J. Med. Chem.*, 1995, **38**, 366-378.
45. G. J. Bridger, R. T. Skerlj, S. Padmanabhan, S. A. Martellucci, G. W. Henson, M. J. Abrams, H. C. Joao, M. Witvrouw, K. DeVreese, R. Pauwels and E. DeClercq, *J. Med. Chem.*, 1996, **39**, 109-119.
46. A. Larochelle, A. Krouse, M. Metzger, D. Orlic, R. E. Donahue, S. Fricker, G. Bridger, C. E. Dunbar and P. Hematti, *Blood*, 2006, **107**, 3772-3778.
47. G. Karponi, N. Psatha, C. W. Lederer, J. E. Adair, F. Zervou, N. Zogas, M. Kleanthous, C. Tsatalas, A. Anagnostopoulos, M. Sadelain, I. Riviere, G. Stamatoyannopoulos and E. Yannaki, *Blood*, 2015, **126**, 616-619.
48. W. C. Liles, H. E. Broxmeyer, E. Rodger, B. Wood, K. Hubel, S. Cooper, G. Hangoc, G. J. Bridger, G. W. Henson, G. Calandra and D. C. Dale, *Blood*, 2003, **102**, 2728-2730.
49. E. De Clercq, *Med. Res. Rev.*, 2015, **35**, 698-719.
50. G. Calandra, J. McCarty, J. McGuirk, G. Tricot, S. A. Crocker, K. Badel, B. Grove, A. Dye and G. Bridger, *Bone Marrow Transplant.*, 2008, **41**, 331-338.
51. Y. Gazitt, C. O. Freytes, C. Akay, K. Badel and G. Calandra, *Stem Cells Dev.*, 2007, **16**, 657-666.
52. N. Flomenberg, J. DiPersio and G. Calandra, *Acta Haematol.*, 2005, **114**, 198-205.
53. S. Devine, Y. Gazitt and G. Calandra, *J. Clin. Oncol.*, 2005, **23**, 3872-3873.

54. H. E. Broxmeyer, *Preclinical Experience with AMD3100 for Mobilization of Hematopoietic Stem and Progenitor Cells*, Springer US, 2012.
55. V. De Falco, V. Guarino, E. Avilla, M. D. Castellone, P. Salerno, G. Salvatore, P. Faviana, F. Basolo, M. Santoro and R. M. Melillo, *Cancer Res.*, 2007, **67**, 11821-11829.
56. J. B. Rubin, A. L. Kung, R. S. Klein, J. A. Chan, Y. P. Sun, K. Schmidt, M. W. Kieran, A. D. Luster and R. A. Segal, *Proc. Natl. Acad. Sci. U. S. A.*, 2003, **100**, 13513-13518.
57. J.-K. Li, L. Yu, Y. Shen, L.-S. Zhou, Y.-C. Wang and J.-H. Zhang, *World J. Gastroenterol.*, 2008, **14**, 2308-2313.
58. J. A. Este, C. Cabrera, E. De Clercq, S. Struyf, J. Van Damme, G. Bridger, R. T. Skerlj, M. J. Abrams, G. Henson, A. Gutierrez, B. Clotet and D. Schols, *Mol. Pharmacol.*, 1999, **55**, 67-73.
59. E. Declerco, N. Yamamoto, R. Pauwels, M. Baba, D. Schols, H. Nakashima, J. Balzarini, Z. Debyser, B. A. Murrer, D. Schwartz, D. Thornton, G. Bridger, S. Fricker, G. Henson, M. Abrams and D. Picker, *Proc. Natl. Acad. Sci. U. S. A.*, 1992, **89**, 5286-5290.
60. G. J. Bridger, R. T. Skerlj and E. De Clercq, *Adv. Antiviral Res.*, 1999, **3**, 161-229.
61. R. Smith, D. Huskens, D. Daelemans, R. E. Mewis, C. D. Garcia, A. N. Cain, T. N. C. Freeman, C. Pannecouque, E. De Clercq, D. Schols, T. J. Hubin and S. J. Archibald, *Dalton Trans.*, 2012, **41**, 11369-11377.
62. G. C. Valks, G. McRobbie, E. A. Lewis, T. J. Hubin, T. M. Hunter, P. J. Sadler, C. Pannecouque, E. De Clercq and S. J. Archibald, *J. Med. Chem.*, 2006, **49**, 6162-6165.
63. G. McRobbie, G. C. Valks, C. J. Empson, A. Khan, J. D. Silversides, C. Pannecouque, E. De Clercq, S. G. Fiddy, A. J. Bridgeman, N. A. Young and S. J. Archibald, *Dalton Trans.*, 2007, 5008-5018.
64. A. Khan, G. Nicholson, J. Greenman, L. Madden, G. McRobbie, C. Pannecouque, E. De Clercq, R. Ullom, D.L. Maples, R.D. Maples, J.D. Silversides, T.J. Hubin and S.J. Archibald, *J. Am. Chem. Soc.*, 2009, **131**, 3416-3417.
65. M. Thelen, *Nat. Immunol.*, 2001, **2**, 129-134.
66. A. Mueller and P. G. Strange, *Int. J. Biochem. Cell Biol*, 2004, **36**, 35-38.
67. F. Cocchi, A. L. Devico, A. Garzinodemo, S. K. Arya, R. C. Gallo and P. Lusso, *Science*, 1995, **270**, 1811-1815.
68. G. Alkhatib, C. Combadiere, C. C. Broder, Y. Feng, P. E. Kennedy, P. M. Murphy and E. A. Berger, *Science*, 1996, **272**, 1955-1958.

69. R. S. Y. Wong, V. Bodart, M. Metz, J. Labrecque, G. Bridger and S. P. Fricker, *Mol. Pharmacol.*, 2008, **74**, 1485-1495.
70. T. Liu, Z. Y. Weng, X. W. Dong and Y. Z. Hu, *Mini-Rev. Med. Chem.*, 2010, **10**, 1277-1292.
71. K. M. Haney, F. Zhang, C. K. Arnatt, Y. Y. Yuan, G. Li, J. L. Ware, D. A. Gewirtz and Y. Zhang, *Bioorg. Med. Chem. Lett.*, 2011, **21**, 5159-5163.
72. D. Aldinucci and A. Colombatti, *Mediators Inflamm.*, 2014, **2014**, 292376-292376.
73. J. Labrecque, M. Metz, G. Lau, M. C. Darkes, R. S. Y. Wong, D. Bogucki, B. Carpenter, G. Chen, T. Li, S. Nan, D. Schols, G. J. Bridger, S. P. Pricker and R. T. Skerlj, *Virol. J.*, 2011, **413**, 231-243.
74. G. G. Vaday, D. M. Peehl, P. A. Kadam and D. M. Lawrence, *Prostate*, 2006, **66**, 124-134.
75. R. I. Connor, K. E. Sheridan, D. Ceradini, S. Choe and N. R. Landau, *J. Exp. Med.*, 1997, **185**, 621-628.
76. T. Theobald, *Sampson's Textbook of Radiopharmacy* pharmaceutical press, 2011, 1 Lambeth High Street London UK fourth edn.
77. F. Reynolds and K. A. Kelly, *Molecular imaging*, 2011, **10**, 407-419.
78. S. Achilefu, *Chem. Rev.*, 2010, **110**, 2575-2578.
79. M. Baker, *Nature*, 2010, **463**, 977-980.
80. S. Bhattacharyya and M. Dixit, *Dalton Trans.*, 2011, **40**, 6112-6128.
81. Z. B. Li and P. S. Conti, *Adv. Drug Del. Rev.*, 2010, **62**, 1031-1051.
82. P. W. Miller, N. J. Long, R. Vilar and A. D. Gee, *Angewandte Chemie-International Edition*, 2008, **47**, 8998-9033.
83. M. E. Phelps, *Proc. Natl. Acad. Sci. U. S. A.*, 2000, **97**, 9226-9233.
84. H. F. Huang, K. Liang, Y. P. Liu, S. T. Huang and T. W. Chu, *Prog Chem*, 2011, **23**, 1501-1506.
85. S. G. Deeks, M. Smith, M. Holodniy and J. O. Kahn, *JAMA*, 1997, **277**, 145-153.
86. A. Rahmim and H. Zaidi, *Nucl. Med. Commun.*, 2008, **29**, 193-207.
87. T. J. Wadas, E. H. Wong, G. R. Weisman and C. J. Anderson, *Chem. Rev.*, 2010, **110**, 2858-2902.
88. C. J. Anderson and M. J. Welch, *Chem. Rev.*, 1999, **99**, 2219-2234.
89. S. Liu, *Chem. Soc. Rev.*, 2004, **33**, 445-461.
90. S. V. Smith, *J. Inorg. Biochem.*, 2004, **98**, 1874-1901.
91. M. Shokeen and C. J. Anderson, *Acc. Chem. Res.*, 2009, **42**, 832-841.
92. R. D. Shannon, *Acta Crystallogr. Sect. A*, 1976, **32**, 751-767.
93. M. D. Bartholomae, *Inorg. Chim. Acta*, 2012, **389**, 36-51.

94. C. F. Ramogida and C. Orvig, *Chem. Commun.*, 2013, **49**, 4720-4739.
95. A. Al-Nahhas, Z. Win, T. Szyszko, A. Singh, S. Khan and D. Rubello, *Eur. J. Nucl. Med. Mol. Imag.*, 2007, **34**, 1897-1901.
96. S. Mirzadeh and R. M. Lambrecht, *J. Radioanal. Nucl. Chem.*, 1996, **202**, 7-102.
97. K. P. Zhernosekov, D. V. Filosofov, R. P. Baum, P. Aschoff, H. Bihl, A. A. Razbash, M. Jahn, M. Jennewein and F. Rösch, *J. Nucl. Med.*, 2007, **48**, 1741-1748.
98. S. Liu, *Adv. Drug Del. Rev.*, 2008, **60**, 1347-1370.
99. J. P. Holland, M. J. Williamson, J. S. Lewis, *Mol. Imaging*, 2010, **9**, 1-20.
100. M. Fani, J. P. André and H. R. Maecke, *Contrast Media Mol. Imaging*, 2008, **3**, 53-63.
101. M. A. Green and M. J. Welch, *Int. J. Rad. Appl. Instrum B*, 1989, **16**, 435-448.
102. M. Asti, G. De Pietri, A. Fraternali, E. Grassi, R. Sghedoni, F. Fioroni, F. Roesch, A. Versari and D. Salvo, *Nucl. Med. Biol.*, **35**, 721-724.
103. M. D. Bartholomä, *Inorg. Chim. Acta*, 2012, **389**, 36-51.
104. L. O. Gerlach, J. S. Jakobsen, K. P. Jensen, M. R. Rosenkilde, R. T. Skerlj, U. Ryde, G. J. Bridger and T. W. Schwartz, *Biochem. (Mosc.)*, 2003, **42**, 710-717.
105. T. M. Hunter, S. J. Paisey, H. S. Park, L. Cleghorn, A. Parkin, S. Parsons and P. J. Sadler, *J. Inorg. Biochem.*, 2004, **98**, 713-719.
106. R. M. Izatt, K. Pawlak, J. S. Bradshaw and R. L. Bruening, *Chem. Rev.*, 1991, **91**, 1721-2085.
107. K. R. Adam, M. Antolovich, I. M. Atkinson, A. J. Leong, L. F. Lindoy, B. J. McCool, R. L. Davis, C. H. L. Kennard and P. A. Tasker, *Chem. Commun.*, 1994, 1539-1540.
108. R. K. Singh and M. A. Khan, *Int. J. Quantum Chem*, 2011, **111**, 4174-4185.
109. T. A. Tyson, K. O. Hodgson, B. Hedman and G. R. Clark, *Acta Crystallogr. Sect. C*, 1990, **46**, 1638-1640.
110. X. Y. Liang and P. J. Sadler, *Chem. Soc. Rev.*, 2004, **33**, 246-266.
111. K. L. Haas and K. J. Franz, *Chem. Rev.*, 2009, **109**, 4921-4960.
112. E. J. Billo, *Inorg. Chem.*, 1984, **23**, 236-238.
113. E. J. Billo, *Inorg. Chem.*, 1984, **23**, 2223-2227.
114. L. Y. Martin, L. J. Dehayes, L. J. Zompa and D. H. Busch, *J. Am. Chem. Soc.*, 1974, **96**, 4046-4048.
115. X. Y. Liang, J. A. Parkinson, M. Weishaupl, R. O. Gould, S. J. Paisey, H. S. Park, T. M. Hunter, C. A. Blindauer, S. Parsons and P. J. Sadler, *J. Am. Chem. Soc.*, 2002, **124**, 9105-9112.
116. M. A. Donnelly and M. Zimmer, *Inorg. Chem.*, 1999, **38**, 1650-1658.

117. X. Y. Liang, M. Weishaupl, J. A. Parkinson, S. Parsons, P. A. McGregor and P. J. Sadler, *Chem. Eur. J* 2003, **9**, 4709-4717.
118. M. Kodama and E. Kimura, *Dalton Trans.*, 1977, 2269-2276.
119. T. M. Hunter, I. W. McNae, D. P. Simpson, A. M. Smith, S. Moggach, F. White, M. D. Walkinshaw, S. Parsons and P. J. Sadler, *Chem. Eur. J.*, 2007, **13**, 40-50.
120. A. Khan, G. Nicholson, J. Greenman, L. Madden, G. McRobbie, C. Pannecouque, E. De Clercq, R. Ullom, D. L. Maples, R. D. Maples, J. D. Silversides, T. J. Hubin and S. J. Archibald, *J. Am. Chem. Soc.*, 2009, **131**, 3416-+.
121. R. Smith, D. Huskens, D. Daelemans, R. E. Mewis, C. D. Garcia, A. N. Cain, T. N. C. Freeman, C. Pannecouque, E. D. Clercq, D. Schols, T. J. Hubin and S. J. Archibald, *Dalton Trans.*, 2012, **41**, 11369-11377.
122. R. Smith, D. Huskens, D. Daelemans, R. E. Mewis, C. D. Garcia, A. N. Cain, T. N. C. Freeman, C. Pannecouque, E. D. Clercq, D. Schols, T. J. Hubin and S. J. Archibald, *Dalton Trans.*, 2012, **41**, 11369-11377.
123. A. Khan, G. Nicholson, J. Greenman, L. Madden, G. McRobbie, C. Pannecouque, E. De Clercq, R. Ullom, D. L. Maples, R. D. Maples, J. D. Silversides, T. J. Hubin and S. J. Archibald, *JACS*, 2009, **131**, 3416–3417.
124. R. Kowallick, M. Neuburger, M. Zehnder and T. A. Kaden, *Helv. Chim. Acta*, 1997, **80**, 948-959.
125. M. Micheloni, P. Paoletti, S. Burki and T. A. Kaden, *Helv. Chim. Acta*, 1982, **65**, 587-594.
126. K. P. Wainwright, *Inorg. Chem.*, 1980, **19**, 1396-1398.
127. M. Le Baccon, F. Chuburu, L. Toupet, H. Handel, M. Soibinet, I. Dechamps-Olivier, J. P. Barbiere and M. Aplincourt, *New J. Chem.*, 2001, **25**, 1168-1174.
128. P. Gluzinski, J. W. Krajewski, Z. Urbanczyklipkowska, J. Bleidelis and A. Kemme, *Acta Crystallogr. Sect. B-Struct. Sci.*, 1982, **38**, 3038-3041.
129. J. D. Silversides, B. P. Burke and S. J. Archibald, *Comptes Rendus Chimie*, 2013, **16**, 524-530.
130. A. Khan, J. D. Silversides, L. Madden, J. Greenman and S. J. Archibald, *Chem. Commun.*, 2007, DOI: 10.1039/b614557d, 416-418.
131. J. D. Silversides, R. Smith and S. J. Archibald, *Dalton Trans.*, 2011, **40**, 6289-6297.
132. J. D. Silversides, C. C. Allan and S. J. Archibald, *Dalton Trans.*, 2007, DOI: 10.1039/b615329a, 971-978.
133. B. H. Abdulwahaab, B. P. Burke, J. Domarkas, J. D. Silversides, T. J. Prior and S. J. Archibald, *J. Org. Chem.*, 2016, **81**, 890-898.
134. R. A. Kolinski, *Pol. J. Chem.*, 1995, **69**, 1039-1045.

135. J. Plutnar, J. Havlickova, J. Kotek, P. Hermann and I. Lukes, *New J. Chem.*, 2008, **32**, 496-504.
136. E. H. Wong, G. R. Weisman, D. C. Hill, D. P. Reed, M. E. Rogers, J. S. Condon, M. A. Fagan, J. C. Calabrese, K. C. Lam, I. A. Guzei and A. L. Rheingold, *J. Am. Chem. Soc.*, 2000, **122**, 10561-10572.
137. E. K. Barefield, K. A. Foster, G. M. Freeman and K. D. Hodges, *Inorg. Chem.*, 1986, **25**, 4663-4668.
138. L. Siegfried and T. A. Kaden, *Helv. Chim. Acta*, 2005, **88**, 380-390.
139. K. Biber and H. W. G. M. Boddeke, in *Chemokine Receptors as Drug Targets*, eds. M. J. Smit, S. A. Lira and R. Leurs, 2011, vol. 46, pp. 151-166.
140. F. Balkwill, *Nat. Rev. Cancer*, 2004, **4**, 540-550.
141. M. Kucia, K. Jankowski, R. Reca, M. Wysoczynski, L. Bandura, D. J. Allendorf, J. Zhang, J. Ratajczak and M. Z. Ratajczak, *J. Mol. Histol.*, 2004, **35**, 233-245.
142. G. A. Donzella, D. Schols, S. W. Lin, J. A. Este, K. A. Nagashima, P. J. Maddon, G. P. Allaway, T. P. Sakmar, G. Henson, E. De Clercq and J. P. Moore, *Nat. Med.*, 1998, **4**, 72-77.
143. N. I. Tarasova, R. H. Stauber and C. J. Michejda, *J. Biol. Chem.*, 1998, **273**, 15883-15886.
144. F. Andre, W. Xia, R. Conforti, Y. Wei, T. Boulet, G. Tomasic, M. Spielmann, M. Zoubir, N. Berrada, R. Arriagada, G. N. Hortobagyi, M.-C. Hung, L. Pusztai, S. Delaloge, S. Michiels and M. Cristofanilli, *Oncologist*, 2009, **14**, 1182-1188.
145. B. C. Schmid, M. Rudas, G. A. Rezniczek, S. Leodolter and R. Zeillinger, *Breast Cancer Res. Treat.*, 2004, **84**, 247-250.
146. I.-K. Na, C. Scheibenbogen, C. Adam, A. Stroux, P. Ghadjar, E. Thiel, U. Keilholz and S. E. Coupland, *Hum. Pathol.*, 2008, **39**, 1751-1755.
147. H. J. Lee, S. W. Kim, H. Y. Kim, S. Li, H. J. Yun, K. S. Song, S. Kim and D. Y. Jo, *Int. J. Oncol.*, 2009, **34**, 473-480.
148. T. Akashi, K. Koizumi, K. Tsuneyama, I. Saiki, Y. Takano and H. Fuse, *Cancer Sci.*, 2008, **99**, 539-542.
149. S. Otsuka, A. C. Klimowicz, K. Kopciuk, S. K. Petrillo, M. Konno, D. Hao, H. Muzik, E. Stolte, W. Boland, D. Morris, A. M. Magliocco and D. G. Bebb, *J. Thorac. Oncol.*, 2011, **6**, 1169-1178.
150. J. Kuil, T. Buckle and F. W. B. van Leeuwen, *Chem. Soc. Rev.*, 2012, **41**, 5239-5261.
151. S. Lee, J. Xie and X. Chen, *Chem. Rev.*, 2010, **110**, 3087-3111.
152. J. Kuil, A. H. Velders and F. W. B. van Leeuwen, *Bioconj. Chem.*, 2010, **21**, 1709-1719.

153. D. A. Mankoff, J. M. Link, H. M. Linden, L. Sundararajan and K. A. Krohn, *J. Nucl. Med.*, 2008, **49**, 149S-163S.
154. R. B. Maksym, M. Tarnowski, K. Grymula, J. Tarnowska, M. Wysoczynski, R. Liu, B. Czerny, J. Ratajczak, M. Kucia and M. Z. Ratajczak, *Eur. J. Pharmacol.*, 2009, **625**, 31-40.
155. M. Schottelius and H.-J. Wester, *Methods*, 2009, **48**, 161-177.
156. B. Furusato, A. Mohamed, M. Uhlen and J. S. Rhim, *Pathol. Int.*, 2010, **60**, 497-505.
157. S. Nimmagadda, M. Pullambhatla and M. G. Pomper, *J. Nucl. Med.*, 2009, **50**, 1124-1130.
158. H. Tamamura, H. Tsutsumi and N. Fujii, *Mini-Rev. Med. Chem.*, 2006, **6**, 989-995.
159. N. Fujii, S. Oishi, K. Hiramatsu, T. Araki, S. Ueda, H. Tamamura, A. Otaka, S. Kusano, S. Terakubo, H. Nakashima, J. A. Broach, J. O. Trent, Z. X. Wang and S. C. Peiper, *Angew. Chem. Int. Ed. Engl.*, 2003, **42**, 3251-3253.
160. T. Narumi, R. Hayashi, K. Tomita, K. Kobayashi, N. Tanahara, H. Ohno, T. Naito, E. Kodama, M. Matsuoka, S. Oishi and N. Fujii, *Org. Biomol. Chem.*, 2010, **8**, 616-621.
161. H.-J. Wester, I. Dijkgraaf, M. Anton, U. Schumacher, W. Brandau, O. Demmer, H. Kessler and M. Schwaiger, *J. Labelled Comp. Radiopharm.*, 2009, **52**, 211-212.
162. O. Demmer, E. Gourni, U. Schumacher, H. Kessler and H.-J. Wester, *ChemMedChem*, 2011, **6**, 1789-1791.
163. E. Gourni, O. Demmer, M. Schottelius, C. D'Alessandria, S. Schulz, I. Dijkgraaf, U. Schumacher, M. Schwaiger, H. Kessler and H.-J. Wester, *J. Nucl. Med.*, 2011, **52**, 1803-1810.
164. H. J. Wester, U. Keller, M. Schottelius, A. Beer, K. Philipp-Abbrederis, F. Hoffmann, J. Simecek, C. Gerngross, M. Lassmann, K. Herrmann, N. Pellegata, M. Rudelius, H. Kessler and M. Schwaiger, *Theranostics*, 2015, **5**, 618-630.
165. K. Philipp-Abbrederis, K. Herrmann, S. Knop, M. Schottelius, M. Eiber, K. Lueckerath, E. Pietschmann, S. Habringer, C. Gerngross, K. Franke, M. Rudelius, A. Schirbel, C. Lapa, K. Schwamborn, S. Steidle, E. Hartmann, A. Rosenwald, S. Kropf, A. J. Beer, C. Peschel, H. Einsele, A. K. Buck, M. Schwaiger, K. Goetze, H.-J. Wester and U. Keller, *EMBO Mol Med*, 2015, **7**, 477-487.
166. O. Jacobson, I. D. Weiss, L. Szajek, J. M. Farber and D. O. Kiesewetter, *Biorg. Med. Chem.*, 2009, **17**, 1486-1493.
167. S. Nimmagadda, M. Pullambhatla, K. Stone, G. Green, Z. M. Bhujwalla and M. G. Pomper, *Cancer Res.*, 2010, **70**, 3935-3944.

168. I. D. Weiss, O. Jacobson, D. O. Kiesewetter, J. P. Jacobus, L. P. Szajek, X. Chen and J. M. Farber, *Mol. Imag. Biol.*, 2012, **14**, 106-114.
169. R. A. De Silva, K. Peyre, M. Pullambhatla, J. J. Fox, M. G. Pomper and S. Nimmagadda, *J. Nucl. Med.*, 2011, **52**, 986-993.
170. L. E. Woodard, R. A. De Silva, B. B. Azad, A. Lisok, M. Pullambhatla, W. G. Lesniak, R. C. Mease, M. G. Pomper and S. Nimmagadda, *Nucl. Med. Biol.*, 2014, **41**, 552-561.
171. N. Bernier, M. Allali, R. Tripier, F. Conan, V. Patinec, S. Develay, M. Le Baccon and H. Handel, *New J. Chem.*, 2006, **30**, 435-441.
172. B. Lee, M. Sharron, L. J. Montaner, D. Weissman and R. W. Doms, *Proc. Natl. Acad. Sci. U. S. A.*, 1999, **96**, 5215-5220.
173. S. Harada, Y. Koyanagi and N. Yamamoto, *Science*, 1985, **229**, 563-566.
174. C. Pannecouque, D. Daelemans and E. De Clercq, *Nat. Protoc.*, 2008, **3**, 427-434.
175. R. Pauwels, J. Balzarini, M. Baba, R. Snoeck, D. Schols, P. Herdewijn, J. Desmyter and E. Declercq, *J. Virol. Methods*, 1988, **20**, 309-321.
176. D. Schols, S. Struyf, J. VanDamme, J. A. Este, G. Henson and E. DeClercq, *J. Exp. Med.*, 1997, **186**, 1383-1388.
177. S. P. Fricker, V. Anastassov, J. Cox, M. C. Darkes, O. Grujic, S. R. Idzan, J. Labrecque, G. Lau, R. M. Mosi, K. L. Nelson, L. Qin, Z. Santucci and R. S. Y. Wong, *Biochem. Pharmacol.*, 2006, **72**, 588-596.
178. K. Princen, S. Hatse, K. Vermeire, E. De Clercq and D. Schols, *Cytometry Part A*, 2003, **51A**, 35-45.
179. C. A. Boswell, X. K. Sun, W. J. Niu, G. R. Weisman, E. H. Wong, A. L. Rheingold and C. J. Anderson, *J. Med. Chem.*, 2004, **47**, 1465-1474.
180. X. K. Sun, M. Wuest, G. R. Weisman, E. H. Wong, D. P. Reed, C. A. Boswell, R. Motekaitis, A. E. Martell, M. J. Welch and C. J. Anderson, *J. Med. Chem.*, 2002, **45**, 469-477.
181. S. J. Paisey and P. J. Sadler, *Chem. Commun.*, 2004, 306-307.
182. D. N. Pandya, A. V. Dale, J. Y. Kim, H. Lee, Y. S. Ha, G. I. An and J. Yoo, *Bioconj. Chem.*, 2012, **23**, 330-335.
183. C. A. Boswell, C. A. S. Regino, K. E. Baidoo, K. J. Wong, D. E. Milenic, J. A. Kelley, C. C. Lai and M. W. Brechbiel, *Biorg. Med. Chem.*, 2009, **17**, 548-552.
184. R. Mannhold and H. van de Waterbeemd, *J. Comput.-Aided Mol. Des.*, 2001, **15**, 337-354.
185. H. van de Waterbeemd, D. A. Smith, K. Beaumont and D. K. Walker, *J. Med. Chem.*, 2001, **44**, 1313-1333.

186. J. R. Proudfoot, *Bioorg. Med. Chem. Lett.*, 2005, **15**, 1087-1090.
187. H. Kubinyi, *Progress in drug research. Fortschritte der Arzneimittelforschung. Progres des recherches pharmaceutiques*, 1979, **23**, 97-198.
188. H. Kubinyi, *Arzneim.-Forsch.*, 1979, **29-2**, 1067-1080.
189. M. T. D. Cronin, *Current Computer-Aided Drug Design*, 2006, **2**, 405-413.
190. C. A. Lipinski, F. Lombardo, B. W. Dominy and P. J. Feeney, *Adv. Drug Del. Rev.*, 2001, **46**, 3-26.
191. C. A. Lipinski, F. Lombardo, B. W. Dominy and P. J. Feeney, *Adv. Drug Del. Rev.*, 1997, **23**, 3-25.
192. M. Oppermann, *Cell. Signal.*, 2004, **16**, 1201-1210.
193. G. Soria and A. Ben-Baruch, *Cancer Lett.*, 2008, **267**, 271-285.
194. M. Abe, K. Hiura, J. Wilde, K. Moriyama, T. Hashimoto, S. Ozaki, S. Wakatsuki, M. Kosaka, S. Kido, D. Inoue and T. Matsumoto, *Blood*, 2002, **100**, 2195-2202.
195. D. Lv, Y. Zhang, H.-J. Kim, L. Zhang and X. Ma, *Cellular & Molecular Immunology*, 2013, **10**, 303-310.
196. Y. Oba, J. W. Lee, L. A. Ehrlich, H. Y. Chung, D. F. Jelinek, N. S. Callander, R. Horuk, S. J. Choi and G. D. Roodman, *Exp. Hematol.*, 2005, **33**, 272-278.
197. E. Terpos, M. Politou, R. Szydlo, J. M. Goldman, J. F. Apperley and A. Rahemtulla, *Br. J. Haematol.*, 2003, **123**, 106-109.
198. M. Roussou, A. Tasidou, M. A. Dimopoulos, E. Kastritis, M. Migkou, D. Christoulas, M. Gavriatopoulou, F. Zagouri, C. Matsouka, D. Anagnostou and E. Terpos, *Leukemia*, 2009, **23**, 2177-2181.
199. S. Lentzsch, M. Gries, M. Janz, R. Bargou, B. Dorken and M. Y. Mapara, *Blood*, 2003, **101**, 3568-3573.
200. C. Moller, T. Stromberg, M. Juremalm, K. Nilsson and G. Nilsson, *Leukemia*, 2003, **17**, 203-210.
201. D. Aldinucci, D. Lorenzon, L. Cattaruzza, A. Pinto, A. Gloghini, A. Carbone and A. Colombatti, *Int. J. Cancer*, 2008, **122**, 769-776.
202. M. Fischer, M. Juremalm, N. Olsson, C. Backlin, C. Sundstrom, K. Nilsson, G. Enblad and G. Nilsson, *Int. J. Cancer*, 2003, **107**, 197-201.
203. D. Aldinucci, A. Gloghini, A. Pinto, A. Colombatti and A. Carbone, *Leuk. Lymphoma*, 2012, **53**, 195-201.
204. I. Bieche, F. Lerebours, S. Tozlu, M. Espie, M. Marty and R. Lidereau, *Clin. Cancer. Res.*, 2004, **10**, 6789-6795.
205. Y. Niwa, H. Akamatsu, H. Niwa, H. Sumi, Y. Ozaki and A. Abe, *Clin. Cancer. Res.*, 2001, **7**, 285-289.

206. G. Luboshits, S. Shina, O. Kaplan, S. Engelberg, D. Nass, B. Lifshitz-Mercer, S. Chaitchik, I. Keydar and A. Ben-Baruch, *Cancer Res.*, 1999, **59**, 4681-4687.

207. H. Seidl, E. Richtig, H. Tilz, M. Stefan, U. Schmidbauer, M. Asslabler, K. Zatloukal, M. Herlyn and H. Schaider, *Hum. Pathol.*, 2007, **38**, 768-780.

208. U. Mrowietz, U. Schwenk, S. Maune, J. Bartels, M. Kupper, I. Fichtner, J. M. Schroder and D. Schadendorf, *Br. J. Cancer*, 1999, **79**, 1025-1031.

209. S. Mattei, M. P. Colombo, C. Melani, A. Silvani, G. Parmiani and M. Herlyn, *Int. J. Cancer*, 1994, **56**, 853-857.

210. H. K. Kim, K. S. Song, Y. S. Park, Y. H. Kang, Y. J. Lee, K. R. Lee, H. K. Kim, K. W. Ryu, J. M. Bae and S. Kim, *Eur. J. Cancer*, 2003, **39**, 184-191.

211. Z. Cao, X. Xu, X. Luo, L. Li, B. Huang, X. Li, D. Tao, J. Hu and J. Gong, *J. Huazhong Univ. Sci. Technol. Med. Sci.*, 2011, **31**, 342-347.

212. B. Cambien, P. Richard-Fiardo, B. F. Karimdjee, V. Martini, B. Ferrua, B. Pitard, H. Schmid-Antomarchi and A. Schmid-Alliana, *PLoS ONE*, 2011, **6**.

213. S. Tsukishiro, N. Suzumori, H. Nishikawa, A. Arakawa and K. Suzumori, *Gynecol. Oncol.*, 2006, **102**, 542-545.

214. K. Maeda, D. Das, H. Nakata and H. Mitsuya, *Expert Opin. Emerg. Drugs*, 2012, **17**, 135-145.

215. R. Kondru, J. Zhang, C. Ji, T. Mirzadegan, D. Rotstein, S. Sankuratri and M. Dioszegi, *Mol. Pharmacol.*, 2008, **73**, 789-800.

216. A. Junker, A. K. Kokornaczyk, A. J. M. Zweemer, B. Frehland, D. Schepmann, J. Yamaguchi, K. Itami, A. Faust, S. Hermann, S. Wagner, M. Schaefers, M. Koch, C. Weiss, L. H. Heitman, K. Kopka and B. Wuensch, *Org. Biomol. Chem.*, 2015, **13**, 2407-2422.

217. T. Dragic, V. Litwin, G. P. Allaway, S. R. Martin, Y. X. Huang, K. A. Nagashima, C. Cayanan, P. J. Maddon, R. A. Koup, J. P. Moore and W. A. Paxton, *Nature*, 1996, **381**, 667-673.

218. T. Dragic, A. Trkola, D. A. D. Thompson, E. G. Cormier, F. A. Kajumo, E. Maxwell, S. W. Lin, W. W. Ying, S. O. Smith, T. P. Sakmar and J. P. Moore, *Proc. Natl. Acad. Sci. U. S. A.*, 2000, **97**, 5639-5644.

219. A. Trkola, T. Dragic, J. Arthos, J. M. Binley, W. C. Olson, G. P. Allaway, C. ChengMayer, J. Robinson, P. J. Maddon and J. P. Moore, *Nature*, 1996, **384**, 184-187.

220. J. Zhang, Y. Fu, G. Li, R. Y. Zhao and J. R. Lakowicz, *Biochem. Biophys. Res. Commun.*, 2011, **407**, 63-67.

221. H. Kobayashi and P. L. Choyke, *Acc. Chem. Res.*, 2011, **44**, 83-90.

222. J. Zhang, Y. Fu, G. Li, K. Nowaczyk, R. Y. Zhao and J. R. Lakowicz, *Biochem. Biophys. Res. Commun.*, 2010, **400**, 111-116.
223. H. P. Luehmann, E. D. Pressly, L. Detering, C. Wang, R. Pierce, P. K. Woodard, R. J. Gropler, C. J. Hawker and Y. Liu, *J. Nucl. Med.*, 2014, **55**, 629-634.
224. M. Shiraishi, Y. Aramaki, M. Seto, H. Imoto, Y. Nishikawa, N. Kanzaki, M. Okamoto, H. Sawada, O. Nishimura, M. Baba and M. Fujino, *J. Med. Chem.*, 2000, **43**, 2049-2063.
225. N. Kanzaki, M. Shiraishi, Y. Iizawa, M. Baba, O. Nishimura and M. Fujino, *Drugs of the Future*, 2000, **25**, 252-258.
226. T. Ikemoto, T. Ito, H. Hashimoto, T. Kawarasaki, A. Nishiguchi, H. Mitsudera, M. Wakimasu and K. Tomimatsu, *Org. Process Res. Dev.*, 2000, **4**, 520-525.
227. K. Kato, T. Takita and H. Umezawa, *Tetrahedron Lett.*, 1980, **21**, 4925-4926.
228. M. Schlosser and Z. Brich, *Helv. Chim. Acta*, 1978, **61**, 1903-1911.
229. A. Junker, D. Schepmann, J. Yamaguchi, K. Itami, A. Faust, K. Kopka, S. Wagner and B. Wuensch, *Org. Biomol. Chem.*, 2014, **12**, 177-186.
230. Y. H. So and J. P. Heeschen, *J. Org. Chem.*, 1997, **62**, 3552-3561.
231. M. Shiraishi, K. Kato, S. Terao, Y. Ashida, Z. Terashita and G. Kito, *J. Med. Chem.*, 1989, **32**, 2214-2221.
232. G. J. Stasiuk and N. J. Long, *Chem. Commun.*, 2013, **49**, 2732-2746.
233. P. Antunes, M. Ginj, H. Zhang, B. Waser, R. P. Baum, J. C. Reubi and H. Maecke, *Eur. J. Nucl. Med. Mol. Imaging*, 2007, **34**, 982-993.
234. E. Blom, B. Langstrom and I. Velikyan, *Bioconj. Chem.*, 2009, **20**, 1146-1151.
235. C. Decristoforo, I. H. Gonzalez, J. Carlsen, M. Rupprich, M. Huisman, I. Virgolini, H.-J. Wester and R. Haubner, *Eur. J. Nucl. Med. Mol. Imag.*, 2008, **35**, 1507-1515.
236. C. Montalbetti and V. Falque, *Tetrahedron*, 2005, **61**, 10827-10852.
237. D. J. Berry, Y. Ma, J. R. Ballinger, R. Tavare, A. Koers, K. Sunassee, T. Zhou, S. Nawaz, G. E. D. Mullen, R. C. Hider and P. J. Blower, *Chem. Commun.*, 2011, **47**, 7068-7070.
238. C. L. Ferreira, E. Lamsa, M. Woods, Y. Duan, P. Fernando, C. Bensimon, M. Kordos, K. Guenther, P. Jurek and G. E. Kiefer, *Bioconj. Chem.*, 2010, **21**, 531-536.
239. D. Bradley, G. Williams and M. Lawton, *J. Org. Chem.*, 2010, **75**, 8351-8354.